

# Generalized Bayesian Likelihood-Free Inference Using Scoring Rules Estimators

Lorenzo Pacchiardi<sup>1\*</sup>, Ritabrata Dutta<sup>2</sup>

<sup>1</sup>*Department of Statistics, University of Oxford, UK*

<sup>2</sup>*Department of Statistics, University of Warwick, UK*

15th March 2022

## Abstract

We propose a framework for Bayesian Likelihood-Free Inference (LFI) based on Generalized Bayesian Inference. To define the generalized posterior, we use Scoring Rules (SRs), which evaluate probabilistic models given an observation. In LFI, we can sample from the model but not evaluate the likelihood; for this reason, we employ SRs with easy empirical estimators. Our framework includes novel approaches and popular LFI techniques (such as Bayesian Synthetic Likelihood) and enjoys posterior consistency in a well-specified setting when a *strictly-proper* SR is used (i.e., one whose expectation is uniquely minimized when the model corresponds to the data generating process). In general, our framework does *not* approximate the standard posterior; as such, it is possible to achieve outlier robustness, which we prove is the case for the Kernel and Energy Scores. We also discuss a strategy for tuning the learning rate in the generalized posterior suitable for the LFI setup. We run simulations studies with correlated pseudo-marginal Markov Chain Monte Carlo and compare with related approaches on standard benchmarks and challenging intractable-likelihood models from meteorology and ecology.

## 1 Introduction

This work is concerned with performing inference for intractable-likelihood models, for which it is impossible or very expensive to evaluate the likelihood  $p(y|\theta)$  for an observation  $y$ , but from which it is easy to simulate for any parameter value  $\theta$ . Given  $y$  and a prior  $\pi(\theta)$  on the parameters, the standard Bayesian posterior is  $\pi(\theta|y) \propto \pi(\theta)p(y|\theta)$ . However, obtaining that explicitly or sampling from it with Markov Chain Monte Carlo (MCMC) techniques is impossible without having access to the likelihood.

Standard Likelihood-Free Inference (LFI) techniques exploit model simulations to approximate the exact posterior distribution when the likelihood is unavailable. Broadly, two categories of approaches exist, differing for the kind of approximation: methods in the first category [Price et al., 2018, An et al., 2020, Thomas et al., 2020] replace the intractable likelihood with a surrogate one whose parameters are estimated from simulations. The second category is constituted by Approximate Bayesian Computation (ABC) methods [Lintusaari et al., 2017, Bernton et al., 2019], which implicitly approximate the likelihood by weighting parameter values according to the mismatch between observed and simulated data.

In this work, we extend the first category above by building on the generalized Bayesian inference setup [Bissiri et al., 2016, Jewson et al., 2018, Knoblauch et al., 2019]: given a generic loss  $\ell(y, \theta)$  between data  $y$  and parameter  $\theta$ , the following update for beliefs on parameter values can be defined:

$$\pi(\theta|y) \propto \pi(\theta) \exp(-w \cdot \ell(y, \theta)); \quad (1)$$

this allows to learn about the parameter value minimizing the expected loss over the data generating process<sup>1</sup> and respects Bayesian additivity (i.e., the posterior obtained by sequentially updating the

\*Corresponding author: lorenzo.pacchiardi@stats.ox.ac.uk.

<sup>1</sup>Indeed setting  $\ell(y, \theta) = -\log p(y|\theta)$  and  $w = 1$  recovers the standard Bayes update, which learns about the parameter value minimizing the KL divergence [Bissiri et al., 2016].

belief with a set of observations does not depend on the order the observations are received). Here, the learning rate  $w$  controls speed of learning.

In the following, we will distinguish between a statistical model (or distribution)  $P_\theta$  and its likelihood function  $p(y|\theta)$ . In general, the update in Eq. (1) does not require the quantity  $\theta$  to parametrize a statistical model  $P_\theta$ . In LFI, however, we cannot evaluate  $p(y|\theta)$ , but a model  $P_\theta$  is present. Therefore, we propose to take  $\ell(y, \theta)$  to be a Scoring Rule (SR)  $S(P_\theta, y)$ , which assesses the performance of  $P_\theta$  for an observation  $y$ , thus obtaining the *Scoring Rule posterior*  $\pi_S$ . If  $S(P_\theta, y)$  can be estimated with samples from  $P_\theta$ , we can apply this approach in a LFI setting without worrying about the missing likelihood  $p(y|\theta)$ . Thus, our main contribution is: *we introduce an LFI framework based on Scoring Rules, which comprehends previously introduced LFI methods and novel ones. Additionally, for some Scoring Rules, the resulting posterior enjoys outlier robustness while asymptotically concentrating on the true parameter value in a well-specified setting.*

Specifically,  $\pi_S$  concentrates asymptotically on the minimizer of the expected Scoring Rule, provided such minimizer is unique; for well-specified models, the minimizer is the true parameter value if so-called *strictly proper* SRs are used. To state this, we rely on previous results in Miller [2021], for which we provide assumptions for our setup. We also point out that the popular Bayesian Synthetic Likelihood (BSL, Price et al. 2018) does not use a strictly proper SR, hence leading to some failures. Further, in general our framework does *not* approximate the standard Bayesian posterior, as it is the case for commonly-used LFI techniques; by relaxing this requirement, outlier robustness can be achieved, as we show for the Kernel and Energy Score. For the same SRs, we also establish a finite sample generalization bound.

Finally, we discuss a tuning strategy for the learning rate  $w$  which is suitable for the SR posterior in a LFI scenario and compare our Kernel and Energy Score posteriors with related approaches via simulation studies. To sample from the SR posteriors, we employ pseudo-marginal MCMC [Andrieu et al., 2009], inside which simulations from  $P_{\theta'}$  are generated for each proposed  $\theta'$ . To reduce the stickiness typical of pseudo-marginal chains, we exploit correlated pseudo-marginal MCMC [Dahlin et al., 2015, Deligiannidis et al., 2018], which was validated for BSL in Picchini et al. [2022]. We study posterior concentration with the g-and-k model (in both well-specified and misspecified case) and outlier robustness on a normal location example and two challenging intractable-likelihood time-series models from meteorology and ecology.

The rest of this manuscript is organized as follows. In Sec. 2, which contains most of our contributions, we first review Scoring Rules and define the SR posterior; we then discuss theoretical properties, sampling strategy and our heuristics for tuning  $w$ . Next, we discuss the relation of our approach with previous works in Sec. 3, showing how some popular LFI approaches are instances of the SR posterior. Our simulation studies are presented in Sec. 4 and we conclude and suggest future directions in Sec. 5.

## 1.1 Notation

We will denote respectively by  $\mathcal{X} \subseteq \mathbb{R}^d$  and  $\Theta \subseteq \mathbb{R}^p$  the data and parameter space, which we assume to be Borel sets. We will assume the observations are generated by a distribution  $P_0$  and use  $P_\theta$  and  $p(\cdot|\theta)$  to denote the distribution and likelihood of our model. Generic distributions will be indicated by  $P$  or  $Q$ , while  $S$  will denote a generic Scoring Rule. Other upper-case letters will denote random variables while lower-case ones will denote observed (fixed) values. We will denote by  $Y$  or  $y$  the observations (correspondingly random variables and realizations) and  $X$  or  $x$  the simulations. Subscripts will denote sample index and superscripts vector components. Also, we will respectively denote by  $\mathbf{Y}_n = \{Y_i\}_{i=1}^n \in \mathcal{X}^n$  and  $\mathbf{y}_n = \{y_i\}_{i=1}^n \in \mathcal{X}^n$  a set of random and fixed observations. Similarly,  $\mathbf{X}_m = \{X_j\}_{j=1}^m \in \mathcal{X}^m$  and  $\mathbf{x}_m = \{x_j\}_{j=1}^m \in \mathcal{X}^m$  denote a set of random and fixed model simulations. Finally,  $\perp$  will denote independence between random variables, while  $X \sim P$  indicates a random variable distributed according to  $P$ .

## 2 Bayesian inference using Scoring Rules

A Scoring Rule (SR, Gneiting and Raftery, 2007)  $S$  is a function of a probability distribution over  $\mathcal{X}$  and of an observation in  $\mathcal{X}$ . In probabilistic forecasting,  $S(P, y)$  represents the *penalty* incurred when

stating a forecast  $P$  for an observation  $y$ .<sup>2</sup>

Assuming that  $y$  is a realization of a random variable  $Y$  with distribution  $Q$ , the expected Scoring Rule is defined as:

$$S(P, Q) := \mathbb{E}_{Y \sim Q} S(P, Y),$$

where we overload notation in the second argument of  $S$ . The Scoring Rule  $S$  is *proper* relative to a set of distributions  $\mathcal{P}(\mathcal{X})$  over  $\mathcal{X}$  if

$$S(Q, Q) \leq S(P, Q) \quad \forall P, Q \in \mathcal{P}(\mathcal{X}),$$

i.e., if the expected Scoring Rule is minimized in  $P$  when  $P = Q$ . Moreover,  $S$  is *strictly proper* relative to  $\mathcal{P}(\mathcal{X})$  if  $P = Q$  is the unique minimum:

$$S(Q, Q) < S(P, Q) \quad \forall P, Q \in \mathcal{P}(\mathcal{X}) \text{ s.t. } P \neq Q;$$

when minimizing an expected strictly proper Scoring Rule, a forecaster provides their true belief [Gneiting and Raftery, 2007].

The divergence related to a proper Scoring Rule [Dawid and Musio, 2014] can be defined as  $D(P, Q) := S(P, Q) - S(Q, Q) \geq 0$ . Notice that  $P = Q \implies D(P, Q) = 0$ , but there may be  $P \neq Q$  such that  $D(P, Q) = 0$ . However, if  $S$  is strictly proper,  $D(P, Q) = 0 \iff P = Q$ , which is the commonly used condition to define a statistical divergence (as for instance the Kullback-Leibler, or KL, divergence). Therefore, each strictly proper Scoring Rule corresponds to a statistical divergence between probability distributions.

Consider now a set of observations  $\mathbf{y}_n \in \mathcal{X}^n$  by a distribution  $P_0$ . We introduce the SR posterior for  $S$  by setting  $\ell(y, \theta) = S(P_\theta, y)$  in the general Bayes update in Eq. (1):

$$\pi_S(\theta | \mathbf{y}_n) \propto \pi(\theta) \exp \left\{ -w \sum_{i=1}^n S(P_\theta, y_i) \right\}. \quad (2)$$

The standard Bayes posterior is recovered from Eq. (2) by setting  $w = 1$  and  $S(P_\theta, y) = -\log p(y|\theta)$ . Such choice of  $S$  is called the *log score*, is strictly proper, and corresponds to the Kullback-Leibler (KL) divergence. With the same  $S$ ,  $w \neq 1$  yields the fractional posterior [Holmes and Walker, 2017, Bhattacharya et al., 2019].

**Remark 1 (Bayesian additivity).** *The posterior in Eq. (2) satisfies Bayesian additivity (also called coherence, Bissiri et al. 2016): sequentially updating the belief with a set of observations does not depend on the order the observations are received. Some related approaches do not satisfy this property, notably the ABC posterior [Lintusaari et al., 2017, Bernton et al., 2019]. Additionally, methods building an estimate of the data generating density using all observations  $\{y_i\}_{i=1}^n$  break additivity (as for instance the Hellinger posterior considered in Jewson et al. [2018]).*

In Sec. 2.1, we review some Scoring Rules which can be conveniently estimated with intractable-likelihood models. Some properties of the SR posterior are discussed in Sec. 2.2. In Sec. 2.3 and Sec. 2.4, we show how to sample from the SR posterior using pseudo-marginal MCMC and propose a heuristic way to set the value of  $w$ .

## 2.1 Scoring Rules for LFI

Under the assumed LFI setup, we can sample from  $P_\theta$ ; therefore, we are interested in SRs for which estimators can be easily obtained using generated samples. Specifically, we will estimate  $S(P_\theta, y)$  with  $\hat{S}(\mathbf{x}_m^{(\theta)}, y)$ , where  $\mathbf{x}_m^{(\theta)} = \{x_j^{(\theta)}\}_{j=1}^m$  is a set of samples  $x_j^{(\theta)} \sim P_\theta$ , and  $\hat{S}$  is such that  $\hat{S}(\mathbf{X}_m^{(\theta)}, y) \rightarrow S(P_\theta, y)$  in probability as  $m \rightarrow \infty$  (i.e., it estimates the SR consistently). Below, we discuss three SRs with such an estimator.

---

<sup>2</sup>Some authors [Gneiting and Raftery, 2007] use the convention of  $S(P, y)$  representing a *reward* rather than a penalty, which is equivalent up to change of sign.

**Dawid-Sebastiani score** The Dawid-Sebastiani (DS) score is defined as:

$$S_{\text{DS}}(P, y) = \ln |\Sigma_P| + (y - \mu_P)^T \Sigma_P^{-1} (y - \mu_P), \quad (3)$$

where  $\mu_P$  and  $\Sigma_P$  are the mean vector and covariance matrix of  $P$ . The DS score is the negative log-likelihood of a multivariate normal distribution with mean  $\mu_P$  and covariance matrix  $\Sigma_P$ , up to some constants. Therefore, it is equivalent to the log score when  $P$  is a multivariate normal distribution.

For a set of distributions  $\mathcal{P}(\mathcal{X})$  with well-defined second moments, this SR is proper but not strictly so: several distributions of that class may yield the same score, as long as the two first moments match [Gneiting and Raftery, 2007]. It is strictly proper if distributions in  $\mathcal{P}(\mathcal{X})$  are determined by their first two moments, as it is the case for the normal distribution.

Using  $S_{\text{DS}}$  in Eq. (2) with  $w = 1$  leads to the popular Bayesian Synthetic Likelihood approach (see Sec. 3). In an LFI setup, an empirical estimator  $\hat{S}_{\text{DS}}$  can be obtained by inserting any estimator of the mean and covariance matrix in Eq. (3).

**Energy score** The energy score is given by:

$$S_{\text{E}}^{(\beta)}(P, y) = 2 \cdot \mathbb{E} \left[ \|X - y\|_2^\beta \right] - \mathbb{E} \left[ \|X - X'\|_2^\beta \right], \quad X \perp\!\!\!\perp X' \sim P,$$

where  $\beta \in (0, 2)$ . This is a strictly proper Scoring Rule for the class  $\mathcal{P}_\beta(\mathcal{X})$  of probability measures  $P$  such that  $\mathbb{E}_{X \sim P} \|X\|^\beta < \infty$  [Gneiting and Raftery, 2007]. The related divergence is the square of the energy distance, which is a metric between probability distributions (Rizzo and Székely 2016; see Appendix C.1)<sup>3</sup>. An unbiased estimate can be obtained by unbiasedly estimating the expectations in  $S_{\text{E}}^{(\beta)}$ :

$$\hat{S}_{\text{E}}^{(\beta)}(\mathbf{x}_m, y) = \frac{2}{m} \sum_{j=1}^m \|x_j - y\|_2^\beta - \frac{1}{m(m-1)} \sum_{\substack{j,k=1 \\ k \neq j}}^m \|x_j - x_k\|_2^\beta.$$

We will fix  $\beta = 1$  in the rest of this work and we will write  $S_{\text{E}}$  in place of  $S_{\text{E}}^{(1)}$ .

**Kernel score** When  $k(\cdot, \cdot)$  is a positive definite kernel, the kernel Scoring Rule for  $k$  can be defined as [Gneiting and Raftery, 2007]:

$$S_k(P, y) = \mathbb{E}[k(X, X')] - 2 \cdot \mathbb{E}[k(X, y)], \quad X \perp\!\!\!\perp X' \sim P.$$

The corresponding divergence is the squared Maximum Mean Discrepancy (MMD, Gretton et al., 2012) relative to  $k$  (see Appendix C.2).

The Kernel Score is proper for the class of probability distributions for which  $\mathbb{E}[k(X, X')]$  is finite (by Theorem 4 in Gneiting and Raftery [2007]). Additionally, it is strictly proper under conditions which ensure that the MMD is a metric for probability distributions on  $\mathcal{X}$  (see Appendix C.2). These conditions are satisfied, among others, by the Gaussian kernel (which we will use in this work):

$$k(x, y) = \exp \left( -\frac{\|x - y\|_2^2}{2\gamma^2} \right),$$

in which  $\gamma$  is a scalar bandwidth. Similarly to the Energy Score, an unbiased estimate is:

$$\hat{S}_k(\mathbf{x}_m, y) = \frac{1}{m(m-1)} \sum_{\substack{j,k=1 \\ k \neq j}}^m k(x_j, x_k) - \frac{2}{m} \sum_{j=1}^m k(x_j, y).$$

---

<sup>3</sup>The probabilistic forecasting literature [Gneiting and Raftery, 2007] use a different convention for the energy score and the subsequent kernel score, which amounts to multiplying our definitions by 1/2. We follow here the convention used in the statistical inference literature [Rizzo and Székely, 2016, Chérif-Abdellatif and Alquier, 2020, Nguyen et al., 2020]

**Remark 2 (Likelihood principle).** *In general, the SR posterior in Eq. (2) does not satisfy the likelihood principle, according to which all information to update beliefs about model parameters is contained in the likelihood value at the observation. This principle is instead satisfied by the standard Bayes posterior. In Jewson et al. [2018], the authors argue that the likelihood principle is sensible when the model is well specified, but it is not in an  $M$ -open setup. Additionally, we add, for likelihood-free inference the likelihood is unavailable in the first place, so that it may be preferable replacing it with a Scoring Rule not respecting the likelihood principle but for which an easy estimator is available.*

**Remark 3 (Non-invariance to change of data coordinates).** *Violation of the likelihood principle implies that the SR posterior is in general not invariant to change of the coordinates used for representing the observations. This is a property common to loss-based frequentist estimators and to the generalized posterior obtained from them [Matsubara et al., 2021]; see Appendix B for more details.*

## 2.2 Properties of the Scoring Rule posterior

### 2.2.1 Asymptotic normality

We first show that the SR posterior satisfies (under some conditions) a Bernstein-von Mises theorem ensuring asymptotic normality. Without loss of generality, we fix here  $w = 1$  (other values can be absorbed in the definition of  $S$ ). The proof relies on the following assumptions:

**A1** The expected Scoring Rule  $S(P_\theta, P_0)$  is finite for all  $\theta \in \Theta$ ; further, it has a unique minimizer:

$$\theta^\star = \arg \min_{\theta \in \Theta} S(P_\theta, P_0) = \arg \min_{\theta \in \Theta} D(P_\theta, P_0).$$

Additionally,  $H_\star := \nabla_\theta^2 S(P_\theta, P_0)|_{\theta=\theta^\star}$  is positive definite.

**A2** Let us denote  $S'''(P_\theta, y)_{jkl} = \frac{\partial^3}{\partial \theta_j \partial \theta_k \partial \theta_l} S(P_\theta, y)$ . There exists an open neighborhood  $E \subseteq \mathbb{R}^d$  of  $\theta^\star$  whose closure  $\bar{E} \subseteq \Theta$  is such that, for all  $j, k, l \in \{1, \dots, d\}$ :

- $\theta \rightarrow S'''(P_\theta, y)_{jkl}$  is continuous in  $E$  and exists in  $\bar{E}$  for any fixed  $y \in \mathcal{X}$ ,
- $y \rightarrow S'''(P_\theta, y)_{jkl}$  is measurable for any fixed  $\theta \in \bar{E}$ ,
- $\mathbb{E}_{P_0} \sup_{\theta \in \bar{E}} |S'''(P_\theta, y)_{jkl}| < \infty$ .

**A3** For  $E$  defined above, there exists a compact  $K \subseteq E$ , with  $\theta^\star$  in the interior of  $K$ , such that:

$$P_0 \left\{ \liminf_n \inf_{\theta \in \Theta \setminus K} \frac{1}{n} \sum_{i=1}^n S(P_\theta, Y_i) > S(P_{\theta^\star}, P_0) \right\} = 1.$$

**A4** The prior has a density  $\pi(\theta)$  with respect to Lebesgue measure;  $\pi(\theta)$  is continuous and positive at  $\theta^\star$ .

Assumption **A3** is a regularity condition which can be replaced with clearer (but less general) Assumptions; see Appendix A.1.2. In Assumption **A1**,  $H_\star$  generalizes the standard Fisher information, which can be obtained by setting  $S(P_\theta, y) = -\log p(y|\theta)$ . Additionally, uniqueness of  $\theta^\star$  is obtained by strictly proper  $S$  and a well-specified model (in which case observations were generated from  $P_{\theta^\star}$ ). If the model class is misspecified, a strictly proper  $S$  does not guarantee a unique minimizer (as in fact there may be pathological cases where multiple minimizers exist).

**Theorem 1.** *Let Assumptions **A1** to **A4** be true. Then, there is a sequence  $\hat{\theta}^{(n)}(\mathbf{Y}_n)$  which converges almost surely to  $\theta^\star$  as  $n \rightarrow \infty$ . Denote now by  $\pi_S^*(\cdot|\mathbf{Y}_n)$  the density of  $\sqrt{n}(\theta - \hat{\theta}^{(n)}(\mathbf{Y}_n))$  when  $\theta \sim \pi_S(\cdot|\mathbf{Y}_n)$ . Then as  $n \rightarrow \infty$ , with probability 1 over  $\mathbf{Y}_n$ :*

$$\int_{\mathbb{R}} |\pi_S^*(s|\mathbf{Y}_n) - \mathcal{N}(s|0, H_\star^{-1})| ds \rightarrow 0,$$

where  $\mathcal{N}(\cdot|0, \Sigma)$  denotes the density of a multivariate normal distribution with zero mean vector and covariance matrix  $\Sigma$ .

Proof of Theorem 1 is reported in Appendix A.1.2 and uses a result for general Bayes posteriors with generic losses found in Miller [2021].

Theorem 1 implies that the SR posterior concentrates, with probability 1, on the parameter value minimizing the expected SR, if that minimizer is unique. If the model is well specified and  $S$  is strictly proper, the SR posterior concentrates therefore on the true parameter value; this property is usually referred to as *posterior consistency*.

**Remark 4 (Non-invariance to change of data coordinates – continued).** *Following on from Remark 3, notice that  $\theta^*$  depends on the data coordinates, unless the model is well specified and  $S$  is strictly proper. If that is not the case, SR posteriors using different data coordinates will concentrate on different parameter values in general. This property is coherent with the SR posterior learning about the parameter value which minimizes the expected Scoring Rule, which in turn depends on the chosen coordinate system. See Appendix B for more details.*

## 2.2.2 Finite sample generalization bound

We now consider the Energy and Kernel Score posteriors and their corresponding divergences, and provide a bound on the probability of deviation of the posterior expectation of the divergence from the minimum divergence achievable by the model. The bound holds with finite number of samples and does not require the model to be well specified nor the minimizer of the divergence to be unique. Such kind of results are usually referred to as generalization bounds [Chérif-Abdellatif and Alquier, 2020]. For our bound to hold, we require the following *prior mass condition*:

**A5** The prior has density  $\pi(\theta)$  (with respect to Lebesgue measure) which satisfies

$$\int_{B_n(\alpha_1)} \pi(\theta) d\theta \geq e^{-\alpha_2 \sqrt{n}}$$

for some constants  $\alpha_1, \alpha_2 > 0$  and for all positive  $n \in \mathbb{N}$ , where we define the sets:

$$B_n(\alpha_1) := \{\theta \in \Theta : |D(P_\theta, P_0) - D(P_{\theta^*}, P_0)| \leq \alpha_1 / \sqrt{n}\},$$

where  $D$  is a divergence and  $\theta^* \in \arg \min_{\theta \in \Theta} D(P_\theta, P_0)$ , which is assumed to be nonempty.

Assumption **A5** constrains the amount of prior mass given to  $D$ -balls with size decreasing as  $n^{-1/2}$  to decrease slower than  $e^{-\alpha_2 \sqrt{n}}$  for some  $\alpha_2$ . It is therefore a weak condition, as it bounds the mass by a quickly decreasing function while the radius is decreasing more slowly. Similar assumptions are taken in Chérif-Abdellatif and Alquier 2020, Matsubara et al. 2021, where some examples of explicit verification can be found.

Our result (proved in Appendix A.2) further assumes either a bounded kernel  $k$  for the Kernel Score posterior, or bounded  $\mathcal{X}$  for the Energy Score posterior.

**Theorem 2.** *The following two statements hold for any  $\epsilon > 0$ :*

1. *Let the kernel  $k$  be such that  $0 \leq \sup_{x,y \in \mathcal{X}} k(x,y) \leq \kappa < \infty$ , and let  $D_k$  be the divergence associated to  $S_k$ . Consider  $\theta^* \in \arg \min_{\theta \in \Theta} D_k(P_\theta, P_0)$ ; if the prior  $\pi(\theta)$  satisfies Assumption **A5** for  $D_k$ , we have for the kernel Score posterior  $\pi_{S_k}$ :*

$$P_0 \left( \left| \int_{\Theta} D_k(P_\theta, P_0) \pi_{S_k}(\theta | \mathbf{Y}_n) d\theta - D_k(P_{\theta^*}, P_0) \right| \geq \epsilon \right) \leq 2e^{-\frac{1}{2} \left( \frac{\sqrt{n}\epsilon - \alpha_1 - \alpha_2/w}{8\kappa} \right)^2}.$$

2. *Assume the space  $\mathcal{X}$  is bounded such that  $\sup_{x,y \in \mathcal{X}} \|x - y\|_2 \leq B < \infty$ , and let  $D_E^{(\beta)}$  be the divergence associated with  $S_E^{(\beta)}$ . Consider  $\theta^* \in \arg \min_{\theta \in \Theta} D_E^{(\beta)}(P_\theta, P_0)$ ; if the prior  $\pi(\theta)$  satisfies Assumption **A5** for  $D_E^{(\beta)}$ , we have for the Energy score posterior  $\pi_{S_E^{(\beta)}}$ :*

$$P_0 \left( \left| \int_{\Theta} D_E^{(\beta)}(P_\theta, P_0) \pi_{S_E^{(\beta)}}(\theta | \mathbf{Y}_n) d\theta - D_E^{(\beta)}(P_{\theta^*}, P_0) \right| \geq \epsilon \right) \leq 2e^{-\frac{1}{2} \left( \frac{\sqrt{n}\epsilon - \alpha_1 - \alpha_2/w}{8B^\beta} \right)^2}.$$

As  $\epsilon$  or  $n$  increases, the bound on the probability tends to 0; for  $n \rightarrow \infty$ , this implies that the SR posterior concentrates on those parameter values for which the model achieves minimum divergence from the data generating process  $P_0$ , ensuring therefore consistency in the well-specified case. With respect to Theorem 1, Theorem 2 provides guarantees on the infinite sample behavior of the SR posterior even when  $\theta^*$  is not unique; however, this result does not describe the specific form of the asymptotic distribution, which Theorem 1 instead does.

### 2.2.3 Global bias-robustness

We establish now robustness with respect to contamination in the dataset for the Kernel Score posterior with bounded kernel and the Energy Score posterior with bounded  $\mathcal{X}$ . A similar result can be found in Matsubara et al. [2021].

First, consider the empirical distribution of the observations  $\hat{P}_n = \frac{1}{n} \sum_{i=1}^n \delta_{y_i}$ . If we define:

$$L(\theta, \hat{P}_n) := \frac{1}{n} \sum_{i=1}^n S(P_\theta, y_i) = \mathbb{E}_{Y \sim \hat{P}_n} S(P_\theta, Y)$$

for a Scoring Rule  $S$ , the SR posterior in Eq. (2) can be rewritten as:

$$\pi_S(\theta | \mathbf{y}_n) = \pi_S(\theta | \hat{P}_n) \propto \pi(\theta) \exp \left\{ -wnL(\theta, \hat{P}_n) \right\}.$$

Next, consider the  $\epsilon$ -contamination distribution  $\hat{P}_{n,\epsilon,z} = (1 - \epsilon)\hat{P}_n + \epsilon\delta_z$ , obtained by perturbing the fixed empirical distribution with an outlier  $z$  of weight  $\epsilon$ . In this setup, the *posterior influence function* [Ghosh and Basu, 2016] can be defined as:

$$\text{PIF} \left( z, \theta, \hat{P}_n \right) := \left. \frac{d}{d\epsilon} \pi_S \left( \theta | \hat{P}_{n,\epsilon,z} \right) \right|_{\epsilon=0},$$

which measures the rate of change of the posterior in  $\theta$  when an infinitesimal perturbation in  $z$  is added to the observations. The SR posterior is said to be globally bias-robust if:

$$\sup_{\theta \in \Theta} \sup_{z \in \mathcal{X}} \left| \text{PIF} \left( z, \theta, \hat{P}_n \right) \right| < \infty.$$

**Theorem 3.** *Assume the prior  $\pi(\theta)$  is bounded over  $\Theta$ ; the following two independent statements hold:*

1. *Consider a kernel  $k$  such that  $0 \leq \sup_{x,y \in \mathcal{X}} k(x,y) \leq \kappa < \infty$ ; then, the Kernel Score posterior  $\pi_{S_k}(\cdot | \mathbf{y}_n)$  is globally bias-robust.*
2. *Alternatively, assume the space  $\mathcal{X}$  is bounded; then, the Energy Score posterior  $\pi_{S_E^{(\beta)}}(\cdot | \mathbf{y}_n)$  is globally bias-robust for all  $\beta \in (0, 2)$ .*

Proof is given in Appendix A.3. The Gaussian kernel (used across this work, see Sec. 2.1) is bounded. Our theoretical result does not hold for the Energy Score posterior when  $\mathcal{X}$  is unbounded. However, in practice we still find the Energy Score posterior to be robust to outliers in examples with unbounded  $\mathcal{X}$  (see Sec. 4.2).

## 2.3 Sampling the Scoring Rule posterior

In implementing our proposed approach, we use an MCMC where, for each proposed value of  $\theta$ , we simulate  $\mathbf{x}_m^{(\theta)} = \{x_j^{(\theta)}\}_{j=1}^m$  and estimate the target in Eq. (2) with:

$$\pi(\theta) \exp \left\{ -w \sum_{i=1}^n \hat{S}(\mathbf{x}_m^{(\theta)}, y_i) \right\}. \quad (4)$$

This procedure is an instance of pseudo-marginal MCMC [Andrieu et al., 2009], with target:

$$\pi_{\hat{S}}^{(m)}(\theta|\mathbf{y}_n) \propto \pi(\theta)p_{\hat{S}}^{(m)}(\mathbf{y}_n|\theta), \quad (5)$$

where:

$$\begin{aligned} p_{\hat{S}}^{(m)}(\mathbf{y}_n|\theta) &= \mathbb{E} \left[ \exp \left\{ -w \sum_{i=1}^n \hat{S}(\mathbf{X}_{\mathbf{m}}^{(\theta)}, y_i) \right\} \right] \\ &= \int \exp \left\{ -w \sum_{i=1}^n \hat{S}(\mathbf{x}_{\mathbf{m}}^{(\theta)}, y_i) \right\} \prod_{j=1}^m p(x_j^{(\theta)}|\theta) dx_1^{(\theta)} dx_2^{(\theta)} \dots dx_m^{(\theta)}. \end{aligned}$$

For a single draw  $\mathbf{x}_{\mathbf{m}}^{(\theta)}$ , the quantity in Eq. (4) is in fact a non-negative and unbiased estimate of the target in Eq. (5); this approach is similar to what is proposed in Drovandi et al. [2015] for inference with auxiliary likelihoods, which has also been used by Price et al. [2018] for BSL. As it was already the case for the latter, the target  $\pi_{\hat{S}}^{(m)}(\theta|\mathbf{y}_n)$  is not the same as  $\pi_S(\theta|\mathbf{y}_n)$  and depends on the number of simulations  $m$ ; in fact, in general:

$$\mathbb{E} \left[ \exp \left\{ -w \sum_{i=1}^n \hat{S}(\mathbf{X}_{\mathbf{m}}^{(\theta)}, y_i) \right\} \right] \neq \exp \left\{ -w \sum_{i=1}^n S(P_{\theta}, y_i) \right\},$$

even if  $\hat{S}(\mathbf{x}_{\mathbf{m}}^{(\theta)}, y)$  is an unbiased estimate of  $S(P_{\theta}, y)$ . However, it is possible to show that, as  $m \rightarrow \infty$ ,  $\pi_{\hat{S}}^{(m)}$  converges to  $\pi_S$ :

**Theorem 4.** *If  $\hat{S}(\mathbf{X}_{\mathbf{m}}^{(\theta)}, y_i)$  converges in probability to  $S(P_{\theta}, y_i)$  as  $m \rightarrow \infty$  for all  $i = 1, \dots, n$ , then, under some minor technical assumptions:*

$$\lim_{m \rightarrow \infty} \pi_{\hat{S}}^{(m)}(\theta|\mathbf{y}_n) = \pi_S(\theta|\mathbf{y}_n), \quad \forall \theta \in \Theta.$$

The above result is an extension of the one in Drovandi et al. [2015] for Bayesian inference with an auxiliary likelihood. We provide complete statement and proof of Theorem 4 in Appendix A.4.

**Remark 5 (Properties of pseudo-marginal MCMC target).** *Our results in Sec. 2.2 refer to the “exact” SR posterior  $\pi_S$  (Eq. 2), which, for finite  $m$ , is different from the pseudo-marginal MCMC target  $\pi_{\hat{S}}^{(m)}$  in Eq. (5). Similarly to what was done in Frazier et al. [2021c] for BSL, it could be possible to show asymptotic normality of  $\pi_{\hat{S}}^{(m)}$  when both  $n \rightarrow \infty$  and  $m \rightarrow \infty$  at the same time; we leave this for future work. Additionally, while  $\pi_S$  satisfies Bayesian additivity (see Remark 1),  $\pi_{\hat{S}}^{(m)}$  does not in general.*

## 2.4 Choice of $w$

In the generalized posterior distribution (Eq. 1),  $w$  represents the amount of information, with respect to prior information, one observation brings to the decision maker. For the standard Bayesian update,  $w$  is fixed to 1, which yields the optimal way to process information in a well-specified scenario [Zellner, 1988]. When the model is misspecified, some works have argued for the use of  $w \neq 1$  in the standard Bayes update [Grünwald and Van Ommen, 2017, Holmes and Walker, 2017, Wu and Martin, 2020], and suggested criteria to select  $w$ . Many strategies for setting  $w$  for generalized Bayesian inference with a generic loss have also been proposed (see Bissiri et al. 2016, Syring and Martin 2019, Lyddon et al. 2019 and Loaiza-Maya et al. 2021, among others). Most of these approaches are however inapplicable to the SR posterior for a LFI setting: Grünwald and Van Ommen [2017] and Syring and Martin [2019] require to obtain the posterior with different values of  $w$ , which is computationally costly; Holmes and Walker [2017] and Lyddon et al. [2019] exploit derivatives of the loss with respect to  $\theta$ , which are inaccessible when the likelihood itself is unavailable; Holmes and Walker [2017], Lyddon et al. [2019] and Syring and Martin [2019] estimate the value of  $\theta$  yielding the minimum expected loss, which



cannot be obtained easily in LFI; finally, Loaiza-Maya et al. [2021] requires samples from the exact posterior.

We propose therefore a heuristics to select  $w$  without repeated posterior inferences, and without relying on knowledge of the likelihood function. Notice that, as remarked by Bissiri et al. [2016]:

$$\log \underbrace{\left\{ \frac{\pi_S(\theta|y)}{\pi_S(\theta'|y)} / \frac{\pi(\theta)}{\pi(\theta')} \right\}}_{\text{BF}(\theta, \theta'; y)} = -w \{S(P_\theta, y) - S(P_{\theta'}, y)\} \iff w = -\frac{\log \text{BF}(\theta, \theta'; y)}{S(P_\theta, y) - S(P_{\theta'}, y)},$$

where  $\text{BF}(\theta, \theta'; y)$  denotes the Bayes Factor of  $\theta$  with respect to  $\theta'$  for observation  $y$ . Therefore,  $w$  can be determined by fixing  $\text{BF}(\theta, \theta'; y)$  for a single choice of  $\theta, \theta', y$ .

Assume the user has access to another posterior  $\tilde{\pi}(\theta|y)$  which is obtained by means of a (in general misspecified) likelihood  $\tilde{p}(y|\theta)$ , with corresponding Bayes Factor  $\widetilde{\text{BF}}$ ; for some  $\theta, \theta', y$ , setting:

$$w = -\frac{\log \widetilde{\text{BF}}(\theta, \theta'; y)}{S(P_\theta, y) - S(P_{\theta'}, y)},$$

would ensure  $\widetilde{\text{BF}}(\theta, \theta'; y) = \text{BF}(\theta, \theta'; y)$ . In practice, we have no reason to prefer a specific choice of  $(\theta, \theta')$ ; thus, we set  $w$  to be the median of  $-\frac{\log \widetilde{\text{BF}}(\theta, \theta'; y)}{S(P_\theta, y) - S(P_{\theta'}, y)}$  over values of  $(\theta, \theta')$  sampled from the prior. The median (with respect to the mean) leads to a strategy which is robust to outliers in the computation of the above ratio. Additionally, if  $P_\theta$  is an intractable-likelihood model, we estimate  $w$  by replacing  $S(P_\theta, y)$  with  $\hat{S}(\mathbf{x}_m^{(\theta)}, y)$ , by generating data  $\mathbf{x}_m^{(\theta)}$  for each considered values of  $\theta$ .

**Remark 6 (Posterior invariance with data rescaling).** *Following on from Remark 3, we highlight here that the Kernel and Energy Score posteriors are invariant to an affine transformation of the data ( $Z = a \cdot Y + b$  for  $a, b \in \mathbb{R}$ ), albeit non-invariant to a generic transformation of the data coordinates. Specifically, the Kernel Score posterior with Gaussian kernel is invariant to such transformations with  $w_Z = w_Y$ , provided the kernel bandwidth is scaled too, while the Energy Score posterior is invariance when  $w_Z \cdot a^\beta = w_Y$ ; both are ensured by our heuristics for selecting  $w$ .*

### 3 Related approaches

**Bayesian Synthetic Likelihood (BSL).** Synthetic Likelihood (SL) [Wood, 2010] replaces the exact likelihood of the model  $P_\theta$  with a normal distribution<sup>4</sup> for each value of  $\theta$ , with mean  $\mu_\theta$  and covariance matrix  $\Sigma_\theta$ . In a Bayesian setting, Price et al. [2018] defined therefore the following posterior (Bayesian Synthetic Likelihood, BSL):

$$\pi_{\text{SL}}(\theta|y) \propto \pi(\theta) \mathcal{N}(y; \mu_\theta, \Sigma_\theta),$$

where  $\mathcal{N}(y; \mu_\theta, \Sigma_\theta)$  denotes the multivariate normal density with mean vector  $\mu_\theta$  and variance matrix  $\Sigma_\theta$  evaluated in  $y$ . As mentioned in Sec. 2.1, BSL is a specific case of our SR posterior (Eq. 2) when  $w = 1$  and the non-strictly proper Dawid-Sebastiani (DS) SR is used.

Commonly, samples from the BSL posterior are obtained by running a pseudo-marginal MCMC in which empirical estimates of  $\mu_\theta$  and  $\Sigma_\theta$  are obtained from model simulations; that is analogous to the sampling approach we discussed in Sec. 2.3. However, some variational approximations have also been proposed [Ong et al., 2018a]. Several different estimates of  $\Sigma_\theta$  (or of the Gaussian likelihood altogether) have been tested within BSL [Ledoit and Wolf, 2004, Price et al., 2018, An et al., 2019]; under our formulation, those correspond to alternative ways of estimating the DS Scoring Rule.

<sup>4</sup>In BSL (and in the subsequent semi-parametric version), the data is usually summarized with a statistics function before applying the normal density; this is done as certain statistics are approximately normal (e.g., sums of large number of variables by Central Limit Theorem arguments). Here, we keep the same notation as the rest of our work, remarking that applying a statistics function to the data corresponds to redefining the data space  $\mathcal{X}$  and the data generating process.

Additionally, in investigating the asymptotics of BSL, a different regime from ours (Sec. 2.2.1) has been traditionally considered [Frazier et al., 2021a,c]: an increasing number of observations (not necessarily i.i.d.) are used to estimate one single set of summary statistics, which are then used in the definition of the posterior. In our setup, instead, each observation contributes to the posterior with a new term in a multiplicative fashion (this also holds for the non-i.i.d. setting of Loaiza-Maya et al. [2021]).

**Semi-parametric BSL (semiBSL)** Semi-parametric BSL (semiBSL, An et al. 2020) considers a Gaussian copula modeling the dependency between the different components in  $P_\theta$  and poses no constraints on marginal densities. The semiBSL likelihood is thus:

$$p_{\text{semiBSL}}(y|\theta) = c_{R_\theta}(F_{\theta,1}(y^1), \dots, F_{\theta,d}(y^d)) \prod_{k=1}^d f_{\theta,k}(y^k), \quad (6)$$

where  $f_{\theta,k}$  and  $F_{\theta,k}$  are respectively the marginal density and Cumulative Density Functions (CDFs) for the  $k$ -th component of the model, and where  $c_R(u)$  denotes the Gaussian copula density for  $u \in [0, 1]^d$  and correlation matrix  $R \in [-1, 1]^{d \times d}$ .

As in BSL, An et al. [2020] used a pseudo-marginal MCMC where simulations from  $P_\theta$  are used to obtain an estimate of the correlation matrix of the Gaussian copula  $\hat{R}_\theta$  as well as Kernel Density Estimates (KDE) of the marginals  $\hat{f}_{\theta,k}$  (from which  $\hat{F}_{\theta,k}$  are obtained by integration). More details are given in Appendix C.3. We can connect semiBSL to our framework by rewriting Eq. (6) as:

$$p_{\text{semiBSL}}(y|\theta) = \exp \left\{ - \sum_{k=1}^d S_{\log} \left( P_\theta^k, y^k \right) - S_{Gc}(C_\theta, (F_{\theta,1}(y^1), \dots, F_{\theta,d}(y^d))) \right\},$$

where  $P_\theta^k$  is the distribution associated to the model for the  $k$ -th component,  $C_\theta$  is the copula associated to  $P_\theta$  and  $S_{Gc}(C, u)$  is the copula Scoring Rule associated to the Gaussian copula; we show in Appendix C.3 that this is a proper, but not strictly so, Scoring Rule for copula random variables. Consistent estimators of the marginal and copula SRs can be obtained using  $\hat{R}_\theta$ ,  $\hat{f}_{\theta,k}$  and  $\hat{F}_{\theta,k}$ .

**Remark 7 (Synthetic Likelihood and model misspecification).** *BSL and semiBSL are instances of standard Bayesian inference with a misspecified likelihood. As mentioned before (Sec. 2.4), some works argued for  $w \neq 1$  in the case of misspecified likelihoods [Holmes and Walker, 2017]. Specifically, setting  $w < 1$  attributes more importance to prior information, but still allows information to accumulate through the likelihood, if the decision maker believes that some aspects of the misspecified likelihood are representative of the data generating process. It would be of interest to understand whether setting  $w < 1$  would improve the performance of BSL and semiBSL for misspecified models. We leave this for future exploration.*

**MMD-Bayes** In Chérif-Abdellatif and Alquier [2020], the following posterior, termed MMD-Bayes, is considered:

$$\pi_{\text{MMD}}(\theta|\mathbf{y}_n) \propto \pi(\theta) \exp \left\{ -\beta \cdot D_k \left( P_\theta, \hat{P}_n \right) \right\},$$

where  $\beta > 0$  and  $D_k \left( P_\theta, \hat{P}_n \right)$  denotes the squared MMD (see Appendix C.2) between the empirical measure of the observations  $\hat{P}_n = \frac{1}{n} \sum_{i=1}^n \delta_{y_i}$  and the model distribution  $P_\theta$ .

MMD-Bayes is a specific case of our SR posterior (Eq. 2) when the kernel Scoring Rule  $S_k$  is used (see Appendix C.2.1 for a proof). However, Chérif-Abdellatif and Alquier [2020] adopted a variational approximation to sample from  $\pi_{\text{MMD}}$  in the LFI setting, while we exploit pseudo-marginal MCMC.

**Ratio Estimation** The standard Bayes posterior can be written as  $\pi(\theta|y) = \pi(\theta) \cdot r(y; \theta)$ , with  $r(y; \theta) = \frac{p(y|\theta)}{p(y)}$ . The Ratio Estimation (RE) approach [Thomas et al., 2020] builds an approximate posterior by estimating  $\log r(y; \theta)$  with some function  $\hat{h}^\theta(y)$  and considering  $\pi_{\text{re}}(\theta|y) \propto \pi(\theta) \exp(\hat{h}^\theta(y))$ .

Thomas et al. [2020] run an MCMC where, for each proposed  $\theta$ ,  $m$  samples  $\mathbf{x}_{\mathbf{m}}^{(\theta)}$  are generated from  $P_\theta$ . These, together with a set of  $m$  reference samples  $\mathbf{x}_{\mathbf{m}}^{(r)} = \{x_j^{(r)}\}_{j=1}^m$  from the marginal data distribution<sup>5</sup>, are used to fit a logistic regression yielding  $\hat{h}^\theta(y)$ . Logistic regression is an optimization problem in which the best function of  $\mathcal{X}$  in distinguishing between the two sets of samples is selected.

<sup>5</sup>Which are obtained by drawing  $\theta_j \sim p(\theta)$ ,  $x_j \sim p(\cdot|\theta_j)$ , and discarding  $\theta_j$ .

In general, the number of reference samples and samples from the model can be different, see Appendix C.4; we make this choice here for the sake of simplicity.

If  $m \rightarrow \infty$  and all scalar functions are considered, the optimum  $h_\star^\theta$  is equal to  $\log r(y; \theta)$ . For finite data, however, the corresponding optimum  $\hat{h}_m^\theta$  is only an approximation of the ratio (as discussed in Appendix C.4). RE is therefore a specific case of our SR posterior framework with  $w = 1$  and:

$$\hat{S}_{\text{RE}}(\mathbf{x}_m^{(\theta)}, \mathbf{x}_m^{(r)}, y) = -\hat{h}_m^\theta(y)$$

which, differently from the other SR estimators considered previously, also depends on the reference samples. Due to what we discussed above,  $\hat{S}_{\text{RE}}$  converges in probability to the log-score (up to a constant term in  $\theta$ ) for  $m \rightarrow \infty$ .

The above argument relies on optimizing over all functions in logistic regression; in practice, the optimization is restricted to a set of functions  $\mathcal{H}$  (for instance, a linear combination of predictors). In this case, the infinite data optimum  $h_{\mathcal{H}\star}^\theta(y)$  does not correspond to  $\log r(y; \theta)$  (see Appendix C.4), but to the best possible approximation in  $\mathcal{H}$  in some sense. Therefore, Ratio Estimation with a restricted set of functions  $\mathcal{H}$  cannot be written exactly under our SR posterior framework. However, very flexible function classes (as for instance neural networks) can produce reasonable approximations to the log score for large values of  $m$ .

**Other related approaches** Scoring Rules have been previously used to generalize Bayesian inference in Jewson et al. [2018], Giummolè et al. [2019], Loaiza-Maya et al. [2021]. Specifically, Giummolè et al. [2019] considered an update similar to ours, but fixed  $w = 1$  and adjusted the parameter value (similarly to what was done in Pauli et al., 2011 and Ruli et al., 2016) so that the posterior has the same asymptotic covariance matrix as the frequentist minimum Scoring Rule estimator. Instead, Loaiza-Maya et al. [2021] considered a time-series setting in which the task is to learn about the parameter value which yields the best prediction, given the previous observations. Finally, Jewson et al. [2018] motivated Bayesian inference using general divergences (beyond the KL one which underpins standard Bayesian inference) in an M-open setup, and discussed posteriors which employ estimators of the divergences from observed data; some of these estimators can be written using Scoring Rules. However, none of the above works considered explicitly the LFI setup.

A work released few weeks after the first version of the present manuscript [Matsubara et al., 2021] investigates the generalized posterior obtained by using a Kernel Stein Discrepancy [Chwialkowski et al., 2016, Liu et al., 2016]. This posterior is shown to satisfy robustness and consistency properties, and is computationally convenient for doubly-intractable models (i.e., for which the likelihood is available, but only up to the normalizing constant). In contrast, our work focuses on intractable-likelihood models.

Finally, Dellaporta et al. [2022], published months after the release of the first version of our work, introduced a new LFI method which, similar to ours, enjoys outlier robustness and posterior consistency; however, their method is derived from the Bayesian non-parametric learning framework of Lyddon et al. [2018] rather than the generalized Bayesian posterior of Bissiri et al. [2016].

## 4 Simulation studies

We present here simulation studies to illustrate our approach. Precisely, we first study the concentration of different methods belonging to the SR posterior framework (the Energy and Kernel Scores, BSL and semiBSL) in Sec. 4.1; next, in Sec. 4.2, we consider the effect of outliers in the observed dataset and compare with the SMC ABC posterior of Del Moral et al. [2012], a popular LFI method belonging to a different framework.

Throughout, we consider  $\beta = 1$  in the Energy Score and define the Kernel Score via the Gaussian kernel with bandwidth set from simulations as illustrated in Appendix D. The LFI techniques are run using the ABCpy Python library [Dutta et al., 2021], while the PyMC3 library [Salvatier et al., 2016] is used to sample from the standard Bayes posterior when that is available. Code for reproducing all results is available at this link.

As mentioned in Sec. 2.3, we use pseudo-marginal MCMC to sample from the SR posterior. When the posterior is narrow, however, vanilla pseudo-marginal approaches [Andrieu et al., 2009] can have a “sticky” behavior, due to the variability in estimating the target. To reduce this issue, correlated

pseudo-marginal MCMC has been suggested [Dahlin et al., 2015, Deligiannidis et al., 2018] and explicitly tested for BSL in Picchini et al. [2022]; the idea is to keep track of the random numbers used in simulating the model and reusing them for subsequent proposed parameter values. This correlates the target estimates at subsequent steps and reduces the chances of the chain getting stuck due to atypical random number draws. Specifically, the  $m$  simulations used in the posterior estimate (Eq. 4) are split in  $G$  groups; at each MCMC step, a new set of random numbers is proposed for the simulations in a randomly chosen group (alongside the proposed value for  $\theta$ ), and accepted or rejected in the standard way. Additionally, when  $\Theta$  is bounded, we run the MCMC on a transformed unbounded space.

The algorithm described above is a valid pseudo-marginal MCMC and therefore targets Eq. (5) which, as mentioned before, is not the same as the original SR posterior defined in Eq. (2). However, as shown in Theorem 4, the former converges to the latter as  $m \rightarrow \infty$ . In Appendix G, we report experimental studies showing how, for  $m$  above some threshold (typically few hundreds), the MCMC target is roughly constant. On the contrary, very small values of  $m$  lead to unsatisfactory MCMC performance. Finally, we refer to Appendix F for further simulation studies on two additional models (MA(2) and M/G/1), on which we also empirically evaluate the effect of different values of  $w$ .

#### 4.1 Concentration with the g-and-k model

Here, we study concentration of the posteriors belonging to the SR posterior framework with an increasing number of observations. We will consider both a well-specified and misspecified case; in the former, if a strictly proper SR (such as the Energy or Kernel Score) is used, the unique minimizer  $\theta^*$  is the parameter value from which data are generated; the posterior will therefore concentrate on  $\theta^*$  for large  $n$  (see Theorem 1). Indeed, in our experiments below we observe concentration for the Energy or Kernel Score posteriors but not for BSL and semiBSL. In the misspecified case, it is hard to verify analytically whether a unique  $\theta^*$  exists, for both proper and strictly proper SRs; we proceed therefore by studying the behavior of the posterior with increasing  $n$  and deduce from this whether  $\theta^*$  is unique or not for the different SRs. Additionally, we experience difficulties in sampling for BSL and semiBSL for large  $n$ , while this is not the case for the Energy and Kernel Score posteriors.

We consider the univariate g-and-k model and its multivariate extension; the univariate g-and-k distribution [Prangle, 2017] is defined in terms of the inverse of its cumulative distribution function  $F^{-1}$ . Given a quantile  $q$ , we define:

$$F^{-1}(q) = A + B \left[ q + 0.8 \frac{1 - e^{-gz(q)}}{1 + e^{-gz(q)}} \right] (1 + z(q)^2)^k z(q),$$

where the parameters  $A, B, g, k$  are broadly associated to the location, scale, skewness and kurtosis of the distribution, and  $z(q)$  denotes the  $q$ -th quantile of the standard normal distribution  $\mathcal{N}(0, 1)$ . Likelihood evaluation for this model is costly as it requires numerical inversion of  $F^{-1}$ ; instead, sampling is immediate by drawing  $z \sim \mathcal{N}(0, 1)$  and inputting it in place of  $z(q)$  in the expression above. A multivariate extension was first considered in the LFI literature in Drovandi and Pettitt [2011]; here we follow the setup of Jiang [2018]. Specifically, we consider drawing a multivariate normal  $(Z^1, \dots, Z^5) \sim \mathcal{N}(0, \Sigma)$ , where  $\Sigma \in \mathbb{R}^{5 \times 5}$  has a sparse correlation structure:  $\Sigma_{kk} = 1$ ,  $\Sigma_{kl} = \rho$  for  $|k - l| = 1$  and 0 otherwise; each component of  $Z$  is then transformed as in the univariate case. The sets of parameters are therefore  $\theta = (A, B, g, k)$  for the univariate case and  $\theta = (A, B, g, k, \rho)$  for the multivariate one. We use uniform priors on  $[0, 4]^4$  for the univariate case and  $[0, 4]^4 \times [-\sqrt{3}/3, \sqrt{3}/3]$  for the multivariate case.

In both setups, we perform inference with our SR methods, BSL and semiBSL (excluding semiBSL for the univariate g-and-k, as that is defined for multivariate distributions only) setting the number of simulations per parameter value to  $m = 500$ ,  $G = 500$  and run MCMC for 110000 steps, of which 10000 are burned in. We repeat this with 1, 5, 10, 15, 20 up to 100 observations spaced by 5.

##### 4.1.1 Well-specified case

For both univariate and multivariate case, we consider synthetic observations generated from parameter values  $A^* = 3$ ,  $B^* = 1.5$ ,  $g^* = 0.5$ ,  $k^* = 1.5$  and  $\rho^* = -0.3$  (notice  $\rho$  is not used in the univariate

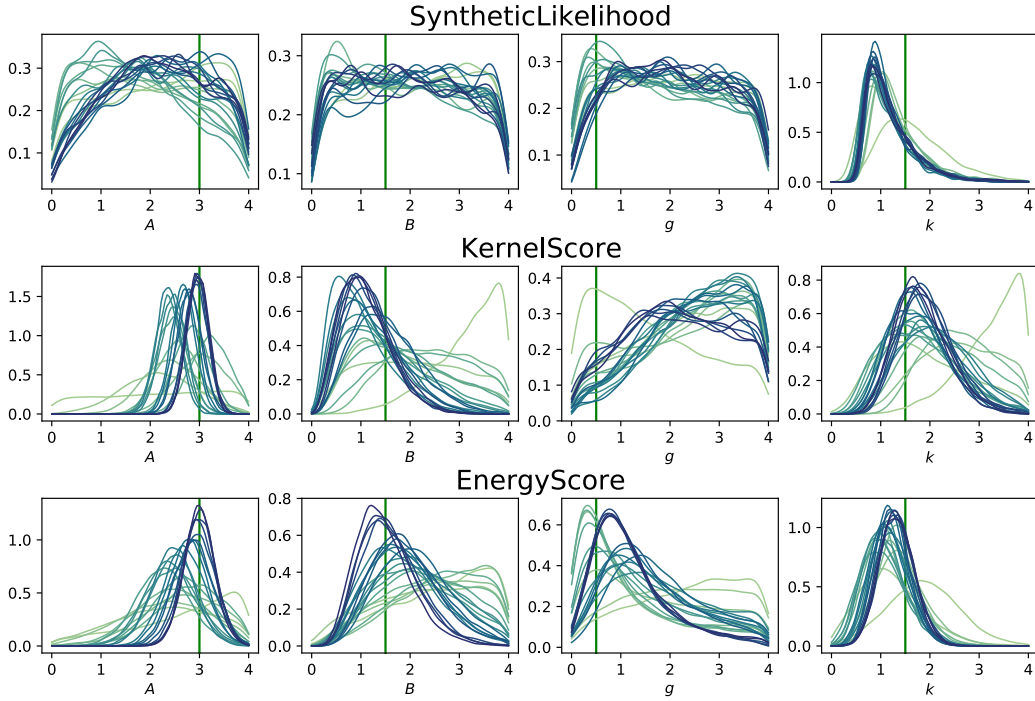


Figure 1: Marginal posterior distributions for the different parameters for the well-specified univariate g-and-k model, with increasing number of observations ( $n = 1, 5, 10, 15, \dots, 100$ ). Darker (respectively lighter) colors denote a larger (smaller) number of observations. The densities are obtained by KDE on the MCMC output thinned by a factor 10. The Energy and Kernel Score posteriors concentrate around the true parameter value (green vertical line), while BSL does not.

case). For the SR posteriors, we fix  $w$  by employing our suggested heuristics with one single observation (Sec. 2.4), using as a reference BSL. The used values of  $w$  are reported in Appendix E.1.1, together with the proposal sizes for MCMC and the resulting acceptance rates.

For the univariate g-and-k, Fig. 1 reports the marginal posterior distributions for each parameter at different number of observations for the considered methods. With increasing  $n$ , the BSL posterior does not concentrate (except for the parameter  $k$ ); the Energy Score posterior concentrates close to the true value for all parameters (green vertical line), while the Kernel Score posterior performs slightly worse, not being able to concentrate for the parameter  $g$  (albeit this may happen with an even larger  $n$ , which we did not consider here). The poor performance of BSL is due to violation of the underlying normality assumption (which is to say, the scoring rule used by BSL is not strictly proper for this example), while the concentration of the Energy and Kernel Score posteriors are in line with them being strictly proper SRs.

Similar results for the multivariate g-and-k are reported in Fig. 2. For this example, the MCMCs targeting the semiBSL and BSL posteriors do not converge beyond respectively 1 and 10 observations; those results are therefore deferred to Fig. 8 in Appendix. Instead, with the Kernel and Energy Scores we do not experience such a problem. The Energy Score concentrates well on the exact parameter value in this case too, while the Kernel Score is able to concentrate well for some parameters ( $g$  and  $k$ ) and some concentration can be observed for  $\rho$ ; however, the Kernel Score posterior marginals for  $A$  and  $B$  are flatter and noisier (it may be that larger  $n$  leads to more concentrate posterior for  $A$  and  $B$  as well, but we did not research this further).

We investigate now the poor performance of semiBSL and BSL, by fixing  $n = 20$  and running MCMC with 10 different initializations. The chains look “sticky” and, after a short transient, get stuck in different regions of  $\Theta$  (see Fig. 9 in Appendix). This behavior can be explained by large variance in the estimates of the pseudo-marginal MCMC target. We repeat therefore the same experiments increasing the number of simulations  $m$ , as that decreases the variance of the target estimates (more details in Appendix E.1.2); larger values of  $m$  slightly increase the acceptance rate for BSL but do not almost change that for semiBSL. Additionally, while the BSL assumptions are unreasonable for this

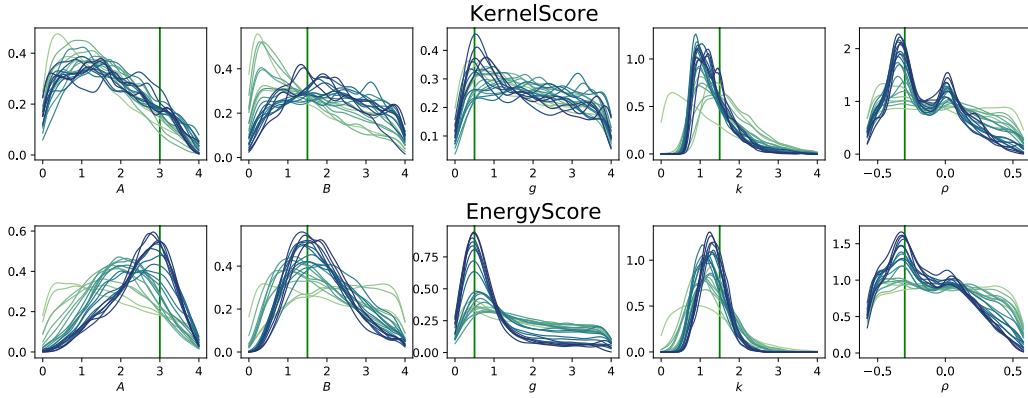


Figure 2: Marginal posterior distributions for the different parameters for the well-specified multivariate g-and-k model, with increasing number of observations ( $n = 1, 5, 10, 15, \dots, 100$ ). Darker (respectively lighter) colors denote a larger (smaller) number of observations. The densities are obtained by KDE on the MCMC output thinned by a factor 10. The Energy Score posterior concentrates well around the true parameter value (green vertical line), with the Kernel Score one performing slightly worse.

model, the multivariate g-and-k fulfills the assumptions underlying semiBSL: in fact, applying a one-to-one transformation to each component of a random vector does not change the copula structure, which is Gaussian in this case. It is therefore surprising that the performance of semiBSL degrades so rapidly when  $n$  increases.

#### 4.1.2 Misspecified setup

Here, we consider as data generating process the Cauchy distribution, which has fatter tails than the g-and-k one. For the univariate case, the univariate Cauchy is used; for the multivariate case, the five components of each observation are drawn independently from the univariate Cauchy distribution (i.e., no correlation between components). For the SR posteriors, we use the values of  $w$  which were obtained with our heuristics in the well-specified case; additional experimental details are reported in Appendix E.1.3.

For the univariate g-and-k, we report the marginal posteriors in Fig. 3. The Energy and Kernel Score posteriors concentrate on a similar parameter value; the BSL posterior concentrates as well (differently from the well-specified case), albeit on a slightly different parameter value (specially for  $B$  and  $k$ ). Therefore, with this kind of misspecification,  $\theta^*$  is unique both when using the strictly proper Kernel and Energy Scores, as well as the non-strictly proper Dawid-Sebastiani Score (corresponding to BSL).

To assess out-of-sample performance of the inferred posterior, we implement the following posterior predictive check: given draws from a posterior  $\pi(\theta|\mathbf{y}_n)$ , we generate simulations from the model for the corresponding parameter value, which are therefore samples from the posterior predictive:

$$p(y_{\text{new}}|\mathbf{y}_n) = \int p(y_{\text{new}}|\theta)\pi(\theta|\mathbf{y}_n)d\theta.$$

From these samples, we estimate the Energy and Kernel Score between the posterior predictive distribution and the observations  $\mathbf{y}_n$ , which assess how well the posterior predictive matches the original observation. Results for  $n = 100$  observations are reported in Table 1: not surprisingly, the posterior predictive obtained for the Kernel Score posterior minimizes the Kernel Score, and similarly for the Energy Score. Indeed, the SR posterior concentrates on the parameter value which achieves the lowest expected SR.

For the multivariate g-and-k, we experienced the same issue with MCMC as in the well-specified case for BSL and semiBSL; therefore, we do not report those results. Marginals for the Energy and Kernel Score posteriors can be seen in Fig. 4; both posteriors concentrate for all parameters except for  $\rho$  (which describes correlation among different components in the observations, here absent). For the

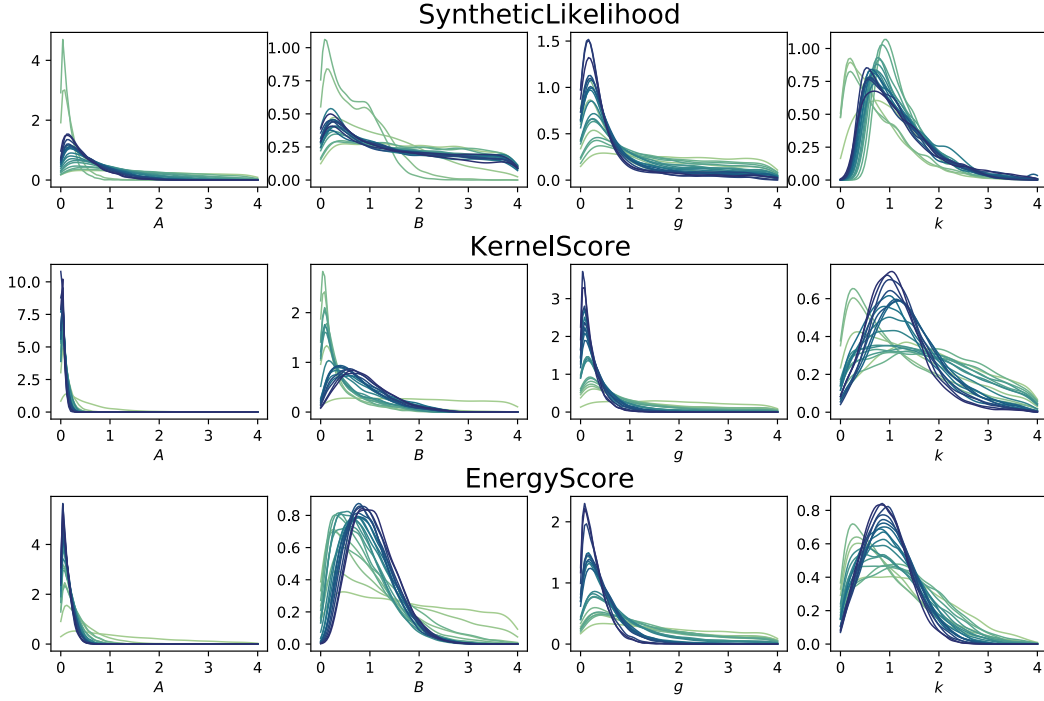


Figure 3: Marginal posterior distributions for the different parameters for the univariate g-and-k model, with increasing number of observations ( $n = 1, 5, 10, 15, \dots, 100$ ) generated from the Cauchy distribution. Darker (respectively lighter) colors denote a larger (smaller) number of observations. The densities are obtained by KDE on the MCMC output thinned by a factor 10. The Energy and Kernel Score posteriors concentrate around the same parameter value, while BSL concentrates on slightly different one (specially for  $B$  and  $k$ ).

other parameters, the two methods concentrate on very similar parameter values, with slightly larger difference for  $k$ , for which the Kernel Score posterior does not concentrate very well.

As before, we report the posterior predictive check results for  $n = 100$  observations in Table 1; here, the Energy Score posterior yields better posterior predictive according to both the Energy and Kernel Score. However, notice that the Kernel Score values for the two methods are very close.

	Misspecified univariate g-and-k			Misspecified multivariate g-and-k	
	BSL	Kernel Score	Energy Score	Kernel Score	Energy Score
Energy Score	49046.1828	41540.6385	<b>36912.0548</b>	243599.3863	<b>227662.0929</b>
Kernel Score	-7296.1355	<b>-8088.4518</b>	-8052.7533	-8856.8503	<b>-8867.2898</b>

Table 1: Posterior predictive check for misspecified univariate and multivariate g-and-k, for  $n = 100$ . Each column refers to a different posterior (column headline), while rows report the estimated Energy or Kernel Score between posterior predictive and the observations. Lower values are better, and bold denotes smallest values.

## 4.2 Robustness to outliers

We now study the performance of the Kernel and Energy Score posteriors in presence of outliers. From our result in Theorem 3, we expect the Kernel Score to be outlier robust, which is empirically verified; however, even the Energy Score posterior shows some robustness. In practice, we consider a normal model and two challenging time-series models from meteorology and ecology. For the first, we compare with the standard Bayes posterior while, for the others, with the SMC ABC one of Del Moral et al. [2012].



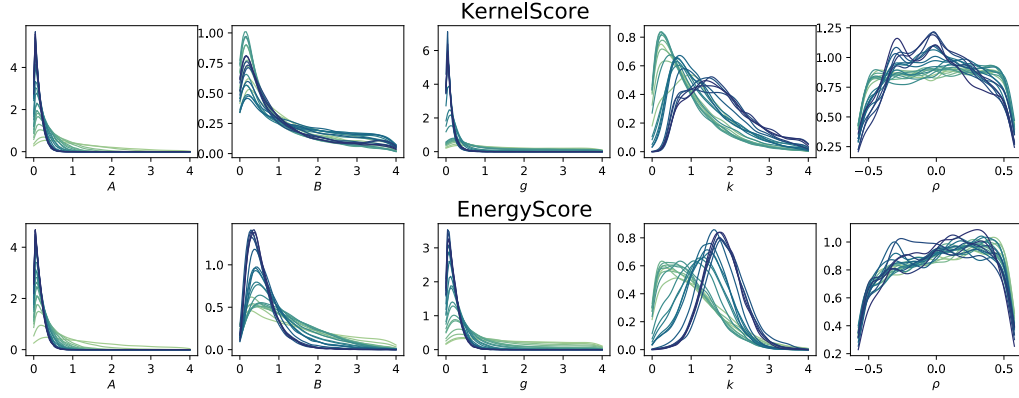


Figure 4: Marginal posterior distributions for the different parameters for the multivariate g-and-k model, with increasing number of observations ( $n = 1, 5, 10, 15, \dots, 100$ ) generated from the Cauchy distribution. Darker (respectively lighter) colors denote a larger (smaller) number of observations. The densities are obtained by KDE on the MCMC output thinned by a factor 10. Both Energy and Kernel Score posteriors concentrate on a very similar parameter value, with slightly larger difference for  $k$ .

#### 4.2.1 Simple normal location model

First, we consider a univariate normal model with fixed standard deviation  $P_\theta = \mathcal{N}(\theta, 1)$ . As was done in Matsubara et al. [2021], we consider 100 observations, a proportion  $1 - \epsilon$  of which is generated by  $P_\theta$  with  $\theta = 1$ , while the remaining proportion  $\epsilon$  is generated by  $\mathcal{N}(z, 1)$  for some value of  $z$ . Therefore,  $\epsilon$  and  $z$  control respectively the number and location of outliers. The prior distribution on  $\theta$  is set to  $\mathcal{N}(0, 1)$ . To perform inference with our proposed SR posterior, we use  $m = 500$ ,  $G = 50$  and 60000 MCMC steps, of which 40000 are burned-in. Additionally, we perform standard Bayesian inference (as the likelihood is available here). For the SR posteriors,  $w$  is fixed in order to get approximately the same posterior variance as standard Bayes in the well-specified case ( $\epsilon = 0$ ); values are reported in Appendix E.2, together with the proposal sizes for MCMC and the resulting acceptance rates.

We consider  $\epsilon$  taking values in  $(0, 0.1, 0.2)$  and  $z$  in  $(1, 3, 5, 7, 10, 20)$ ; in Fig. 5, some results are shown. Results for all combinations of  $z$  and  $\epsilon$  are available in Fig. 11 in Appendix. The Kernel Score posterior is highly robust with respect to outliers, while the Energy Score posterior performs slightly worse. As expected, the standard Bayes posterior shifts significantly when either  $\epsilon$  or  $z$  are increased. We highlight that Theorem 3 only ensures robustness for small values of  $\epsilon$  and all values of  $z$  for the Kernel Score posterior, which is in fact experimentally verified (the robustness result for the Energy Score posterior does not apply here as  $\mathcal{X}$  is unbounded); however, we find empirically that both SR posteriors are more robust than the standard Bayes one. when both  $z$  and  $\epsilon$  are increased.

Finally, this example satisfies the BSL assumptions, which should therefore recover the standard Bayes posterior. However, our simulation results with BSL were unsatisfactory; specifically, BSL is able to reproduce the standard Bayes posterior when no outliers are present or when  $z$  is close to 1; in all other cases, MCMC does not converge and presents a sticky behavior, similar to what was already mentioned in Sec. 4.1. Further details on this are given in Appendix E.2.

#### 4.2.2 Real-life time-series examples

We consider now two time-series examples. In both cases, simulation outputs are high dimensional; we therefore reduce the dimensionality via a set of summary statistics. For both models, we consider 10 observations generated from parameter values  $\theta^*$  and replace either 0, 1 or 2 of them with outliers generated from  $\theta^{\text{out}}$ , corresponding to outlier proportions  $\epsilon = 0, 0.1$  and  $0.2$ .

Here, we focus on the Kernel Score posterior, as that was shown to be more robust to outliers theoretically (Theorem 3) and empirically on the normal location example. Results for the Energy SR posterior are reported in Appendices E.3 and E.4. We compare with the posterior obtained via the SMC ABC of Del Moral et al. [2012], which we run for 100 steps, 1000 posterior particles and



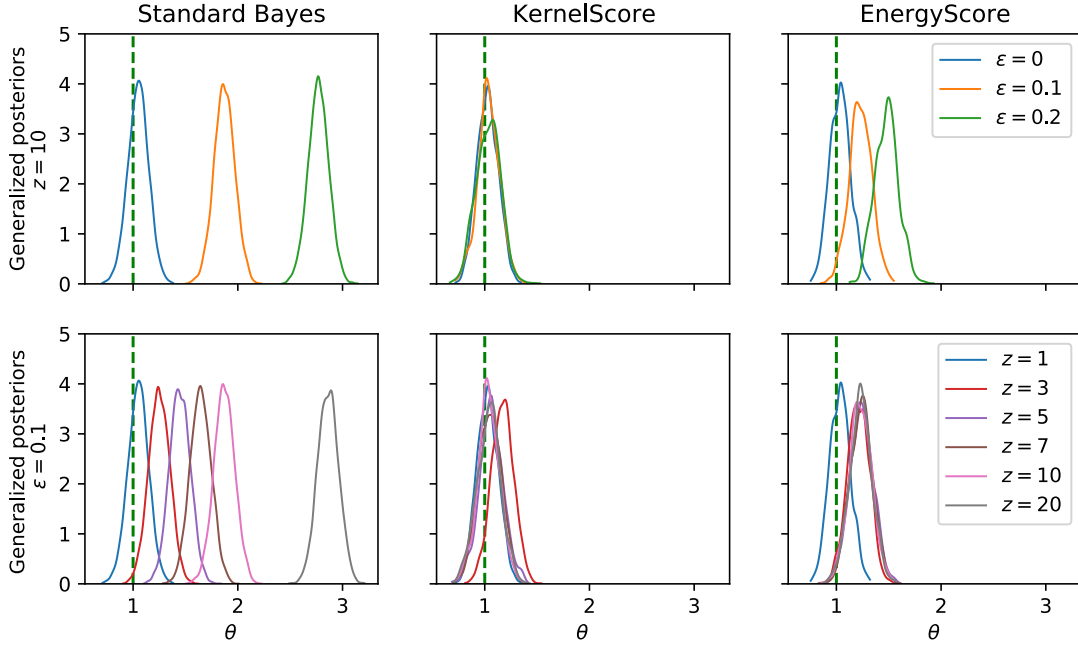


Figure 5: Posterior distribution for the misspecified normal location model, following experimental setup introduced in Matsubara et al. [2021]. First row: fixed outliers location  $z = 10$  and varying proportion  $\epsilon$ ; second row: fixed outlier proportion  $\epsilon$ , varying location  $z$ . From both rows, it can be seen that both Kernel and Energy score are more robust with respect to Standard Bayes. The densities are obtained by KDE on the MCMC output thinned by a factor 10.

10 simulations per parameter value. We attempted running BSL and semiBSL but the correlated pseudo-marginal MCMC was unable to run satisfactorily, similar to what reported before.

For both models, the SMC ABC posterior is broad; for the first model below, that is also the case for the Kernel Score one. In these cases, the outliers do not seem to strongly impact the posteriors, which already cover large part of the parameter space. Therefore, we assess performance via two different posterior predictive checks: the first is that introduced for the misspecified g-and-k (Sec. 4.1), which we apply on the summary statistics values. For the second check, we compute the Energy and Kernel score between posterior predictive samples and observations at each time-step of the raw time-series. We then compare the values obtained via the Kernel Score posterior and the SMC ABC one; at a given time-step, lower values for the former imply that our method better represents the data distribution at that time-step. To measure outlier robustness, both checks are carried out with respect to the observations generated from  $\theta^*$  only. Results are in Figures 6 and 7 and are discussed separately for the two models below.

**Lorenz96 model** The Lorenz96 model [Lorenz, 1996] is a chaotic system used as a toy model of atmospheric behavior and includes interacting slow and fast scale variables; it is an important benchmark for meteorological techniques [Arnold et al., 2013] and was previously studied in the LFI literature [Thomas et al., 2020, Jarvenpaa et al., 2020, Pacchiardi and Dutta, 2022]. We use here a version of the Lorenz96 model introduced by Wilks [2005], in which the effect of the fast variables on the slow ones is replaced by a stochastic effective term which depends on a set of parameters. Specifically, the model is defined by the following set of Ordinary Differential Equations (ODEs):

$$\frac{dy_k}{dt} = -y_{k-1}(y_{k-2} - y_{k+1}) - y_k + 10 - g(y_k, t; \theta); \quad k = 1, \dots, K,$$

where cyclic boundary conditions imply that we take  $K + 1 = 1$  in the indices. The effective term  $g$  depends on parameters  $\theta = (b_0, b_1, \sigma_e, \phi)$ , and is defined upon discretizing the ODEs with a time-step  $\Delta t$ :

$$g(y, t; \theta) = b_0 + b_1 y + \phi \cdot r(t - \Delta t) + \sigma_e(1 - \phi^2)^{1/2} \eta(t), \quad \eta(t) \sim \mathcal{N}(0, 1).$$

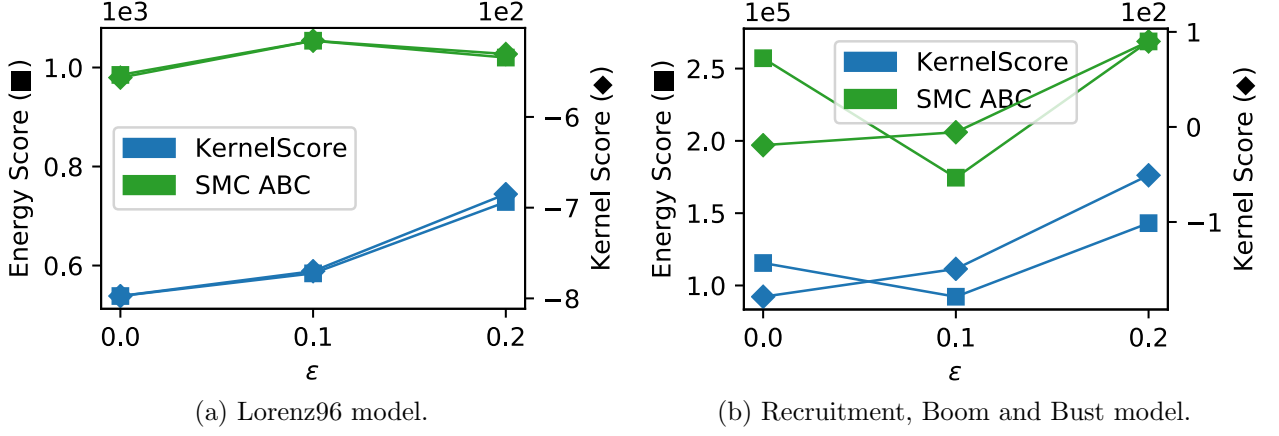


Figure 6: Posterior predictive check: estimated scores on the statistics between posterior predictive and observations from  $\theta^*$ . In each panel, different colors denote posteriors obtained with different methods. Squares (respectively diamonds) denote estimated Energy (Kernel) Score, whose scale is reported in left (right) vertical axis. Lower is better.

In practice, we took  $K = 8$ ,  $\Delta t = 1/30$  and integrated the model using a 4th order Runge-Kutta integrator on the interval  $t \in [0, 1.5]$ , starting from initial condition  $y(0)$  independent on parameter values. The integration output is an 8-dimensional time-series with 45 time-steps; to reduce data dimensionality, we compute the statistics introduced in Hakkaraian et al. [2012]: the temporal mean and variance of  $y_k(t)$ , the auto-covariance of  $y_k(t)$  with time lag 1, and the covariance of  $y_k(t)$  with its two neighbors  $y_{k-1}(t)$  and  $y_{k+1}(t)$ . All above quantities are then averaged over the index  $k$ , leading to a 6-dimensional set of statistics.

We take  $\theta^* = (2, 0.8, 1.7, 0.4)$  and  $\theta^{\text{out}} = (1.41, 0.1, 2.4, 0.95)$ . In Fig. 14 in Appendix, we compare graphically simulations from  $\theta^*$  and  $\theta^{\text{out}}$ . As prior distribution, we consider a uniform on the region  $[1.4, 2.2] \times [0, 1] \times [1.5, 2.5] \times [0, 1]$ . We then set  $w$  for the Kernel Score posterior with our heuristics (Sec. 2.4), using a single observation generated from  $\theta^*$ . Next, we run inference for the Kernel Score posteriors with  $m = 200$ ,  $G = 10$  and 25000 MCMC steps, of which 5000 are burned-in; we also run the SMC ABC algorithm of Del Moral et al. [2012].

In Fig. 6a, we report the posterior predictive check results on the statistics values; Fig. 7a shows instead the difference between SR values at each time-step of the raw time-series between the SMC ABC and Kernel Score posterior. These results show how the posterior predictive distribution obtained with the Kernel Score better match the observations from  $\theta^*$ , for all outlier proportions  $\epsilon$ . More details, results with the Energy Score and posterior plots can be found in Appendix E.3.

**Recruitment, boom and bust model** The recruitment, boom and bust model was studied in Fasiolo et al. [2018] and An et al. [2020]; it is a discrete stochastic temporal model representing the population size of some group over time. At each time-step  $t$ , the population size  $N_t$  induces the distribution for  $N_{t+1}$  via the following distribution:

$$N_{t+1} \sim \begin{cases} \text{Poisson}(N_t(1+r)) + \epsilon_t, & \text{if } N_t \leq \kappa \\ \text{Binom}(N_t, \alpha) + \epsilon_t, & \text{if } N_t > \kappa \end{cases}$$

where  $\epsilon_t \sim \text{Poisson}(\beta)$  is a stochastic term and  $\theta = (r, \kappa, \alpha, \beta)$  are a set of parameters. We simulate the model for 300 steps, discarding the first 50 as burn-in (resulting thus in 250 steps). We reduce data dimensionality with the following summary statistics (following An et al., 2020): first, denoting as  $\mathbf{N} = (N_1, N_2, \dots, N_{250})$  the full sequence, we construct the differences  $\mathbf{d} = \{N_t - N_{t-1}, i = 2, \dots, 250\}$  and ratios  $\mathbf{r} = \{N_t/N_{t-1}, i = 2, \dots, 250\}$ ; then, we consider mean, variance, skewness and kurtosis of  $\mathbf{N}$ ,  $\mathbf{d}$  and  $\mathbf{r}$  as our summary statistics, resulting in 12 statistics.

We take  $\theta^* = (0.4, 50.0, 0.09, 0.05)$  and  $\theta^{\text{out}} = (0.9, 70.0, 0.80, 0.05)$ . We consider a uniform prior on the region  $[0, 1] \times [10, 80] \times [0, 1] \times [0, 1]$ . For this model, setting  $w$  with our heuristics (Sec. 2.4) using a single observation generated from  $\theta^*$  yielded a large value (see Appendix E.4) with which

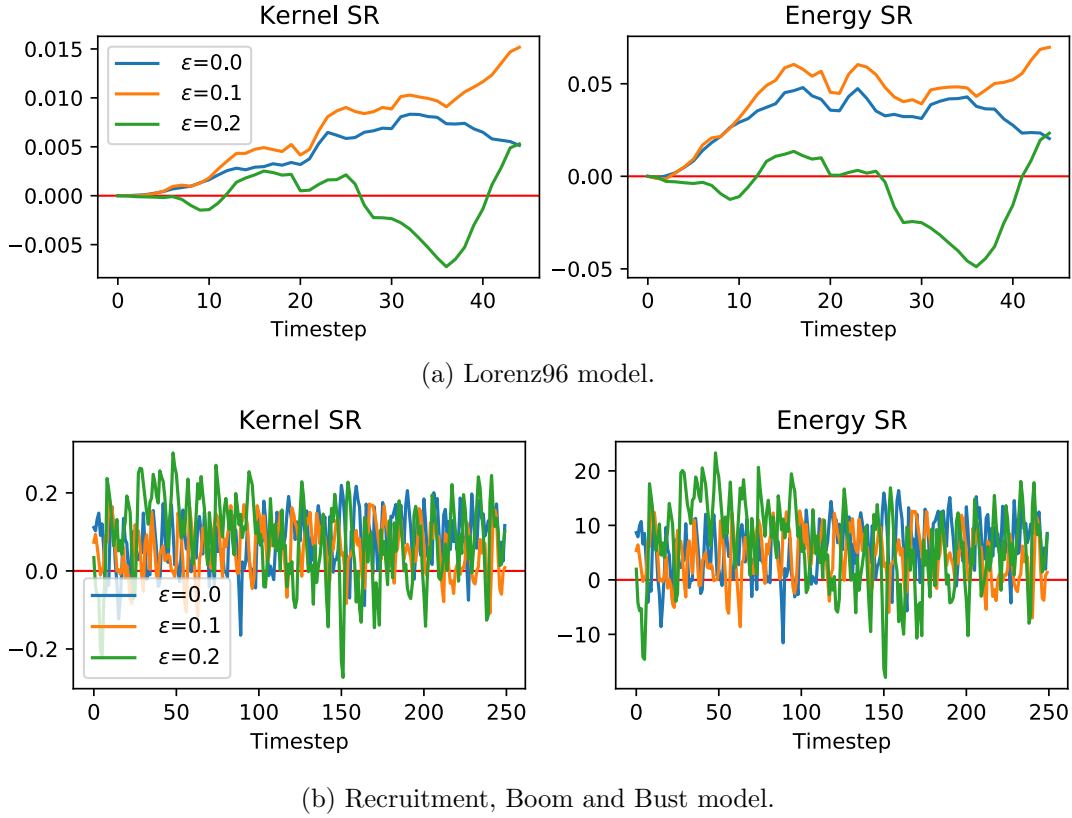


Figure 7: Posterior predictive check: difference of SR at each time-step (with respect to observations from  $\theta^*$ ) between posterior predictive obtained from the SMC ABC posterior and the Kernel Score one. Left (respectively right) panels report Kernel (resp. Energy) SR values. Positive values indicate the Kernel Score posterior better represents the distribution at that time-step than the SMC ABC one, which happens for most time-steps and  $\epsilon$  for both models. Red horizontal line denotes 0.

sampling was impractical due to extreme concentration of the posterior. We therefore hand-picked  $w = 20$  for the Kernel Score posterior and run inference with  $m = 200$ ,  $G = 10$  and 55000 MCMC steps, of which 5000 are burned-in. Again, we also consider the SMC ABC posterior.

In Fig. 6b, we report the posterior predictive check results on the statistics values; Fig. 7b shows instead the difference between SR values at each time-step of the raw time-series between the SMC ABC and Kernel Score posterior. Again, the Kernel Score posterior yields a predictive distribution better matching the observations from  $\theta^*$  for all outlier proportions  $\epsilon$ . More details can be found in Appendix E.4, where we report posterior plots and results with the Energy Score posterior.

## 5 Conclusion

We introduced a way to perform Likelihood-Free Inference based on Generalized Bayesian Inference using Scoring Rules (SR), which includes popular LFI approaches [Price et al., 2018, Thomas et al., 2020, Chérif-Abdellatif and Alquier, 2020] as special cases. The SR posterior is computationally convenient for intractable-likelihood models when the chosen SR can be easily estimated from samples. For some SRs, it asymptotically recovers the exact parameter value in a well-specified setting.

The SR posterior does *not* aim to approximate the standard Bayes posterior, as most LFI methods do: it is instead a generalized posterior, therefore learning about the parameter value minimizing the expected SR; importantly, outlier robustness is achieved as a consequence of this relaxation. We hope new research directions are inspired by this novel connection between the Generalized Bayesian and LFI frameworks; here, we suggest the following extensions:

- many more Scoring Rules exist [Gneiting and Raftery, 2007, Dawid and Musio, 2014, Ziel and Berk, 2019], some of which may be successfully applied for LFI.

- Other heuristics to tune  $w$  beyond our proposal in Sec. 2.4 could be designed, which would ideally be motivated by the goal of inference or any downstream task. All strategies however need to work with the constraints posed by intractable-likelihood models (discussed in Sec. 2.4).
- Even with the correlated strategy, the pseudo-marginal MCMC used in our simulations had a low acceptance rate in some cases (Sec. 4.1). The SR posterior could be alternatively sampled using random weight particle filters [Del Moral et al., 2007, Fearnhead et al., 2008]. Alternatively, variational inference methods could be exploited, similarly to what was done in Ong et al. [2018b], Chérif-Abdellatif and Alquier [2020] and Frazier et al. [2021b] for related methods.
- Generalized Bayesian approaches are often motivated with robustness arguments with respect to model misspecification, as the standard Bayes posterior may perform poorly in this setup [Bissiri et al., 2016, Jewson et al., 2018, Knoblauch et al., 2019]. Most LFI techniques are approximations of the true posterior, and as such are unsuited to a misspecified setup (albeit an emerging literature investigating the effect of misspecification in LFI exists, see Ridgway [2017], Frazier et al. [2017], Frazier [2020], Frazier et al. [2020], Fujisawa et al. [2021]). Although we provided an outlier robustness result, it would be of interest to better study the behavior of the SR posterior with more general forms of model misspecification.

## Acknowledgment

LP is supported by the EPSRC and MRC through the OxWaSP CDT programme (EP/L016710/1), which also funds the computational resources used to perform this work. RD is funded by EPSRC (grant nos. EP/V025899/1, EP/T017112/1) and NERC (grant no. NE/T00973X/1).

We thank Jeremias Knoblauch, François-Xavier Briol, Takuo Matsubara, Geoff Nicholls and Sebastian Schmon for valuable feedback and suggestions on earlier versions of this work. We also thank Alex Shestopaloff for providing code for exact MCMC for the M/G/1 model.

## References

- Z. An, L. F. South, D. J. Nott, and C. C. Drovandi. Accelerating Bayesian synthetic likelihood with the graphical lasso. *Journal of Computational and Graphical Statistics*, 28(2):471–475, 2019.
- Z. An, D. J. Nott, and C. Drovandi. Robust Bayesian synthetic likelihood via a semi-parametric approach. *Statistics and Computing*, 30(3):543–557, 2020.
- C. Andrieu, G. O. Roberts, et al. The pseudo-marginal approach for efficient Monte Carlo computations. *The Annals of Statistics*, 37(2):697–725, 2009.
- H. Arnold, I. Moroz, and T. Palmer. Stochastic parametrizations and model uncertainty in the Lorenz’96 system. *Philosophical Transactions of the Royal Society A: Mathematical, Physical and Engineering Sciences*, 371(1991):20110479, 2013.
- E. Bernton, P. E. Jacob, M. Gerber, and C. P. Robert. Approximate Bayesian computation with the Wasserstein distance. *Journal of the Royal Statistical Society: Series B (Statistical Methodology)*, 81(2):235–269, 2019. doi: <https://doi.org/10.1111/rssb.12312>. URL <https://rss.onlinelibrary.wiley.com/doi/abs/10.1111/rssb.12312>.
- A. Bhattacharya, D. Pati, and Y. Yang. Bayesian fractional posteriors. *The Annals of Statistics*, 47(1):39–66, 2019.
- P. Billingsley. *Convergence of probability measures*. John Wiley & Sons, 2nd edition, 1999.
- P. G. Bissiri, C. C. Holmes, and S. G. Walker. A general framework for updating belief distributions. *Journal of the Royal Statistical Society. Series B, Statistical methodology*, 78(5):1103, 2016.
- K. Boudt, J. Cornelissen, and C. Croux. The Gaussian rank correlation estimator: robustness properties. *Statistics and Computing*, 22(2):471–483, 2012.
- F.-X. Briol, A. Barp, A. B. Duncan, and M. Girolami. Statistical inference for generative models with maximum mean discrepancy. *arXiv preprint arXiv:1906.05944*, 2019.
- B.-E. Chérif-Abdellatif and P. Alquier. MMD-Bayes: Robust Bayesian estimation via maximum mean discrepancy. In *Symposium on Advances in Approximate Bayesian Inference*, pages 1–21. PMLR, 2020.

- K. Chwialkowski, H. Strathmann, and A. Gretton. A kernel test of goodness of fit. In *International conference on machine learning*, pages 2606–2615. PMLR, 2016.
- J. Dahlin, F. Lindsten, J. Kronander, and T. B. Schön. Accelerating pseudo-marginal Metropolis-Hastings by correlating auxiliary variables. *arXiv preprint arXiv:1511.05483*, 2015.
- A. P. Dawid and M. Musio. Theory and applications of proper scoring rules. *Metron*, 72(2):169–183, 2014.
- P. Del Moral, A. Doucet, and A. Jasra. Sequential Monte Carlo for Bayesian computation. *Bayesian statistics*, 8(1):34, 2007.
- P. Del Moral, A. Doucet, and A. Jasra. An adaptive sequential Monte Carlo method for approximate Bayesian computation. *Statistics and Computing*, 22(5):1009–1020, 2012.
- G. Deligiannidis, A. Doucet, and M. K. Pitt. The correlated pseudomarginal method. *Journal of the Royal Statistical Society: Series B (Statistical Methodology)*, 80(5):839–870, 2018.
- C. Dellaporta, J. Knoblauch, T. Damoulas, and F.-X. Briol. Robust bayesian inference for simulator-based models via the MMD posterior bootstrap. *arXiv preprint arXiv:2202.04744*, 2022.
- C. C. Drovandi and A. N. Pettitt. Likelihood-free Bayesian estimation of multivariate quantile distributions. *Computational Statistics & Data Analysis*, 55(9):2541–2556, 2011.
- C. C. Drovandi, A. N. Pettitt, and A. Lee. Bayesian indirect inference using a parametric auxiliary model. *Statistical Science*, 30(1):72–95, 2015.
- R. Dutta, M. Schoengens, L. Pacchiardi, A. Ummadisingu, N. Widmer, P. Künzli, J.-P. Onnela, and A. Mira. ABCpy: A high-performance computing perspective to approximate bayesian computation. *Journal of Statistical Software*, 100(7):1–38, 2021. doi: 10.18637/jss.v100.i07. URL <https://www.jstatsoft.org/index.php/jss/article/view/v100i07>.
- M. Fasiolo, S. N. Wood, F. Hartig, and M. V. Bravington. An extended empirical saddlepoint approximation for intractable likelihoods. *Electronic Journal of Statistics*, 12(1):1544–1578, 2018.
- P. Fearnhead, O. Papaspiliopoulos, and G. O. Roberts. Particle filters for partially observed diffusions. *Journal of the Royal Statistical Society: Series B (Statistical Methodology)*, 70(4):755–777, 2008.
- D. T. Frazier. Robust and efficient approximate Bayesian computation: A minimum distance approach. *arXiv preprint arXiv:2006.14126*, 2020.
- D. T. Frazier, C. P. Robert, and J. Rousseau. Model misspecification in ABC: consequences and diagnostics. *arXiv preprint arXiv:1708.01974*, 2017.
- D. T. Frazier, C. Drovandi, and R. Loaiza-Maya. Robust approximate Bayesian computation: An adjustment approach. *arXiv preprint arXiv:2008.04099*, 2020.
- D. T. Frazier, C. Drovandi, and D. J. Nott. Synthetic likelihood in misspecified models: Consequences and corrections. *arXiv preprint arXiv:2104.03436*, 2021a.
- D. T. Frazier, R. Loaiza-Maya, G. M. Martin, and B. Koo. Loss-based variational Bayes prediction. *arXiv preprint arXiv:2104.14054*, 2021b.
- D. T. Frazier, D. J. Nott, C. Drovandi, and R. Kohn. Bayesian inference using synthetic likelihood: asymptotics and adjustments. *arXiv preprint arXiv:1902.04827*, 2021c.
- M. Fujisawa, T. Teshima, I. Sato, and M. Sugiyama.  $\gamma$ -ABC: Outlier-robust approximate Bayesian computation based on a robust divergence estimator. In *International Conference on Artificial Intelligence and Statistics*, pages 1783–1791. PMLR, 2021.
- A. Ghosh and A. Basu. Robust Bayes estimation using the density power divergence. *Annals of the Institute of Statistical Mathematics*, 68(2):413–437, 2016.
- J. K. Ghosh and R. Ramamoorthi. *Bayesian nonparametrics*. Springer Science & Business Media, 2003.
- F. Giummolè, V. Mameli, E. Ruli, and L. Ventura. Objective Bayesian inference with proper scoring rules. *Test*, 28(3):728–755, 2019.
- T. Gneiting and A. E. Raftery. Strictly proper scoring rules, prediction, and estimation. *Journal of the American statistical Association*, 102(477):359–378, 2007.
- A. Gretton, K. M. Borgwardt, M. J. Rasch, B. Schölkopf, and A. Smola. A kernel two-sample test. *The Journal of Machine Learning Research*, 13(1):723–773, 2012.

- P. Grünwald and T. Van Ommen. Inconsistency of Bayesian inference for misspecified linear models, and a proposal for repairing it. *Bayesian Analysis*, 12(4):1069–1103, 2017.
- J. Hakkarainen, A. Ilin, A. Solonen, M. Laine, H. Haario, J. Tamminen, E. Oja, and H. Järvinen. On closure parameter estimation in chaotic systems. *Nonlinear processes in Geophysics*, 19(1):127–143, 2012.
- C. Holmes and S. Walker. Assigning a value to a power likelihood in a general Bayesian model. *Biometrika*, 104(2): 497–503, 2017.
- M. Jarvenpää, A. Vehtari, and P. Marttinen. Batch simulations and uncertainty quantification in gaussian process surrogate approximate Bayesian computation. In *Conference on Uncertainty in Artificial Intelligence*, pages 779–788. PMLR, 2020.
- J. Jewson, J. Q. Smith, and C. Holmes. Principles of Bayesian inference using general divergence criteria. *Entropy*, 20(6):442, 2018.
- B. Jiang. Approximate Bayesian computation with Kullback-Leibler divergence as data discrepancy. In *International Conference on Artificial Intelligence and Statistics*, pages 1711–1721, 2018.
- J. Knoblauch, J. Jewson, and T. Damoulas. Generalized variational inference: Three arguments for deriving new posteriors. *arXiv preprint arXiv:1904.02063*, 2019.
- O. Ledoit and M. Wolf. A well-conditioned estimator for large-dimensional covariance matrices. *Journal of multivariate analysis*, 88(2):365–411, 2004.
- J. Lintusaari, M. U. Gutmann, R. Dutta, S. Kaski, and J. Corander. Fundamentals and recent developments in approximate Bayesian computation. *Systematic Biology*, 66(1):e66–e82, 2017. ISSN 1076836X. doi: 10.1093/sysbio/syw077. URL <https://doi.org/10.1093/sysbio/syw077>.
- Q. Liu, J. Lee, and M. Jordan. A kernelized Stein discrepancy for goodness-of-fit tests. In *International conference on machine learning*, pages 276–284. PMLR, 2016.
- R. Loaiza-Maya, G. M. Martin, and D. T. Frazier. Focused Bayesian prediction. *Journal of Applied Econometrics*, 36(5):517–543, 2021.
- E. N. Lorenz. Predictability: A problem partly solved. In *Proc. Seminar on predictability*, volume 1, 1996.
- S. Lyddon, S. Walker, and C. C. Holmes. Nonparametric learning from Bayesian models with randomized objective functions. *Advances in Neural Information Processing Systems*, 31, 2018.
- S. Lyddon, C. Holmes, and S. Walker. General Bayesian updating and the loss-likelihood bootstrap. *Biometrika*, 106(2):465–478, 2019.
- J.-M. Marin, P. Pudlo, C. P. Robert, and R. J. Ryder. Approximate Bayesian computational methods. *Statistics and Computing*, 22(6):1167–1180, 2012.
- T. Matsubara, J. Knoblauch, F.-X. Briol, C. Oates, et al. Robust generalised Bayesian inference for intractable likelihoods. *arXiv preprint arXiv:2104.07359*, 2021.
- C. McDiarmid. On the method of bounded differences. *Surveys in combinatorics*, 141(1):148–188, 1989.
- J. W. Miller. Asymptotic normality, concentration, and coverage of generalized posteriors. *Journal of Machine Learning Research*, 22(168):1–53, 2021.
- B. Nelson. *Foundations and methods of stochastic simulation: a first course*. Springer Science & Business Media, 2013.
- H. D. Nguyen, J. Arbel, H. Lü, and F. Forbes. Approximate Bayesian computation via the energy statistic. *IEEE Access*, 8:131683–131698, 2020.
- V. M. Ong, D. J. Nott, M.-N. Tran, S. A. Sisson, and C. C. Drovandi. Variational Bayes with synthetic likelihood. *Statistics and Computing*, 28(4):971–988, 2018a.
- V. M.-H. Ong, D. J. Nott, M.-N. Tran, S. A. Sisson, and C. C. Drovandi. Likelihood-free inference in high dimensions with synthetic likelihood. *Computational Statistics & Data Analysis*, 128:271–291, 2018b.
- L. Pacchiardi and R. Dutta. Score matched neural exponential families for likelihood-free inference. *Journal of Machine Learning Research*, 23(38):1–71, 2022. URL <http://jmlr.org/papers/v23/21-0061.html>.
- M. Park, W. Jitkrittum, and D. Sejdinovic. K2-ABC: Approximate Bayesian computation with kernel embeddings. In *Artificial Intelligence and Statistics*, 2016.

- F. Pauli, W. Racugno, and L. Ventura. Bayesian composite marginal likelihoods. *Statistica Sinica*, pages 149–164, 2011.
- U. Picchini, U. Simola, and J. Corander. Sequentially Guided MCMC Proposals for Synthetic Likelihoods and Correlated Synthetic Likelihoods. *Bayesian Analysis*, pages 1 – 31, 2022. doi: 10.1214/22-BA1305. URL <https://doi.org/10.1214/22-BA1305>.
- D. Prangle. gk: An R package for the g-and-k and generalised g-and-h distributions. *arXiv preprint arXiv:1706.06889*, 2017.
- L. F. Price, C. C. Drovandi, A. Lee, and D. J. Nott. Bayesian synthetic likelihood. *Journal of Computational and Graphical Statistics*, 27(1):1–11, 2018.
- J. Ridgway. Probably approximate Bayesian computation: nonasymptotic convergence of ABC under misspecification. *arXiv preprint arXiv:1707.05987*, 2017.
- M. L. Rizzo and G. J. Székely. Energy distance. *Wiley interdisciplinary reviews: Computational statistics*, 8(1):27–38, 2016.
- E. Ruli, N. Sartori, and L. Ventura. Approximate Bayesian computation with composite score functions. *Statistics and Computing*, 26(3):679–692, 2016.
- J. Salvatier, T. V. Wiecki, and C. Fonnesbeck. Probabilistic programming in Python using PyMC3. *PeerJ Computer Science*, 2:e55, 2016.
- H. Scheffé. A useful convergence theorem for probability distributions. *The Annals of Mathematical Statistics*, 18(3):434–438, 1947.
- A. Y. Shestopaloff and R. M. Neal. On Bayesian inference for the M/G/1 queue with efficient MCMC sampling. *arXiv preprint arXiv:1401.5548*, 2014.
- N. Syring and R. Martin. Calibrating general posterior credible regions. *Biometrika*, 106(2):479–486, 2019.
- O. Thomas, R. Dutta, J. Corander, S. Kaski, M. U. Gutmann, et al. Likelihood-free inference by ratio estimation. *Bayesian Analysis*, 2020.
- D. S. Wilks. Effects of stochastic parametrizations in the Lorenz’96 system. *Quarterly Journal of the Royal Meteorological Society*, 131(606):389–407, 2005.
- S. N. Wood. Statistical inference for noisy nonlinear ecological dynamic systems. *Nature*, 466(7310):1102, 2010.
- P.-S. Wu and R. Martin. A comparison of learning rate selection methods in generalized bayesian inference. *arXiv preprint arXiv:2012.11349*, 2020.
- A. Zellner. Optimal information processing and Bayes’s theorem. *The American Statistician*, 42(4):278–280, 1988.
- F. Ziel and K. Berk. Multivariate forecasting evaluation: On sensitive and strictly proper scoring rules. *arXiv preprint arXiv:1910.07325*, 2019.

## A Proofs of theoretical results

### A.1 Proof and more details on Theorem 1

#### A.1.1 Discussion and comparison with related results

**Discussion on assumptions** The uniqueness of the minimizer of the expected scoring rule  $\theta^*$  (in Assumption **A1**) is satisfied in a well specified setup if  $S$  is a strictly proper scoring rule (in which case  $P_{\theta^*} = P_0$ ). If the model class is not well specified, a strictly proper  $S$  does not guarantee the minimizer to be unique (as in fact there may be pathological cases where multiple minimizers exist).

Additionally, it may be the case that, for a specific  $P_0$  and misspecified model class  $P_\theta$ , the minimizer of  $S(P_\theta, P_0)$  is unique even if  $S$  is not strictly proper; in fact, in general, being not strictly proper means that there exist at least one pair of values  $\theta^{(1)}, \theta^{(2)}$  for which  $S(P_{\theta^{(1)}}, P_{\theta^{(2)}}) = S(P_{\theta^{(1)}}, P_{\theta^{(1)}})$ , but it may be that the  $\arg \min_{\theta \in \Theta} S(P_\theta, P_0)$  is unique for that specific choice of  $P_0$ , as the minimizer is in a region of the parameter space for which there are no other parameter values which lead to the same value of the scoring rule.

Our proof below builds on Theorem 5 in Miller [2021]; to do so, we require regularity conditions on the third order derivatives of the SR (in Assumptions **A2** or, alternatively, **A2bis** below). It may be possible however to relax these assumptions to assuming  $\theta \rightarrow S(P_\theta, y)$  can be locally written as a quadratic function of  $\theta$ , with bounded coefficient for the third order term; this is usually called a Locally Asymptotically Normal (LAN) condition. With such, it would be possible to apply Theorem 4 in Miller [2021] (more general than Theorem 5) to show our result.

**Related results** Appendix A in Loaiza-Maya et al. [2021] provides a result which holds with non-i.i.d. (independent and identically distributed) data, with a generalized posterior based on Scoring Rules with a similar formulation to ours. Additionally, they replace our assumptions on differentiability (which ensure the existence of the Taylor series expansion in the proof below) with assuming the difference of the cumulative scoring rules have a LAN form. Finally, they only convergence in probability.

Another related result can be found in Matsubara et al. [2021], which studies a generalized posterior based on Kernel Stein Discrepancy; similarly to us, they build on Miller [2021], and provide almost sure convergence. However, they exploit the Theorem 4 in Miller [2021], while we rely on Theorem 5. In Matsubara et al. [2021], third order differentiability conditions are assumed in Matsubara et al. [2021], analogously to our Assumption **A2**. The remaining assumptions in Matsubara et al. [2021] are similar to ours, including prior continuity and uniqueness of the minimizer  $\theta^*$ .

Finally, we remark that, if multiple minimizers of  $S(P_\theta, P_0)$  exist (in finite number), it may be possible to obtain an asymptotic *fractional* normality result, which ensures the SR posterior converges to a mixture of normal distributions centered in the different minimizers; see for instance [Frazier et al., 2021a] for an example of such results in the setting of BSL. We leave this for future work.

### A.1.2 Alternative statements and proof

First, let us reproduce Theorem 5 in Miller [2021], on which our proof is based, for ease of reference. Here, convergence and boundedness for vectors  $v \in \mathbb{R}^p$ , matrices  $M \in \mathbb{R}^{p \times p}$  and tensors  $T \in \mathbb{R}^{p \times p \times p}$  are defined with respect to Euclidean-Frobenius norms, that is:  $|v| = \left(\sum_j v_j^2\right)^{1/2}$ ,  $\|M\| = \left(\sum_{jk} M_{jk}^2\right)^{1/2}$  and  $\|T\| = \left(\sum_{jkl} T_{jkl}^2\right)^{1/2}$ .

**Theorem 5** (Theorem 5 in Miller [2021]). *Let  $\Theta \subseteq \mathbb{R}^p$ . Let  $E \subseteq \Theta$  be open (in  $\mathbb{R}^p$ ) and bounded. Fix  $\theta^* \in E$  and let  $\pi : \Theta \rightarrow \mathbb{R}$  be a probability density with respect to Lebesgue measure. Consider the following family of distributions:*

$$\pi_n(\theta) = \frac{\pi(\theta) \exp(-nf_n(\theta))}{\int_{\Theta} \pi(\theta) \exp(-nf_n(\theta))},$$

where  $f_n : \Theta \rightarrow \mathbb{R}$  is a family of functions. Under the following conditions:

**C1**  $\pi$  is continuous at  $\theta^*$  and  $\pi(\theta^*) > 0$ ,

**C2**  $f_n$  have continuous third derivatives in  $E$ ,

**C3**  $f_n \rightarrow f$  pointwise for some  $f : \Theta \rightarrow \mathbb{R}$ ,

**C4**  $f''(\theta^*)$  is positive definite,

**C5**  $f_n'''$  is uniformly bounded in  $E$ ,

**C6** Either one of the following holds:

- (a) for some compact  $K \subseteq E$ , with  $\theta^*$  in the interior of  $K$ ,  $f(\theta) > f(\theta^*) \forall \theta \in K \setminus \{\theta^*\}$  and  $\liminf_n \inf_{\theta \in \Theta \setminus K} f_n(\theta) > f(\theta^*)$ , or
- (b) each  $f_n$  is convex and  $f'(\theta^*) = 0$ ;



then, there is a sequence  $\theta_n \rightarrow \theta^*$  such that  $f'_n(\theta_n) = 0$  for all  $n$  sufficiently large,  $f_n(\theta_n) \rightarrow f(\theta^*)$  and, letting  $q_n$  be the density of  $\sqrt{n}(\theta - \theta_n)$  when  $\theta \sim \pi_n$ :

$$\int |q_n(s) - \mathcal{N}(s|0, (f''(\theta^*))^{-1})| ds \rightarrow 0 \text{ as } n \rightarrow \infty,$$

that is,  $q_n$  converges to  $\mathcal{N}(0, (f''(\theta^*))^{-1})$  in total variation. Additionally, **C6b** implies **C6a** under the other conditions.

Notice that Theorem 5 considers deterministic  $f_n$  and  $f$ . In order to prove our result, therefore, we will verify the different conditions hold almost surely, which implies almost sure convergence.

Besides the assumptions considered in the main text (i.e. **A1-A4**), it is possible to prove the asymptotic normality result in Theorem 1 under alternative sets of assumptions. For this reason, we introduce the following:

**A2bis** The parameter space  $\Theta$  is open, convex, and bounded; the function  $\theta \rightarrow S(P_\theta, y)$ , for any fixed  $y \in \mathcal{X}$ , can be extended to the closure  $\bar{\Theta}$ . Let us denote  $S'''(P_\theta, y)_{jkl} = \frac{\partial^3}{\partial \theta_j \partial \theta_k \partial \theta_l} S(P_\theta, Y)$ . For all  $j, k, l \in \{1, \dots, d\}$ :

- $\theta \rightarrow S'''(P_\theta, y)_{jkl}$  is continuous in  $\Theta$  and exists in  $\bar{\Theta}$  for any fixed  $y \in \mathcal{X}$ ,
- $y \rightarrow S'''(P_\theta, y)_{jkl}$  is measurable for any fixed  $\theta \in \bar{\Theta}$ ,
- $\mathbb{E}_{P_0} \sup_{\theta \in \bar{\Theta}} |S'''(P_\theta, y)_{jkl}| < \infty$ .

**A3bis** For each  $y \in \mathcal{X}$ , the function:  $\theta \rightarrow S(P_\theta, y)$  is convex.

The following extended form of Theorem 1 includes the formulation in the main text as well as two alternative sets of assumptions.

**Theorem 1 - extended version.** *Under either one of the following sets of assumptions:*

1. **A1, A2, A3, A4** (the set originally used in the main text),
2. **A1, A2, A3bis, A4**,
3. **A1, A2bis, A4**,

*the statement of Theorem 1 in the main text holds.*

We next move to proving our result.

Assumption **A2** is used in the original set of assumptions to ensure the second part of Condition **C6a** holds almost surely. Under set of assumptions 2, convexity of the scoring rules (Assumption **A3bis**) is used to show Condition **C6b**; alternatively, with set of assumptions 3, the constraints on  $\Theta$  are used to imply the second part of Condition **C6a** with probability 1 using Theorem 7 in Miller [2021]. In both cases, Assumption **A2** is not explicitly needed anymore – as in fact it is implied by the remaining assumptions. However, we are unable to remove Assumption **A2** under no constraints on  $\Theta$  or the convexity of  $\theta \rightarrow S(P_\theta, y)$ .

We now give our proof:

*Proof of Theorem 1 - extended version.* In order to obtain our result, we identify

$$f_n(\theta) = \frac{1}{n} \sum_{i=1}^n S(P_\theta, Y_i), \quad f(\theta) = S(P_\theta, P_0);$$

this implies that  $f_n$  is now a random quantity: as such, we show the conditions for Theorem 5 hold almost surely over the stochasticity induced by  $\mathbf{Y}_n$ .

All three sets of assumptions include Assumptions **A1** and **A4**; therefore, under all three sets of assumptions:

- **C1** corresponds to our Assumption **A4**,
- **C3** holds almost surely thanks to the strong law of large numbers, as  $S(P_\theta, P_0)$  is finite  $\forall \theta \in \Theta$  by Assumption **A1**,
- **C4** is implied by Assumption **A1**.

Therefore, we are left with establishing **C2**, **C5** and **C6** separately for the different sets of assumptions.

#### Set of assumptions 1 (used in main text):

- **C2** is implied by our Assumption **A2** to hold with probability 1 for all  $n$ .
- In order to show **C5**, we proceed in similar manner as in Theorem 13 in Miller [2021]. For any  $j, k, l \in \{1, \dots, d\}$ , Assumption **A2** implies that, with probability 1,  $f_n'''(\theta)_{jkl} = \frac{1}{n} \sum_{i=1}^n S'''(P_\theta, Y_i)_{jkl}$  is uniformly bounded on  $\bar{E}$  by the uniform law of large number (Theorem 1.3.3 in Ghosh and Ramamoorthi 2003). Letting  $C_{jkl}(Y_1, Y_2, \dots)$  be such a uniform bound for each  $j, k, l$ , we have that with probability 1, for all  $n \in \mathbb{N}$ ,  $\theta \in \bar{E}$ ,  $\|f_n'''(\theta)\|^2 = \sum_{jkl} (f_n'''(\theta)_{jkl})^2 \leq \sum_{jkl} C_{jkl}(Y_1, Y_2, \dots) < \infty$ . Thus,  $f_n'''(\theta)$  is almost surely uniformly bounded on  $\bar{E}$ , and hence on  $E$ .
- The first part of **C6a** is implied by Assumption **A1**, while the second part holds almost surely by Assumption **A3**.

**Set of assumptions 2:** The only difference here is that we replace Assumption **A3** with the stronger convexity Assumption **A3bis**; therefore, **C2** and **C5** are shown in the same way as with set of assumptions 1.

Next, consider **C6b**: the first part is implied to hold with probability 1 for all  $n$  by Assumption **A3bis**, as the sum of convex functions is convex. The second part is instead consequence of  $\theta^*$  being a stationary point of  $f$  due to Assumption **A1**, and of  $f'(\theta^*)$  existing due to **C4**.

**Set of assumptions 3:** Under these assumptions, we fix  $E = \Theta$  in the statement of Theorem 5, as we consider  $\Theta$  to be open and bounded. With that, we can exploit Assumption **A2bis** and follow the same steps as with set of assumptions 1 to show that, over  $\Theta$ , **C2** and **C5** hold with probability 1.

The first part of **C6a** is implied by Assumption **A1**, for any choice of  $K$ ; it now remains to show the second part. First, Theorem 7 in Miller [2021] implies that  $f_n \rightarrow f$  uniformly almost surely, as in fact  $f_n$  have continuous third derivatives by **C2**,  $f_n'''$  is uniformly bounded with probability 1 by **C5**, and  $f_n \rightarrow f$  with probability 1 due to **C3** holding with probability 1.

Therefore, with probability 1:

$$\liminf_n \inf_{\theta \in \Theta \setminus K} f_n(\theta) = \inf_{\theta \in \Theta \setminus K} f(\theta) > \inf_{\theta \in \Theta} f(\theta) = f(\theta^*),$$

where the first equality is due to uniform convergence allowing to “swap” the infimum and the limit.  $\square$

## A.2 Proof of Theorem 2

First, we prove a finite sample generalization bound which is valid for the generalized Bayes posterior with a generic loss, assuming a concentration property and prior mass condition. Next, we will use this Lemma to prove Theorem 2 reported in the main body of the paper (in Section 2.2.2), by first proving concentration results for Kernel and Energy Scores.

We remark that our Theorem 2 is similar to Theorem 1 in Matsubara et al. [2021] for the kernel Stein Discrepancy (KSD) posterior, but provides a tighter probability bound. As the kernel used in KSD is unbounded, in fact, Matsubara et al. [2021] had to rely on weaker results with respect to the ones used to prove Theorem 2. With a similar approach, a result for unbounded  $k$  or  $\mathcal{X}$  may be obtained in our case; we leave this for future exploration.

### A.2.1 Lemma for generalized Bayes posterior with generic loss

In this Subsection, we consider the following generalized Bayes posterior:

$$\pi_L(\theta|\mathbf{y}_n) \propto \pi(\theta) \exp \{-wnL(\theta, \mathbf{y}_n)\}, \quad (7)$$

where  $\mathbf{y}_n = \{y_i\}_{i=1}^n$  denote the observations,  $\pi$  is the prior and  $L(\theta, \mathbf{y}_n)$  is a generic loss function (which does not need to be additive in  $y_i$ ). Here, the SR posterior for the scoring rule  $S$  corresponds to choosing:

$$L(\theta, \mathbf{y}_n) = \frac{1}{n} \sum_{i=1}^n S(P_\theta, y_i).$$

First, we state a result concerning this form of the posterior which we will use later (taken from Knoblauch et al. 2019), and reproduce here the proof for convenience:

**Lemma 1** (Theorem 1 in Knoblauch et al. [2019]). *Provided that  $\int_{\Theta} \pi(\theta) \exp \{-wnL(\theta, \mathbf{y}_n)\} d\theta < \infty$ ,  $\pi_L(\cdot|\mathbf{y}_n)$  in Eq. (7) can be written as the solution to a variational problem:*

$$\pi_L(\cdot|\mathbf{y}_n) = \arg \min_{\rho \in \mathcal{P}(\Theta)} \{wn\mathbb{E}_{\theta \sim \rho} [L(\theta, \mathbf{y}_n)] + \text{KL}(\rho||\pi)\}, \quad (8)$$

where  $\mathcal{P}(\Theta)$  denotes the set of distributions over  $\Theta$ , and  $\text{KL}$  denotes the KL divergence.

*Proof.* We follow here (but adapt to our notation) the proof given in Knoblauch et al. [2019], which in turn is based on the one for the related result contained in Bissiri et al. [2016].

Notice that the minimizer of the objective in Eq. (8) can be written as:

$$\begin{aligned} \pi^*(\cdot|\mathbf{y}_n) &= \arg \min_{\rho \in \mathcal{P}(\Theta)} \left\{ \int_{\Theta} \left[ \log(\exp \{wnL(\theta, \mathbf{y}_n)\}) + \log \left( \frac{\rho(\theta)}{\pi(\theta)} \right) \right] \rho(\theta) d\theta \right\} \\ &= \arg \min_{\rho \in \mathcal{P}(\Theta)} \left\{ \int_{\Theta} \left[ \log \left( \frac{\rho(\theta)}{\pi(\theta) \exp \{-wnL(\theta, \mathbf{y}_n)\}} \right) \right] \rho(\theta) d\theta \right\}. \end{aligned}$$

As we are only interested in the minimizer  $\pi^*(\cdot|\mathbf{y}_n)$  (and not in the value of the objective), it holds that, for any constant  $Z > 0$ :

$$\begin{aligned} \pi^*(\cdot|\mathbf{y}_n) &= \arg \min_{\rho \in \mathcal{P}(\Theta)} \left\{ \int_{\Theta} \left[ \log \left( \frac{\rho(\theta)}{\pi(\theta) \exp \{-wnL(\theta, \mathbf{y}_n)\} Z^{-1}} \right) \right] \rho(\theta) d\theta - \log Z \right\} \\ &= \arg \min_{\rho \in \mathcal{P}(\Theta)} \{ \text{KL}(\rho(\theta)||\pi(\theta) \exp \{-wnL(\theta, \mathbf{y}_n)\} Z^{-1}) \}. \end{aligned}$$

Now, we can set  $Z = \int_{\Theta} \pi(\theta) \exp \{-wnL(\theta, \mathbf{y}_n)\} d\theta$  (which is finite by assumption) and notice that we get:

$$\pi^*(\cdot|\mathbf{y}_n) = \arg \min_{\rho \in \mathcal{P}(\Theta)} \{ \text{KL}(\rho||\pi_L(\cdot|\mathbf{y}_n)) \},$$

which yields  $\pi^*(\cdot|\mathbf{y}_n) = \pi_L(\cdot|\mathbf{y}_n)$  as the KL is minimized uniquely if the two arguments are the same.  $\square$

Next, we prove a finite sample (as it holds for fixed number of samples  $n$ ) generalization bound. Our statement and proof generalize Lemma 8 in Matsubara et al. [2021] (as we consider a generic loss function  $L(\theta, \mathbf{y}_n)$ , while they consider the Kernel Stein Discrepancy only).

In order to do this, let  $J$  be a function of the parameter  $\theta$ , with  $J(\theta)$  representing some loss (of which we will assume  $L(\theta, \mathbf{y}_n)$  is a finite sample estimate; the meaning of  $J$  will be made clearer in the following and when applying this result to the SR posterior).

We will assume the following *prior mass condition*, which is more generic with respect to the one considered in the main body of this manuscript (Assumption **A5**):

**A5bis** Denote  $\theta^* \in \arg \min_{\theta \in \Theta} J(\theta)$ , which is supposed to be non-empty. The prior has a density  $\pi(\theta)$  (with respect to Lebesgue measure) which satisfies

$$\int_{B_n(\alpha_1)} \pi(\theta) d\theta \geq e^{-\alpha_2 \sqrt{n}}$$

for some constants  $\alpha_1, \alpha_2 > 0$ , where we define the sets

$$B_n(\alpha_1) := \{\theta \in \Theta : |J(\theta) - J(\theta^*)| \leq \alpha_1/\sqrt{n}\}.$$

Assumption **A5bis** constrains the minimum amount of prior mass which needs to be given to  $J$ -balls with decreasing size, and is in general quite a weak condition (similar assumptions are taken in Chérif-Abdellatif and Alquier [2020], Matsubara et al. [2021]).

Next, we state our result, which as mentioned above generalizes Lemma 8 in Matsubara et al. [2021]:

**Lemma 2.** Consider the generalized posterior  $\pi_L(\theta|\mathbf{y}_n)$  defined in Eq. (7), and assume that:

- (concentration) for all  $\delta \in (0, 1]$ :

$$P_0 \{|L(\theta, \mathbf{Y}_n) - J(\theta)| \leq \epsilon_n(\delta)\} \geq 1 - \delta, \quad (9)$$

where  $\epsilon_n(\delta) \geq 0$  is an approximation error term;

- $J(\theta^*) = \min_{\theta \in \Theta} J(\theta)$  is finite;
- Assumption **A5bis** holds.

Then, for all  $\delta \in (0, 1]$ , with probability at least  $1 - \delta$ :

$$\int_{\Theta} J(\theta) \pi_L(\theta|\mathbf{Y}_n) d\theta \leq J(\theta^*) + \frac{\alpha_1 + \alpha_2/w}{\sqrt{n}} + 2\epsilon_n(\delta),$$

where the probability is taken with respect to realisations of the dataset  $\mathbf{Y}_n = \{Y_i\}_{i=1}^n, Y_i \stackrel{iid}{\sim} P_0$  for  $i = 1, \dots, n$ ; this also implies the following statement:

$$P_0 \left( \left| \int_{\Theta} J(\theta) \pi_L(\theta|\mathbf{Y}_n) d\theta - J(\theta^*) \right| \geq \frac{\alpha_1 + \alpha_2/w}{\sqrt{n}} + 2\epsilon_n(\delta) \right) \leq \delta.$$

This result ensures that, with high probability, the expectation over the posterior of  $J(\theta)$  is close to the minimum  $J(\theta^*)$ , provided that the distribution of  $L(\theta, \mathbf{Y}_n)$  (where  $\mathbf{Y}_n \sim P_0^n$  is a random variable) satisfies a concentration bound, which constrains how far  $L(\theta, \mathbf{Y}_n)$  is distributed from the loss function  $J(\theta)$ . Notice that this result does not require the minimizer of  $J$  to be unique.

Typically the approximation error term  $\epsilon_n(\delta)$  is such that  $\epsilon_n(\delta) \xrightarrow{\delta \rightarrow 0} +\infty$  and  $\epsilon_n(\delta) \xrightarrow{n \rightarrow \infty} 0$ . If the second limit is verified, the posterior concentrates, for large  $n$ , on the values of  $\theta$  which minimize  $J$ . In practical cases (as for instance for the SR posterior), it is common to have  $J(\theta) = D(\theta, P_0)$ , i.e., corresponding to a loss function relating  $\theta$  with the data generating process  $P_0$ .

We now prove the result.

*Proof of Lemma 2.* Due to the absolute value in Eq. (9), the following two inequalities hold simultaneously with probability (w.p.) at least  $1 - \delta$ :

$$J(\theta) \leq L(\theta, \mathbf{Y}_n) + \epsilon_n(\delta), \quad (10)$$

$$L(\theta, \mathbf{Y}_n) \leq J(\theta) + \epsilon_n(\delta). \quad (11)$$

Taking expectation with respect to the generalized posterior on both sides of Eq. (10) yields, w.p.  $\geq 1 - \delta$ :

$$\int_{\Theta} J(\theta) \pi_L(\theta|\mathbf{Y}_n) d\theta \leq \int_{\Theta} L(\theta, \mathbf{Y}_n) \pi_L(\theta|\mathbf{Y}_n) d\theta + \epsilon_n(\delta).$$

We now want to apply the identity in Eq. (8); therefore, we add  $(wn)^{-1}\text{KL}(\pi_L(\cdot|\mathbf{Y}_n)\|\pi) \geq 0$  in the right hand side such that, w.p.  $\geq 1 - \delta$ :

$$\int_{\Theta} J(\theta)\pi_L(\theta|\mathbf{Y}_n)d\theta \leq \frac{1}{wn} \left\{ \int_{\Theta} wnL(\theta, \mathbf{Y}_n)\pi_L(\theta|\mathbf{Y}_n)d\theta + \text{KL}(\pi_L(\cdot|\mathbf{Y}_n)\|\pi) \right\} + \epsilon_n(\delta).$$

Now by Eq. (8):

$$\begin{aligned} \int_{\Theta} J(\theta)\pi_L(\theta|\mathbf{Y}_n)d\theta &\leq \frac{1}{wn} \inf_{\rho \in \mathcal{P}(\Theta)} \left\{ \int_{\Theta} wnL(\theta, \mathbf{Y}_n)\rho(\theta)d\theta + \text{KL}(\rho\|\pi) \right\} + \epsilon_n(\delta) \\ &= \inf_{\rho \in \mathcal{P}(\Theta)} \left\{ \int_{\Theta} L(\theta, \mathbf{Y}_n)\rho(\theta)d\theta + \frac{1}{wn}\text{KL}(\rho\|\pi) \right\} + \epsilon_n(\delta), \end{aligned} \quad (12)$$

where  $\mathcal{P}(\Theta)$  denotes the space of probability distributions over  $\Theta$ . Putting now Eq. (11) in Eq. (12) we have, w.p.  $\geq 1 - \delta$ :

$$\int_{\Theta} J(\theta)\pi_L(\theta|\mathbf{Y}_n)d\theta \leq \inf_{\rho \in \mathcal{P}(\Theta)} \left\{ \int_{\Theta} J(\theta)\rho(\theta)d\theta + \frac{1}{wn}\text{KL}(\rho\|\pi) \right\} + 2\epsilon_n(\delta),$$

and using the trivial bound  $J(\theta) \leq J(\theta^*) + |J(\theta) - J(\theta^*)|$  we get:

$$\int_{\Theta} J(\theta)\pi_L(\theta|\mathbf{Y}_n)d\theta \leq J(\theta^*) + \inf_{\rho \in \mathcal{P}(\Theta)} \left\{ \int_{\Theta} |J(\theta) - J(\theta^*)|\rho(\theta)d\theta + \frac{1}{wn}\text{KL}(\rho\|\pi) \right\} + 2\epsilon_n(\delta).$$

Finally, we upper bound the infimum term by exploiting the prior mass condition in Assumption **A5bis**. Specifically, letting  $\Pi(B_n) = \int_{B_n} \pi(\theta)d\theta$ , we take  $\rho(\theta) = \pi(\theta)/\Pi(B_n)$  for  $\theta \in B_n$  and  $\rho(\theta) = 0$  otherwise. By Assumption **A5bis**, we have therefore  $\int_{B_n} |J(\theta) - J(\theta^*)|\rho(\theta)d\theta \leq \alpha_1/\sqrt{n}$  and that  $\text{KL}(\rho\|\pi) = \int_{\Theta} \log(\rho(\theta)/\pi(\theta))\rho(\theta)d\theta = \int_{B_n} -\log(\Pi(B_n))\pi(\theta)d\theta/\Pi(B_n) = -\log \Pi(B_n) \leq \alpha_2\sqrt{n}$ . Thus, we have:

$$\int_{\Theta} J(\theta)\pi_L(\theta|\mathbf{Y}_n)d\theta \leq J(\theta^*) + \frac{\alpha_1 + \alpha_2/w}{\sqrt{n}} + 2\epsilon_n(\delta),$$

as claimed in the first statement.

In order to obtain the second statement, notice that:

$$J(\theta) - J(\theta^*) \geq 0, \quad \forall \theta \in \Theta \implies \int_{\Theta} J(\theta)\pi_L(\theta|\mathbf{Y}_n)d\theta - J(\theta^*) \geq 0;$$

thus:

$$P_0 \left( \left| \int_{\Theta} J(\theta)\pi_L(\theta|\mathbf{Y}_n)d\theta - J(\theta^*) \right| \leq \frac{\alpha_1 + \alpha_2/w}{\sqrt{n}} + 2\epsilon_n(\delta) \right) \geq 1 - \delta;$$

taking the complement yields the result.  $\square$

### A.2.2 Case of Kernel and Energy Score posteriors

We now state and prove concentration results of the form in Eq. (9) for the Kernel and Energy Scores. Here, we will assume  $X \perp\!\!\!\perp X'$ . To this regards, notice that the kernel SR posterior can be written as:

$$\begin{aligned} \pi_{S_k}(\theta|\mathbf{y}_n) &\propto \pi(\theta) \exp \left\{ -w \sum_{i=1}^n [\mathbb{E}_{X, X' \sim P_{\theta}} k(X, X') - 2\mathbb{E}_{X \sim P_{\theta}} k(X, y_i)] \right\} \\ &\propto \pi(\theta) \exp \left\{ -w \sum_{i=1}^n \left[ \mathbb{E}_{X, X' \sim P_{\theta}} k(X, X') - 2\mathbb{E}_{X \sim P_{\theta}} k(X, y_i) + \frac{1}{n-1} \sum_{\substack{j=1 \\ j \neq i}}^n k(y_i, y_j) \right] \right\}, \end{aligned}$$

as in fact the terms  $k(y_i, y_j)$  are independent of  $\theta$ . From the second line in the above expression and the form of the generalized Bayes posterior with generic loss in Eq. (7), we can identify:

$$L(\theta, \mathbf{y}_n) = \mathbb{E}_{X, X' \sim P_{\theta}} k(X, X') - \frac{2}{n} \sum_{i=1}^n \mathbb{E}_{X \sim P_{\theta}} k(X, y_i) + \frac{1}{n(n-1)} \sum_{\substack{i,j=1 \\ i \neq j}}^n k(y_i, y_j). \quad (13)$$

Similarly, the Energy Score posterior can be obtained by identifying in Eq. (7):

$$L(\theta, \mathbf{y}_n) = \frac{2}{n} \sum_{i=1}^n \mathbb{E}_{X \sim P_\theta} \|X - y_i\|_2^\beta - \frac{1}{n(n-1)} \sum_{\substack{i,j=1 \\ i \neq j}}^n \|y_i - y_j\|_2^\beta - \mathbb{E}_{X, X' \sim P_\theta} \|X - X'\|_2^\beta; \quad (14)$$

this can be obtained by simply setting  $k(x, y) = -\|x - y\|_2^\beta$  in Eq. (13), as the Kernel SR with that choice of kernel recovers the Energy SR.

For both SRs,  $L(\theta, \mathbf{Y}_n)$  is an unbiased estimator (with respect to  $Y_i \sim P_0$ ) of the associated divergences; in fact, considering  $X \perp\!\!\!\perp X' \sim P_\theta$  and  $Y \perp\!\!\!\perp Y' \sim P_0$ , the associated divergence for Kernel SR is the squared MMD (see Section 2.1):

$$D_k(P_\theta, P_0) = \mathbb{E}k(X, X') + \mathbb{E}k(Y, Y') - 2\mathbb{E}k(X, Y), \quad (15)$$

while, for the Energy SR, the associated divergence is the squared Energy Distance:

$$D_E^{(\beta)}(P_\theta, P_0) = 2\mathbb{E}\|X - Y\|_2^\beta - \mathbb{E}\|X - X'\|_2^\beta - \mathbb{E}\|Y - Y'\|_2^\beta. \quad (16)$$

In order to prove our concentration results, we will exploit the following Lemma:

**Lemma 3** (McDiarmid's inequality, McDiarmid 1989). *Let  $g$  be a function of  $n$  variables  $\mathbf{y}_n = \{y_i\}_{i=1}^n$ , and let*

$$\delta_i g(\mathbf{y}_n) := \sup_{z \in \mathcal{X}} g(y_1, \dots, y_{i-1}, z, y_{i+1}, \dots, y_n) - \inf_{z \in \mathcal{X}} g(y_1, \dots, y_{i-1}, z, y_{i+1}, \dots, y_n),$$

and  $\|\delta_i g\|_\infty := \sup_{\mathbf{y}_n \in \mathcal{X}^n} |\delta_i g(\mathbf{y}_n)|$ . If  $Y_1, \dots, Y_n$  are independent random variables:

$$P(g(Y_1, \dots, Y_n) - \mathbb{E}g(Y_1, \dots, Y_n) \geq \varepsilon) \leq e^{-2\varepsilon^2 / \sum_{i=1}^n \|\delta_i g\|_\infty^2}.$$

We are now ready to prove two concentration results of the form of Eq. (9). The first holds for the Kernel SR assuming a bounded kernel, while the latter holds for the Energy SR assuming a bounded  $\mathcal{X}$ . Let us start with a simple equality stated in the following Lemma:

**Lemma 4.** *For  $L(\theta, \mathbf{Y}_n)$  defined in Eq. (13) and  $D_k(P_\theta, P_0)$  defined in Eq. (15), we have:*

$$L(\theta, \mathbf{Y}_n) - D_k(P_\theta, P_0) = g(Y_1, Y_2, \dots, Y_n) - \mathbb{E}[g(Y_1, Y_2, \dots, Y_n)]$$

for

$$g(Y_1, Y_2, \dots, Y_n) = \frac{1}{n(n-1)} \sum_{\substack{i,j=1 \\ i \neq j}}^n k(Y_i, Y_j) - \frac{2}{n} \sum_{i=1}^n \mathbb{E}_{X \sim P_\theta} k(X, Y_i). \quad (17)$$

Similar expression holds for  $L(\theta, \mathbf{Y}_n)$  defined in Eq. (14) and  $D_E^{(\beta)}(P_\theta, P_0)$  defined in Eq. (16), by setting  $k(x, y) = -\|x - y\|_2^\beta$ .

*Proof.* First, notice that, for  $L(\theta, \mathbf{Y}_n)$  defined in Eq. (13) and  $D_k(P_\theta, P_0)$  defined in Eq. (15):

$$\begin{aligned} L(\theta, \mathbf{Y}_n) - D_k(P_\theta, P_0) &= \cancel{\mathbb{E}_{X, X' \sim P_\theta} k(X, X')} - \frac{2}{n} \sum_{i=1}^n \mathbb{E}_{X \sim P_\theta} k(X, Y_i) + \frac{1}{n(n-1)} \sum_{\substack{i,j=1 \\ i \neq j}}^n k(Y_i, Y_j) + \\ &\quad - \cancel{\mathbb{E}_{X, X' \sim P_\theta} k(X, X')} - \mathbb{E}_{Y, Y' \sim P_0} [k(Y, Y')] + 2\mathbb{E}_{X \sim P_\theta, Y \sim P_0} [k(X, Y)] \\ &= \frac{1}{n(n-1)} \sum_{\substack{i,j=1 \\ i \neq j}}^n k(Y_i, Y_j) - \frac{2}{n} \sum_{i=1}^n \mathbb{E}_{X \sim P_\theta} k(X, Y_i) + \\ &\quad - (\mathbb{E}_{Y, Y' \sim P_0} [k(Y, Y')] - 2\mathbb{E}_{X \sim P_\theta, Y \sim P_0} [k(X, Y)]) \\ &= g(Y_1, Y_2, \dots, Y_n) - \mathbb{E}[g(Y_1, Y_2, \dots, Y_n)], \end{aligned}$$

where the expectation in the last line is with respect to  $Y_i \sim P_0$ ,  $i = 1, \dots, n$ , and where we set  $g$  as in Eq. (17).  $\square$

Now, we give the concentration result for the kernel SR:

**Lemma 5.** Consider  $L(\theta, \mathbf{y}_n)$  defined in Eq. (13) (corresponding to the loss function defining the Kernel Score posterior) and  $D_k(P_\theta, P_0)$  defined in Eq. (15); if the kernel is such that  $|k(x, y)| \leq \kappa$ , we have:

$$P_0 \left( |L(\theta, \mathbf{Y}_n) - D_k(P_\theta, P_0)| \leq \sqrt{-\frac{32\kappa^2}{n} \log \frac{\delta}{2}} \right) \geq 1 - \delta.$$

*Proof.* First, we write:

$$L(\theta, \mathbf{Y}_n) - D_k(P_\theta, P_0) = g(Y_1, Y_2, \dots, Y_n) - \mathbb{E}[g(Y_1, Y_2, \dots, Y_n)],$$

where  $g$  is defined in Eq. (17) in Lemma 4. Next, notice that:

$$\begin{aligned} P_0(|g(\mathbf{Y}_n) - \mathbb{E}[g(\mathbf{Y}_n)]| \geq \epsilon) &\leq P_0(g(\mathbf{Y}_n) - \mathbb{E}[g(\mathbf{Y}_n)] \geq \epsilon) + P_0(g(\mathbf{Y}_n) - \mathbb{E}[g(\mathbf{Y}_n)] \leq -\epsilon) \\ &= P_0(g(\mathbf{Y}_n) - \mathbb{E}[g(\mathbf{Y}_n)] \geq \epsilon) + P_0(-g(\mathbf{Y}_n) - \mathbb{E}[-g(\mathbf{Y}_n)] \geq \epsilon) \end{aligned}$$

by the union bound. We use now McDiarmid's inequality (Lemma 3) to prove the result. Consider first  $P_0(g(\mathbf{Y}_n) - \mathbb{E}[g(\mathbf{Y}_n)] \geq \epsilon)$ ; thus:

$$\begin{aligned} |\delta_i g(\mathbf{Y}_n)| &= \left| \sup_z \left\{ \frac{2}{n(n-1)} \sum_{\substack{j=1 \\ j \neq i}}^n k(z, Y_j) - \frac{2}{n} \mathbb{E}_{X \sim P_\theta} k(X, z) \right\} - \inf_z \left\{ \frac{2}{n(n-1)} \sum_{\substack{j=1 \\ j \neq i}}^n k(z, Y_j) - \frac{2}{n} \mathbb{E}_{X \sim P_\theta} k(X, z) \right\} \right| \\ &= \left| \sup_z \left\{ \frac{2}{n(n-1)} \sum_{\substack{j=1 \\ j \neq i}}^n k(z, Y_j) - \frac{2}{n} \mathbb{E}_{X \sim P_\theta} k(X, z) \right\} \right| + \left| \sup_z \left\{ \frac{2}{n} \mathbb{E}_{X \sim P_\theta} k(X, z) - \frac{2}{n(n-1)} \sum_{\substack{j=1 \\ j \neq i}}^n k(z, Y_j) \right\} \right| \\ &\leq \sup_z \left| \frac{2}{n(n-1)} \sum_{\substack{j=1 \\ j \neq i}}^n k(z, Y_j) - \frac{2}{n} \mathbb{E}_{X \sim P_\theta} k(X, z) \right| + \sup_z \left| \frac{2}{n} \mathbb{E}_{X \sim P_\theta} k(X, z) - \frac{2}{n(n-1)} \sum_{\substack{j=1 \\ j \neq i}}^n k(z, Y_j) \right| \\ &= 2 \cdot \frac{2}{n} \sup_z \left| \frac{1}{n-1} \sum_{\substack{j=1 \\ j \neq i}}^n k(z, Y_j) - \mathbb{E}_{X \sim P_\theta} k(X, z) \right| \leq \frac{4}{n} \sup_z \left\{ \frac{1}{n-1} \sum_{\substack{j=1 \\ j \neq i}}^n |k(z, Y_j)| + \mathbb{E}_{X \sim P_\theta} |k(X, z)| \right\} \\ &\leq \frac{4}{n} \left\{ \frac{1}{n-1} \sum_{\substack{j=1 \\ j \neq i}}^n \underbrace{\sup_z |k(z, Y_j)|}_{\leq \kappa} + \mathbb{E}_{X \sim P_\theta} \underbrace{\sup_z |k(X, z)|}_{\leq \kappa} \right\} \leq \frac{4}{n} \left\{ \frac{1}{n-1} \cdot (n-1)\kappa + \kappa \right\} = \frac{8\kappa}{n} \end{aligned}$$

As the bound does not depend on  $\mathbf{Y}_n$ , we have that  $\|\delta_i g\|_\infty \leq \frac{8\kappa}{n}$ , from which McDiarmid's inequality (Lemma 3) gives:

$$P_0(g(\mathbf{Y}_n) - \mathbb{E}[g(\mathbf{Y}_n)] \geq \epsilon) \leq \exp \left( -\frac{2\epsilon^2}{n \cdot \frac{64\kappa^2}{n^2}} \right) = e^{-\frac{n\epsilon^2}{32\kappa^2}}.$$

For the bound on the other side, notice that  $\|\delta_i(-g)\|_\infty = \|\delta_i g\|_\infty$ ; therefore, we also have

$$P_0(-g(\mathbf{Y}_n) - \mathbb{E}[-g(\mathbf{Y}_n)] \geq \epsilon) \leq e^{-\frac{n\epsilon^2}{32\kappa^2}},$$

from which:

$$P_0(|g(\mathbf{Y}_n) - \mathbb{E}[g(\mathbf{Y}_n)]| \geq \epsilon) \leq 2e^{-\frac{n\epsilon^2}{32\kappa^2}}.$$

Defining the right hand side of the bound as  $\delta$ , we get:

$$P_0 \left( |g(\mathbf{Y}_n) - \mathbb{E}[g(\mathbf{Y}_n)]| \geq \sqrt{-\frac{32\kappa^2}{n} \log \frac{\delta}{2}} \right) \leq \delta,$$

from which the result is obtained taking the complement.  $\square$

We now give the analogous result for the Energy Score:

**Lemma 6.** Consider  $L(\theta, \mathbf{Y}_n)$  defined in Eq. (14) (corresponding to the loss function defining the Energy Score posterior) and  $D_E^{(\beta)}(P_\theta, P_0)$  defined in Eq. (16); assume that the space  $\mathcal{X}$  is bounded such that  $\sup_{x, y \in \mathcal{X}} \|x - y\|_2 \leq B < \infty$ ; therefore, we have:

$$P_0 \left( \left| L(\theta, \mathbf{Y}_n) - D_E^{(\beta)}(P_\theta, P_0) \right| \leq \sqrt{-\frac{32B^{2\beta}}{n} \log \frac{\delta}{2}} \right) \geq 1 - \delta.$$

*Proof.* We rely on Lemma 5; in fact, recall that the Kernel Score recovers the Energy Score for  $k(x, y) = -\|x - y\|_2^\beta$ . With this choice of  $k$ , Eqs. (13) and (15) (considered in Lemma 5) respectively recover Eqs. (14) and (16).

Additionally, assuming  $\mathcal{X}$  to be bounded ensures that  $|k(x, y)| = \|x - y\|_2^\beta \leq B^\beta$ ; therefore, we can apply Lemma 5 with  $\kappa = B^\beta$ , from which the result follows.  $\square$

We are finally ready to prove our generalization bound:

*Proof of Theorem 2.* The proof consists in verifying the assumptions of Lemma 2, for both the Energy and Kernel Score posteriors. First, notice that **A5** is a specific case of **A5bis** by identifying  $J(\theta) = D_k(P_\theta, P_0)$  or  $J(\theta) = D_E(P_\theta, P_0)$ . We therefore need to verify the first and second assumptions only.

As already mentioned before, the Kernel Score posterior corresponds to the generalized Bayes posterior in Eq. (7) by choosing  $L(\theta, \mathbf{Y}_n)$  defined in Eq. (13); with this choice of  $L(\theta, \mathbf{Y}_n)$ , Lemma 5 holds, which corresponds to the first assumption of Lemma 2 with  $J(\theta) = D_k(P_\theta, P_0)$  ( $D_k$  being the divergence related to the kernel SR, defined in Eq. (15)) and:

$$\epsilon_n(\delta) = \sqrt{-\frac{32\kappa^2}{n} \log \frac{\delta}{2}}.$$

Finally, we have that  $D_k(P_\theta, P_0) \geq 0$ , which ensures the second assumption of Lemma 2. Thus, we have, from Lemma 2:

$$P_0 \left( \left| \int_{\Theta} D_k(P_\theta, P_0) \pi_{S_k}(\theta | \mathbf{Y}_n) d\theta - D_k(P_{\theta^*}, P_0) \right| \geq \frac{1}{\sqrt{n}} \left( \alpha_1 + \frac{\alpha_2}{w} + 8\kappa \sqrt{-2 \log \frac{\delta}{2}} \right) \right) \leq \delta;$$

by defining the deviation term as  $\epsilon$  and inverting the relation, we obtain the result for the kernel Score Posterior.

The same steps can be taken for the the Energy Score posterior; specifically, we notice that it corresponds to the generalized Bayes posterior in Eq. (7) by choosing  $L(\theta, \mathbf{Y}_n)$  defined in Eq. (14); with this choice of  $L(\theta, \mathbf{Y}_n)$ , Lemma 6 holds, which corresponds to the first assumption of Lemma 2 with  $J(\theta) = D_E^{(\beta)}(P_\theta, P_0)$  ( $D_E^{(\beta)}$  being the divergence related to the Energy SR defined in Eq. (16)) and:

$$\epsilon_n(\delta) = \sqrt{-\frac{32B^{2\beta}}{n} \log \frac{\delta}{2}}.$$

Finally, we have that  $D_E^{(\beta)}(P_\theta, P_0) \geq 0$ , which ensures the second assumption of Lemma 2. Thus, we have, from Lemma 2:

$$P_0 \left( \left| \int_{\Theta} D_E^{(\beta)}(P_\theta, P_0) \pi_{S_E^{(\beta)}}(\theta | \mathbf{Y}_n) d\theta - D_E^{(\beta)}(P_{\theta^*}, P_0) \right| \geq \frac{1}{\sqrt{n}} \left( \alpha_1 + \frac{\alpha_2}{w} + 8B^\beta \sqrt{-2 \log \frac{\delta}{2}} \right) \right) \leq \delta;$$

by defining the deviation term as  $\epsilon$  and inverting the relation, we obtain the result for the Energy Score Posterior.  $\square$

We remark here that Theorem 1 in Chérif-Abdellatif and Alquier [2020] proved a similar generalization bound for the Kernel Score posterior holding in expectation (rather than in high probability, as for our bounds), albeit under a slightly different prior mass condition.



### A.3 Proof of Theorem 3

Global bias-robustness was also shown in Matsubara et al. [2021] for their kernel Stein discrepancy (KSD) posterior. In our proof, we will rely on Lemma 5 in Matsubara et al. [2021] (which we state below in our Lemma 7), which establishes sufficient conditions for global bias-robustness to hold for generalized Bayes posterior with generic loss function; we recall that the definition of global bias-robustness is given in Sec. 2.2.3.

Across this Section, we define as  $\hat{P}_n = \frac{1}{n} \sum_{i=1}^n \delta_{y_i}$  the empirical distribution given by the observations  $\mathbf{y}_n = \{y_i\}_{i=1}^n$  (considered to be non-random here) and consider the generalized Bayes posterior:

$$\pi_L(\theta|\hat{P}_n) \propto \pi(\theta) \exp \left\{ -wnL(\theta, \hat{P}_n) \right\}, \quad (18)$$

from which the SR posterior in Eq. (2) with Scoring Rule  $S$  is recovered with:

$$L(\theta, \hat{P}_n) = \frac{1}{n} \sum_{i=1}^n S(P_\theta, y_i) = \mathbb{E}_{Y \sim \hat{P}_n} S(P_\theta, Y),$$

We remark that the notation is here slightly different from Appendix A.2, in which we considered  $L$  to be a function of  $\theta$  and  $\mathbf{y}_n$  (compare Eq. (18) with Eq. (7)). The reason of this will be clear in the following.

We start by stating the result we will rely on, to which we provide proof for ease of reference.

**Lemma 7** (Lemma 5 in Matsubara et al. [2021]). *Let  $\pi_L(\theta|\hat{P}_n)$  be the generalized posterior defined in Eq. (18) for fixed  $n \in \mathbb{N}$ , with a generic loss  $L(\theta, \hat{P}_n)$  and prior  $\pi(\theta)$ . Suppose  $L(\theta, \hat{P}_n)$  is lower-bounded and  $\pi(\theta)$  upper bounded over  $\theta \in \Theta$ , for any  $\hat{P}$ . Denote  $DL(z, \theta, \hat{P}_n) = (d/d\epsilon)L(\theta, \hat{P}_{n,\epsilon,z})|_{\epsilon=0}$ . Then,  $\pi_L$  is globally bias-robust if, for any  $\hat{P}_n$ ,*

1.  $\sup_{\theta \in \Theta} \sup_{z \in \mathcal{X}} |DL(z, \theta, \hat{P}_n)| \pi(\theta) < \infty$ , and
2.  $\int_{\Theta} \sup_{z \in \mathcal{X}} |DL(z, \theta, \hat{P}_n)| \pi(\theta) d\theta < \infty$ .

*Proof.* We follow the proof given in Matsubara et al. [2021] and adapt it to our notation:

First of all, Eq. (17) of Ghosh and Basu [2016] demonstrates that

$$\text{PIF}(z, \theta, \hat{P}_n) = wn\pi_L(\theta|\hat{P}_n) \left( -DL(z, \theta, \hat{P}_n) + \int_{\Theta} DL(z, \theta', \hat{P}_n) \pi_L(\theta'|\hat{P}_n) d\theta' \right),$$

where PIF denotes the posterior influence function defined in Sec. 2.2.3 in the main text.

We can apply Jensen's inequality to get the following upper bound:

$$\sup_{\theta \in \Theta} \sup_{z \in \mathcal{X}} |\text{PIF}(z, \theta, \hat{P}_n)| \leq wn \sup_{\theta \in \Theta} \pi_L(\theta|\hat{P}_n) \left( \sup_{z \in \mathcal{X}} |DL(z, \theta, \hat{P}_n)| + \int_{\Theta} \sup_{z \in \mathcal{X}} |DL(z, \theta', \hat{P}_n)| \pi_L(\theta'|\hat{P}_n) d\theta' \right).$$

Recall now that  $\pi_L(\theta|\hat{P}_n) = \pi(\theta) \exp(-wnL(\theta; \hat{P}_n)) / Z$ , where  $0 < Z < \infty$  is the normalising constant. Thus we can obtain an upper bound  $\pi_L(\theta|\hat{P}_n) \leq \pi(\theta) \exp(-wn \inf_{\theta \in \Theta} L(\theta; \hat{P}_n)) / Z =: C\pi(\theta)$  for some constant  $0 < C < \infty$ , since  $L(\theta, \hat{P}_n)$  is lower bounded by assumption and  $n$  fixed. From this upper bound, we have:

$$\begin{aligned} \sup_{\theta \in \Theta} \sup_{z \in \mathcal{X}} |\text{PIF}(z, \theta, \hat{P}_n)| &\leq wnC \sup_{\theta \in \Theta} \pi(\theta) \left( \sup_{z \in \mathcal{X}} |DL(z, \theta, \hat{P}_n)| + C \int_{\Theta} \sup_{z \in \mathcal{X}} |DL(z, \theta', \hat{P}_n)| \pi(\theta') d\theta' \right) \\ &\leq wnC \sup_{\theta \in \Theta} \left( \pi(\theta) \sup_{z \in \mathcal{X}} |DL(z, \theta, \hat{P}_n)| \right) + \\ &\quad wnC^2 \left( \sup_{\theta \in \Theta} \pi(\theta) \right) \int_{\Theta} \sup_{z \in \mathcal{X}} |DL(z, \theta', \hat{P}_n)| \pi(\theta') d\theta'. \end{aligned}$$

Since  $\sup_{\theta \in \Theta} < \infty$  by assumption, it follows that:

$$\sup_{\theta \in \Theta} \left( \pi(\theta) \sup_{z \in \mathcal{X}} \left| DL(z, \theta, \hat{P}_n) \right| \right) < \infty \quad \text{and} \quad \int_{\Theta} \pi(\theta) \sup_{z \in \mathcal{X}} \left| DL(z, \theta, \hat{P}_n) \right| d\theta < \infty$$

are sufficient conditions for  $\sup_{\theta \in \Theta} \sup_{z \in \mathcal{X}} \left| \text{PIF}(z, \theta, \hat{P}_n) \right| < \infty$ , as claimed.  $\square$

Next, we give the explicit form for  $DL(z, \theta, \hat{P}_n)$  in our case in the following Lemma:

**Lemma 8.** For  $L(\theta, \hat{P}_{n, \epsilon, z}) = \mathbb{E}_{Y \sim \hat{P}_{n, \epsilon, z}} S(P_\theta, Y)$ , we have:

$$DL(z, \theta, \hat{P}_n) = S(P_\theta, z) - \mathbb{E}_{Y \sim \hat{P}_n} S(P_\theta, Y);$$

further, setting  $S = S_k$ , where  $S_k$  is the kernel scoring rule with kernel  $k$ , we have:

$$DL(z, \theta, \hat{P}_n) = 2\mathbb{E}_{X \sim P_\theta} \left[ \mathbb{E}_{Y \sim \hat{P}_n} k(X, Y) - k(X, z) \right];$$

finally, the form for the energy score can be obtained by setting  $k(x, y) = -\|x - y\|_2^\beta$ .

*Proof.* For the first statement, notice that:

$$\mathbb{E}_{Y \sim \hat{P}_{n, \epsilon, z}} S(P_\theta, Y) = (1 - \epsilon) \mathbb{E}_{Y \sim \hat{P}_n} S(P_\theta, Y) + \epsilon S(P_\theta, z),$$

from which differentiating with respect to  $\epsilon$  gives the statement.

For the second statement, recall the form for the kernel SR:

$$S_k(P, z) = \mathbb{E}_{X, X' \sim P} [k(X, X')] - 2\mathbb{E}_{X \sim P} [k(X, z)],$$

from which:

$$\begin{aligned} DL(z, \theta, \hat{P}_n) &= S_k(P_\theta, z) - \mathbb{E}_{\hat{P}_n} S_k(P_\theta, Y) \\ &= \mathbb{E}_{X, X' \sim P_\theta} [k(X, X')] - 2\mathbb{E}_{X \sim P_\theta} [k(X, z)] - \mathbb{E}_{Y \sim \hat{P}_n} [\mathbb{E}_{X, X' \sim P_\theta} [k(X, X')] - 2\mathbb{E}_{X \sim P_\theta} [k(X, Y)]] \\ &= \mathbb{E}_{X, X' \sim P_\theta} [k(X, X')] - 2\mathbb{E}_{X \sim P_\theta} [k(X, z)] - \mathbb{E}_{X, X' \sim P_\theta} [k(X, X')] + 2\mathbb{E}_{Y \sim \hat{P}_n} \mathbb{E}_{X \sim P_\theta} [k(X, Y)] \\ &= 2\mathbb{E}_{X \sim P_\theta} \left[ \mathbb{E}_{Y \sim \hat{P}_n} k(X, Y) - k(X, z) \right]. \end{aligned}$$

$\square$

Finally, we state the proof for Theorem 3:

*Proof of Theorem 3.* The proof consists in verifying the conditions necessary for Lemma 7 for the Kernel and Energy Score posteriors

First, let us consider the Kernel Score posterior and let us show that, under the assumptions of the Theorem,  $L(\theta, \hat{P}_n)$  for the Kernel Score  $S_k$  is lower bounded; specifically, we have:

$$\begin{aligned} L(\theta, \hat{P}_n) &= \frac{1}{n} \sum_{i=1}^n S_k(P_\theta, y_i) = \frac{1}{n} \sum_{i=1}^n \mathbb{E} [k(X, X') - 2k(X, y_i)] \geq -\frac{1}{n} \mathbb{E} \left| \sum_{i=1}^n [k(X, X') - 2k(X, y_i)] \right| \\ &\geq -\frac{1}{n} \sum_{i=1}^n \mathbb{E} [|k(X, X')| + |2k(X, y_i)|] \\ &\geq -\frac{1}{n} \sum_{i=1}^n [\kappa + 2\kappa] = -3\kappa > -\infty, \end{aligned}$$

where all expectations are over  $X, X' \sim P_\theta$  and the bound exploits the fact that  $|k(x, y)| < \kappa$ .

We now need to verify Assumptions 1 and 2 from Lemma 7. For the former, we proceed in a similar way as above by noticing that, for the kernel SR (using Lemma 8):

$$\begin{aligned} \left| DL(z, \theta, \hat{P}_n) \right| &= 2 \left| \mathbb{E}_{X \sim P_\theta} \mathbb{E}_{Y \sim \hat{P}_n} [k(X, Y) - k(X, z)] \right| \\ &\leq 2 \mathbb{E}_{X \sim P_\theta} \mathbb{E}_{Y \sim \hat{P}_n} [|k(X, Y)| + |k(X, z)|] \\ &\leq 2 \mathbb{E}_{X \sim P_\theta} \mathbb{E}_{Y \sim \hat{P}_n} [\kappa + \kappa] = 4\kappa. \end{aligned}$$

Now:

$$\sup_{\theta \in \Theta} \left( \pi(\theta) \sup_{z \in \mathcal{X}} \left| DL(z, \theta, \hat{P}_n) \right| \right) \leq 4\kappa \sup_{\theta \in \Theta} \pi(\theta),$$

which is  $< \infty$  as the prior is assumed to be upper bounded over  $\Theta$ , which verifies Assumption 1. Next:

$$\int_{\Theta} \sup_{z \in \mathcal{X}} \left| DL(z, \theta, \hat{P}_n) \right| \pi(\theta) d\theta \leq 4\kappa \int_{\Theta} \pi(\theta) d\theta = 4\kappa < \infty,$$

which verifies Assumption 2; together, these prove the first statement.

For the statement about the Energy Score posterior, we proceed in similar manner. First, let us show that, under the assumptions of the Theorem,  $L(\theta, \hat{P}_n)$  for the Energy Score  $S_E^{(\beta)}$  is lower bounded; in fact:

$$\begin{aligned} L(\theta, \hat{P}_n) &= \frac{1}{n} \sum_{i=1}^n S_E^{(\beta)}(P_\theta, y_i) = \frac{1}{n} \sum_{i=1}^n \mathbb{E} \left[ 2\|X - y_i\|_2^\beta - \|X - X'\|_2^\beta \right] = \frac{2}{n} \sum_{i=1}^n \mathbb{E} \|X - y_i\|_2^\beta - \mathbb{E} \|X - X'\|_2^\beta \\ &= \underbrace{\frac{2}{n} \sum_{i=1}^n \mathbb{E} \|X - y_i\|_2^\beta - \mathbb{E} \|X - X'\|_2^\beta - \frac{1}{n^2} \sum_{i,j=1}^n \|y_i - y_j\|_2^\beta + \frac{1}{n^2} \sum_{i,j=1}^n \|y_i - y_j\|_2^\beta}_{=D_E^{(\beta)}(P_\theta, \hat{P}_n)}, \end{aligned}$$

where  $D_E^{(\beta)}(P_\theta, \hat{P}_n)$  is the squared Energy Distance between  $P_\theta$  and the empirical distribution  $\hat{P}_n$ ; as the Energy Distance is a distance between probability measures [Rizzo and Székely, 2016],  $D_E^{(\beta)}(P_\theta, \hat{P}_n) \geq 0$ , from which:

$$L(\theta, \hat{P}_n) = D_E^{(\beta)}(P_\theta, \hat{P}_n) + \frac{1}{n^2} \sum_{i,j=1}^n \|y_i - y_j\|_2^\beta \geq 0.$$

Recall that, as we assume  $\mathcal{X}$  to be bounded, there exists  $B < \infty$  such that  $\sup_{x,y \in \mathcal{X}} \|x - y\|_2 \leq B$ . Using this fact, we now need to verify Assumptions 1 and 2 from Lemma 7. For the former, notice that, for the Energy SR (using Lemma 8):

$$\begin{aligned} \left| DL(z, \theta, \hat{P}_n) \right| &= 2 \left| \mathbb{E}_{X \sim P_\theta} \mathbb{E}_{Y \sim \hat{P}_n} [\|X - z\|_2^\beta - \|X - Y\|_2^\beta] \right| \\ &\leq 2 \mathbb{E}_{X \sim P_\theta} \mathbb{E}_{Y \sim \hat{P}_n} \left[ \left| \|X - z\|_2^\beta \right| + \left| \|X - Y\|_2^\beta \right| \right] \\ &\leq 2 \mathbb{E}_{X \sim P_\theta} \mathbb{E}_{Y \sim \hat{P}_n} [B^\beta + B^\beta] = 4B^\beta, \end{aligned}$$

where the last inequality is due to  $z \in \mathcal{X}$  and the boundedness assumptions for  $\mathcal{X}$ . Now:

$$\sup_{\theta \in \Theta} \left( \pi(\theta) \sup_{z \in \mathcal{X}} \left| DL(z, \theta, \hat{P}_n) \right| \right) \leq 4B^\beta \sup_{\theta \in \Theta} \pi(\theta),$$

which is  $< \infty$  as the prior is assumed to be upper bounded over  $\Theta$ , which verifies Assumption 1. Next:

$$\int_{\Theta} \sup_{z \in \mathcal{X}} \left| DL(z, \theta, \hat{P}_n) \right| \pi(\theta) d\theta \leq 4B^\beta \int_{\Theta} \pi(\theta) d\theta = 4B^\beta < \infty,$$

which verifies Assumption 2; together, these prove the second statement.  $\square$

#### A.4 Proof of Theorem 4

In order to prove Theorem 4, we extend the proof for the analogous result for Bayesian inference with an auxiliary likelihood [Drovandi et al., 2015]. Our setup is slightly more general as we do not constraint the update to be defined in terms of a likelihood; notice that the original setup in Drovandi et al. [2015] is recovered when we consider  $S$  being the negative log likelihood, for some auxiliary likelihood.

We recall here for simplicity the useful definitions. We consider the SR posterior:

$$\pi_S(\theta|\mathbf{y}_n) \propto \pi(\theta) \underbrace{\exp \left\{ -w \sum_{i=1}^n S(P_\theta, y_i) \right\}}_{p_S(\mathbf{y}_n|\theta)},$$

Further, we recall the form of the target of the pseudo-marginal MCMC:

$$\pi_{\hat{S}}^{(m)}(\theta|\mathbf{y}_n) \propto \pi(\theta) p_{\hat{S}}^{(m)}(\mathbf{y}_n|\theta),$$

where:

$$\begin{aligned} p_{\hat{S}}^{(m)}(\mathbf{y}_n|\theta) &= \mathbb{E} \left[ \exp \left\{ -w \sum_{i=1}^n \hat{S}(\mathbf{X}_m^{(\theta)}, y_i) \right\} \right] \\ &= \int \exp \left\{ -w \sum_{i=1}^n \hat{S}(\mathbf{x}_m^{(\theta)}, y_i) \right\} \prod_{j=1}^m p(x_j^{(\theta)}|\theta) dx_1 dx_2 \cdots dx_m. \end{aligned}$$

We begin by stating a useful property:

**Lemma 9** (Theorem 3.5 in Billingsley [1999]). *If  $X_n$  is a sequence of uniformly integrable random variables and  $X_n$  converges in distribution to  $X$ , then  $X$  is integrable and  $\mathbb{E}[X_n] \rightarrow \mathbb{E}[X]$  as  $n \rightarrow \infty$ .*

**Remark 8** (Remark 1 in Drovandi et al. [2015]). *A simple sufficient condition for uniform integrability is that for some  $\delta > 0$ :*

$$\sup_n \mathbb{E}[|X_n|^{1+\delta}] < \infty.$$

The result in the main text is the combination of the following two Theorems, which respectively follow Results 1 and 2 in Drovandi et al. [2015]:

**Theorem 6** (Generalizes Result 1 in Drovandi et al. [2015]). *Assume that  $p_{\hat{S}}^{(m)}(\mathbf{y}_n|\theta) \rightarrow p_S(\mathbf{y}_n|\theta)$  as  $m \rightarrow \infty$  for all  $\theta$  with positive prior support; further, assume  $\inf_m \int_{\Theta} p_{\hat{S}}^{(m)}(\mathbf{y}_n|\theta) \pi(\theta) d\theta > 0$  and  $\sup_{\theta \in \Theta} p_S(\mathbf{y}_n|\theta) < \infty$ . Then*

$$\lim_{m \rightarrow \infty} \pi_{\hat{S}}^{(m)}(\theta|\mathbf{y}_n) = \pi_S(\theta|\mathbf{y}_n).$$

*Furthermore, if  $f : \Theta \rightarrow \mathbb{R}$  is a continuous function satisfying  $\sup_m \int_{\Theta} |f(\theta)|^{1+\delta} \pi_S^{(m)}(\theta|\mathbf{y}_n) d\theta < \infty$  for some  $\delta > 0$  then*

$$\lim_{m \rightarrow \infty} \int_{\Theta} f(\theta) \pi_{\hat{S}}^{(m)}(\theta|\mathbf{y}_n) d\theta = \int_{\Theta} f(\theta) \pi_S(\theta|\mathbf{y}_n) d\theta.$$

*Proof.* The first part follows from the fact that the numerator of

$$\pi_{\hat{S}}^{(m)}(\theta|\mathbf{y}_n) = \frac{p_{\hat{S}}^{(m)}(\mathbf{y}_n|\theta) \pi(\theta)}{\int_{\Theta} p_{\hat{S}}^{(m)}(\mathbf{y}_n|\theta) \pi(\theta) d\theta}$$

converges pointwise and the denominator is positive and converges by the bounded convergence theorem.

For the second part, if for each  $m \in \mathbb{N}$ ,  $\theta_m$  is distributed according to  $\pi_{\hat{S}}^{(m)}(\cdot|\mathbf{y}_n)$  and  $\theta$  is distributed according to  $\pi_S(\cdot|\mathbf{y}_n)$  then  $\theta_m$  converges to  $\theta$  in distribution as  $m \rightarrow \infty$  by Scheffé's lemma [Scheffé, 1947]. Since  $f$  is continuous,  $f(\theta_m)$  converges in distribution to  $f(\theta)$  as  $n \rightarrow \infty$  by the continuous mapping theorem and we conclude by application of Remark 8 and Lemma 9.  $\square$

The following gives a convenient way to ensure  $p_{\hat{S}}^{(m)}(\mathbf{y}_n|\theta) \rightarrow p_S(\mathbf{y}_n|\theta)$ :

**Theorem 7** (Generalizes Result 2 in Drovandi et al. [2015]). *Assume that  $\exp\{-w \sum_{i=1}^n \hat{S}(\mathbf{X}_m^{(\theta)}, y_i)\}$  converges in probability to  $p_S(\mathbf{y}_n|\theta)$  as  $m \rightarrow \infty$ . If*

$$\sup_m \mathbb{E} \left[ \left| \exp\left\{-w \sum_{i=1}^n \hat{S}(\mathbf{X}_m^{(\theta)}, y_i)\right\} \right|^{1+\delta} \right] < \infty$$

for some  $\delta > 0$  then  $p_{\hat{S}}^{(m)}(\mathbf{y}_n|\theta) \rightarrow p_S(\mathbf{y}_n|\theta)$  as  $m \rightarrow \infty$ .

*Proof.* The proof follows by applying Remark 8 and Lemma 9.  $\square$

Notice that the convergence in probability of  $\exp\{-w \sum_i \hat{S}(\mathbf{X}_m^{(\theta)}, y_i)\}$  to  $p_S(\mathbf{y}_n|\theta)$  is implied by the convergence in probability of  $\hat{S}(\mathbf{X}_m^{(\theta)}, y_i)$  to  $S(P_\theta, y_i)$  and by the continuity of the exponential function. Therefore, Theorem 4 follows from applying Theorem 7 followed by Theorem 6.

## B Changing data coordinates

We give here some more details on the behavior of the SR posterior when the coordinate system used to represent the data is changed, as mentioned in Remark 3.

**Frequentist estimator** First, we investigate whether the minimum scoring rule estimator (for a strictly proper scoring rule) is affected by a transformation of the data. Specifically, considering a strictly proper  $S$ , we are interested in whether  $\theta_Y^* = \arg \min_{\theta \in \Theta} S(P_\theta^Y, Q_Y) = \arg \min_{\theta \in \Theta} D(P_\theta^Y, Q_Y)$  is the same as  $\theta_Z^* = \arg \min_{\theta \in \Theta} S(P_\theta^Z, Q_Z) = \arg \min_{\theta \in \Theta} D(P_\theta^Z, Q_Z)$ , where  $Z = f(Y) \implies Y \sim Q_Y \iff Z \sim Q_Z$  and  $Y \sim P_\theta^Y \iff Z \sim P_\theta^Z$ . If the model is well specified,  $P_{\theta_Y^*}^Y = Q_Y, P_{\theta_Z^*}^Z = Q_Z \implies \theta_Y^* = \theta_Z^*$ . If the model is misspecified, for a generic SR the minimizer of the expected SR may change according to the parametrization. We remark how this is not a drawback of the frequentist minimum SR estimator but rather a feature, as such estimator is the parameter value corresponding to the model minimizing the chosen expected scoring rule from the data generating process *in that coordinate system*, and is therefore completely reasonable for it to change when the coordinate system is modified.

Notice that a sufficient condition for  $\theta_Y^* = \theta_Z^*$  is  $S(P_\theta^Y, y) = a \cdot S(P_\theta^Z, z) + b$  for  $a > 0, b \in \mathbb{R}$ . This condition is verified when  $S$  is chosen to be the log-score, as in fact:

$$S(P_\theta^Z, f(y)) = -\ln p_Z(f(y)|\theta) = S(P_\theta^Z, y) + \ln |J_f(y)|,$$

where we assumed  $f$  to be a one-to-one function and we applied the change of variable formula to the density  $p_Z$ .

**Generalized Bayesian posterior** For a single observation, let  $\pi_S^Y$  denote the SR posterior conditioned on values of  $Y$ , while  $\pi_S^Z$  denote instead the posterior conditioned on values of  $Z = f(Y)$  for some one-to-one function  $f$ ; in general,  $\pi_S^Y(\theta|y) \neq \pi_S^Z(\theta|f(y))$ . By denoting as  $w_Z$  (respectively  $w_Y$ ) and  $P_\theta^Z$  (respectively  $P_\theta^Y$ ) the weight and model distributions appearing in  $\pi_S^Z$  (resp.  $\pi_S^Y$ ), the equality would in fact require  $w_Z S(P_\theta^Z, f(y)) = w_Y S(P_\theta^Y, y) + C \forall \theta, y$  for some choice of  $w_Z, w_Y$  and for all transformations  $f$ , where  $C$  is a constant in  $\theta$ . Notice that this is satisfied for the standard Bayesian posterior (i.e., with the log-score) with  $w_Z = w_Y = 1$ . Instead, for other scoring rules the above condition cannot be satisfied in general for any choice of  $w_Z, w_Y$ . For instance, consider the kernel SR:

$$S(P_\theta^Z, f(y)) = \mathbb{E}[k(Z, \tilde{Z})] - \mathbb{E}[k(Z, f(y))] = \mathbb{E}[k(f(Y), f(\tilde{Y}))] - \mathbb{E}[k(f(Y), f(y))];$$

for general kernels and functions  $f$ , the above is different from  $S(P_\theta^Y, y) = \mathbb{E}[k(Y, \tilde{Y})] - \mathbb{E}[k(Y, f(x))]$  up to a constant. Therefore, the posterior shape depends on the chosen data coordinates. Considering

the expression for the kernel SR, it is clear that is a consequence of the fact that the likelihood principle is not satisfied (as the kernel SR does not only depend on the likelihood value at the observation). Similar argument holds for the Energy Score posterior as well.

We also remark that this is also the case for BSL [Price et al., 2018], as in that case the model is assumed to be multivariate normal, and changing the data coordinates impacts their normality (in fact it is common practice in BSL to look for transformations of data which yield distribution as close as possible to a normal one).

The theoretical semiBSL posterior [An et al., 2020], instead, is invariant with respect to one-to-one transformation applied independently to each data coordinate, which do not affect the copula structure. Notice however that different data coordinate systems may yield better empirical estimates of the marginal KDEs from model simulations.

## C More details on related techniques

### C.1 Energy Distance

The squared energy distance is a metric between probability distributions [Rizzo and Székely, 2016], and is defined by:

$$D_E^{(\beta)}(P, Q) = 2 \cdot \mathbb{E} \left[ \|X - Y\|_2^\beta \right] - \mathbb{E} \left[ \|X - X'\|_2^\beta \right] - \mathbb{E} \left[ \|Y - Y'\|_2^\beta \right],$$

for  $X \perp\!\!\!\perp X' \sim P$  and  $Y \perp\!\!\!\perp Y' \sim Q$ .

The probabilistic forecasting literature [Gneiting and Raftery, 2007] use a different convention of the energy score and distance, which amounts to multiplying our definitions by  $1/2$ . We follow here the convention used in the statistical inference literature [Rizzo and Székely, 2016, Chérif-Abdellatif and Alquier, 2020, Nguyen et al., 2020].

### C.2 Maximum Mean Discrepancy (MMD)

We follow here Section 2.2 in Gretton et al. [2012]; all proofs of our statements can be found there. Let  $k(\cdot, \cdot) : \mathcal{X} \times \mathcal{X} \rightarrow \mathbb{R}$  be a positive definite and symmetric kernel. Under these conditions, there exists a unique Reproducing kernel Hilbert space (RKHS)  $\mathcal{H}_k$  of real functions on  $\mathcal{X}$  associated to  $k$ .

Now, let's define the Maximum Mean Discrepancy (MMD).

**Definition 1.** Let  $\mathcal{F}$  be a class of functions  $f : \mathcal{X} \rightarrow \mathbb{R}$ ; we define the MMD relative to  $\mathcal{F}$  as:

$$\text{MMD}_{\mathcal{F}}(P, Q) = \sup_{f \in \mathcal{F}} [\mathbb{E}_{X \sim P} f(X) - \mathbb{E}_{Y \sim Q} f(Y)].$$

We will show here how choosing  $\mathcal{F}$  to be the unit ball in an RKHS  $\mathcal{H}_k$  turns out to be computationally convenient, as it allows to avoid computing the supremum explicitly. First, let us define the mean embedding of the distribution  $P$  in  $\mathcal{H}_k$ :

**Lemma 10** (Lemma 3 in Gretton et al. [2012]). *If  $k(\cdot, \cdot)$  is measurable and  $\mathbb{E}_{X \sim P} \sqrt{k(X, X)} < \infty$ , then the mean embedding of the distribution  $P$  in  $\mathcal{H}_k$  is:*

$$\mu_P = \mathbb{E}_{X \sim P} [k(X, \cdot)] \in \mathcal{H}_k.$$

Using this fact, the following Lemma shows that the MMD relative to  $\mathcal{H}_k$  can be expressed as the distance in  $\mathcal{H}_k$  between the mean embeddings:

**Lemma 11** (Lemma 4 in Gretton et al. [2012]). *Assume the conditions in Lemma 10 are satisfied, and let  $\mathcal{F}$  be the unit ball in  $\mathcal{H}_k$ ; then:*

$$\text{MMD}_{\mathcal{F}}^2(P, Q) = \|\mu_P - \mu_Q\|_{\mathcal{H}_k}^2.$$

In general, the MMD is a *pseudo-metric* for probability distributions (i.e., it is symmetric, satisfies the triangle inequality and  $\text{MMD}_{\mathcal{F}}(P, P) = 0$ , Briol et al. 2019). For the probability measures on a compact metric space  $\mathcal{X}$ , the next Lemma states the conditions under which the MMD is a *metric*, which additionally ensures that  $\text{MMD}_{\mathcal{F}}(P, Q) = 0 \implies P = Q$ . Specifically, this holds when the kernel is universal, which requires that  $k(\cdot, \cdot)$  is continuous, and  $\mathcal{H}_k$  being dense in  $C(\mathcal{X})$  with respect to the  $L_\infty$  norm (these conditions are satisfied by the Gaussian and Laplace kernel).

**Lemma 12** (Theorem 5 in Gretton et al. [2012]). *Let  $\mathcal{F}$  be the unit ball in  $\mathcal{H}_k$ , where  $\mathcal{H}_k$  is defined on a compact metric space  $\mathcal{X}$  and has associated continuous kernel  $k(\cdot, \cdot)$ . Then:*

$$\text{MMD}_{\mathcal{F}}(P, Q) = 0 \iff P = Q.$$

This result can be generalized to more general spaces  $\mathcal{X}$ , by considering the notion of characteristics kernel, for which the mean map is injective; it can be shown that the Laplace and Gaussian kernels are characteristics [Gretton et al., 2012], so that MMD for those two kernels is a metric for distributions on  $\mathbb{R}^d$ .

Additionally, the form of MMD for a unit-ball in an RKHS allows easy estimation, as shown next:

**Lemma 13** (Lemma 6 in Gretton et al. [2012]). *Assume that the form for MMD given in Lemma 11 holds; say  $X \perp\!\!\!\perp X' \sim P$ ,  $Y \perp\!\!\!\perp Y' \sim Q$ , and let  $\mathcal{F}$  be the unit ball in  $\mathcal{H}_k$ . Then, you can write:*

$$\text{MMD}_{\mathcal{F}}^2(P, Q) = \mathbb{E}[k(X, X')] + \mathbb{E}[k(Y, Y')] - 2\mathbb{E}[k(X, Y)].$$

In the main body of this work (Section 2.1), we denoted the squared MMD by  $D_k(P, Q)$ .

### C.2.1 Equivalence between MMD-Bayes posterior and $\pi_{S_k}$

Chérif-Abdellatif and Alquier [2020] considered the following posterior, termed MMD-Bayes:

$$\pi_{\text{MMD}}(\theta | \mathbf{y}_n) \propto \pi(\theta) \exp \left\{ -\beta \cdot D_k \left( P_\theta, \hat{P}_n \right) \right\}$$

where  $\beta > 0$  is a temperature parameter and  $D_k \left( P_\theta, \hat{P}_n \right)$  denotes the squared MMD between the empirical measure of the observations  $\hat{P}_n = \frac{1}{n} \sum_{i=1}^n \delta_{y_i}$  and the model distribution  $P_\theta$ .

From the properties of MMD (see Appendix C.2), notice that:

$$\begin{aligned} D_k \left( P_\theta, \hat{P}_n \right) &= \mathbb{E}_{X, X' \sim P_\theta} k(X, X') + \frac{1}{n^2} \sum_{i,j=1}^n k(y_i, y_j) - \frac{2}{n} \sum_{i=1}^n \mathbb{E}_{X \sim P_\theta} k(X, y_i) \\ &= \frac{1}{n} \left( n \cdot \mathbb{E}_{X, X' \sim P_\theta} k(X, X') - 2 \sum_{i=1}^n \mathbb{E}_{X \sim P_\theta} k(X, y_i) \right) + \frac{1}{n^2} \sum_{i,j=1}^n k(y_i, y_j) \\ &= \frac{1}{n} \left( \sum_{i=1}^n S_k(P_\theta, y_i) \right) + \frac{1}{n^2} \sum_{i,j=1}^n k(y_i, y_j), \end{aligned}$$

where we used the expression of the SR scoring rule  $S_k$ , and where the second term is independent on  $\theta$ . Therefore, the MMD-Bayes posterior is equivalent to the SR posterior with kernel scoring rule  $S_k$ , by identifying  $w = \beta/n$ .

### C.3 Semi-Parametric Synthetic Likelihood

We discuss here in more details the semiBSL approach An et al. [2020], introduced in the main body in Sec. 3.

**Copula theory** First, recall that a copula is a multivariate Cumulative Density Function (CDF) such that the marginal distribution for each variable is uniform on the interval  $[0, 1]$ . Consider now a multivariate random variable  $X = (X^1, \dots, X^d)$ , for which the marginal CDFs are denoted by  $F_j(x) = \mathbb{P}(X^j < x)$ ; then, the multivariate random variable built as:

$$(U^1, U^2, \dots, U^d) = (F_1(X^1), F_2(X^2), \dots, F_d(X^d))$$

has uniform marginals on  $[0, 1]$ .

Sklar's theorem exploits copulas to decompose the density  $h$  of  $X^6$ ; specifically, it states that the following decomposition is valid:

$$h(x^1, \dots, x^d) = c(F_1(x^1), \dots, F_d(x^d)) f_1(x^1) \cdots f_d(x^d),$$

where  $f_j$  is the marginal density of the  $j$ -th coordinate, and  $c$  is the density of the copula.

We now review definition and properties of the Gaussian copula, which is defined by a correlation matrix  $R \in [-1, 1]^{d \times d}$ , and has cumulative density function:

$$C_R(u) = \Phi_R(\Phi^{-1}(u^1), \dots, \Phi^{-1}(u^d)),$$

where  $\Phi^{-1}$  is the inverse cdf (quantile function) of a standard normal, and  $\Phi_R$  is the cdf of a multivariate normal with covariance matrix  $R$  and 0 mean. If you define as  $U$  the random variable which is distributed according to  $C_R$ , it can be easily seen that  $R$  is the covariance matrix of the multivariate normal random variable  $Z = \Phi^{-1}(U)$ , where  $\Phi^{-1}$  is applied element-wise. In fact:

$$P(Z \leq \eta) = P(U \leq \Phi(\eta)) = C_R(\Phi(\eta)) = \Phi_R(\eta),$$

where the inequalities are intended component-wise.

By defining as  $\eta$  a  $d$ -vector with components  $\eta^k = \Phi^{-1}(u^k)$ , the Gaussian copula density is:

$$c_R(u) = \frac{1}{\sqrt{|R|}} \exp \left\{ -\frac{1}{2} \eta^\top (R^{-1} - \mathbf{I}_d) \eta \right\},$$

where  $\mathbf{I}_d$  is a  $d$ -dimensional identity matrix, and  $|\cdot|$  denotes the determinant.

**Semiparametric Bayesian Synthetic Likelihood (semiBSL)** The semiBSL approach assumes that the likelihood for the model has a Gaussian copula; therefore, the likelihood for a single observation  $y$  can be written as:

$$p_{\text{semiBSL}}(y|\theta) = c_{R_\theta}(F_{\theta,1}(y^1), \dots, F_{\theta,d}(y^d)) \prod_{k=1}^d f_{\theta,k}(y^k),$$

where  $y^k$  is the  $k$ -th component of  $y$ ,  $f_{\theta,k}$  is the marginal density of the  $k$ -th component and  $F_{\theta,k}$  is the CDF of the  $k$ -th component.

In order to obtain an estimate for it, we exploit simulations from  $P_\theta$  to estimate  $R_\theta$ ,  $f_{\theta,k}$  and  $F_{\theta,k}$ ; this leads to:

$$\begin{aligned} \hat{p}_{\text{semiBSL}}(y|\theta) &= c_{\hat{R}_\theta}(\hat{F}_{\theta,1}(y^1), \dots, \hat{F}_{\theta,d}(y^d)) \prod_{k=1}^d \hat{f}_{\theta,k}(y^k) \\ &= \frac{1}{\sqrt{|\hat{R}_\theta|}} \exp \left\{ -\frac{1}{2} \hat{\eta}_y^\top (\hat{R}_\theta^{-1} - \mathbf{I}_d) \hat{\eta}_y \right\} \prod_{k=1}^d \hat{f}_{\theta,k}(y^k), \end{aligned}$$

where  $\hat{f}_{\theta,k}$  and  $\hat{F}_{\theta,k}$  are estimates for  $f_{\theta,k}$  and  $F_{\theta,k}$ ,  $\hat{\eta}_y = (\hat{\eta}_y^1, \dots, \hat{\eta}_y^d)$ ,  $\hat{\eta}_y^k = \Phi^{-1}(\hat{u}^k)$ ,  $\hat{u}^k = \hat{F}_{\theta,k}(y^k)$ . Moreover,  $\hat{R}_\theta$  is an estimate of the correlation matrix.

---

<sup>6</sup>Provided that the density exists in the first place; a more general version of Sklar's theorem is concerned with general random variables, but we restrict here to the case where densities are available.



We discuss now how the different quantities are estimated. First, a Kernel Density Estimate (KDE) is used for the marginals densities and cumulative density functions. Specifically, given samples  $x_1, \dots, x_m \sim P_\theta$ , a KDE estimate for the  $k$ -th marginal density is:

$$\hat{f}_{\theta,k}(y^k) = \frac{1}{m} \sum_{j=1}^m K_h(y^k - x_j^k),$$

where  $K_h$  is a normalized kernel which is chosen to be Gaussian in the original implementation [An et al., 2020]. The CDF estimates are obtained by integrating the KDE density.

Next, for estimating the correlation matrix, An et al. [2020] proposed to use a robust procedure based on the ranks (grc, Gaussian rank correlation, Boudt et al., 2012); specifically, given  $m$  simulations  $x_1, \dots, x_m \sim P_\theta$ , the estimate for the  $(k, l)$ -th entry of  $R_\theta$  is given by:

$$[\hat{R}_\theta^{\text{grc}}]_{k,l} = \frac{\sum_{j=1}^m \Phi^{-1}\left(\frac{r(x_j^k)}{m+1}\right) \Phi^{-1}\left(\frac{r(x_j^l)}{m+1}\right)}{\sum_{j=1}^m \Phi^{-1}\left(\frac{j}{m+1}\right)^2},$$

where  $r(\cdot) : \mathbb{R} \rightarrow \mathcal{A}$ , where  $\mathcal{A} = \{1, \dots, m\}$  is the rank function.

**Copula scoring rule** Finally, we write down the explicit expression of the copula scoring rule  $S_{Gc}$ , associated to the Gaussian copula. We show that this is a proper, but not strictly so, scoring rule for copula distributions. Specifically, let  $C$  be a distribution for a copula random variable, and let  $u \in [0, 1]^d$ . We define:

$$S_{Gc}(C, u) = \frac{1}{2} \log |R_C| + \frac{1}{2} (\Phi^{-1}(u))^T (R_C^{-1} - \mathbf{I}_d) \Phi^{-1}(u),$$

where  $\Phi^{-1}$  is applied element-wise to  $u$ , and  $R_C$  is the correlation matrix associated to  $C$  in the following way: define the copula random variable  $V \sim C$  and its transformation  $\Phi^{-1}(V)$ ; then,  $\Phi^{-1}(V)$  will have a multivariate normal distribution with mean 0 and covariance matrix  $R_C$ .

Similarly to the Dawid-Sebastiani score (see Sec. 2.1), this scoring rule is proper but not strictly so as it only depends on the first 2 moments of the distribution of the random variable  $\Phi^{-1}(V)$  (the first one being equal to 0). To show this, assume the copula random variable  $U$  has an exact distribution  $Q$  and consider the expected scoring rule:

$$S_{Gc}(C, Q) = \mathbb{E}_{U \sim Q} S_{Gc}(C, U) = \frac{1}{2} \log |R_C| + \mathbb{E}_{U \sim Q} \left[ (\Phi^{-1}(U))^T (R_C^{-1} - \mathbf{I}_d) \Phi^{-1}(U) \right];$$

now, notice that  $\Phi^{-1}(U)$  is a multivariate normal distribution whose marginals are standard normals. Therefore, let us denote as  $R_Q$  the covariance matrix of  $\Phi^{-1}(U)$ , which is a correlation matrix. From the well-known form for the expectation of a quadratic form<sup>7</sup>, it follows that:

$$\begin{aligned} S_{Gc}(C, Q) &= \frac{1}{2} \log |R_C| + \frac{1}{2} \text{Tr} [(R_C^{-1} - \mathbf{I}_d) \cdot R_Q] \\ &= \frac{1}{2} \log |R_C| + \frac{1}{2} \text{Tr} [R_C^{-1} \cdot R_Q] - \frac{1}{2} \text{Tr} [R_Q] \\ &= \underbrace{\frac{1}{2} \left\{ \log \frac{|R_C|}{|R_Q|} - d + \text{Tr} [R_C^{-1} \cdot R_Q] \right\}}_{D_{KL}(Z_Q \| Z_C)} + \frac{1}{2} \log |R_Q| + \frac{d}{2} - \frac{1}{2} \text{Tr} [R_Q], \end{aligned}$$

where  $D_{KL}(Z_Q \| Z_C)$  is the KL divergence between two multivariate normal distributions  $Z_Q$  and  $Z_C$  of dimension  $d$ , with mean 0 and covariance matrix  $R_Q$  and  $R_C$  respectively. Further, notice that the remaining factors do not depend on the distribution  $C$ . Therefore,  $S_{Gc}(C, Q)$  is minimized whenever  $R_C$  is equal to  $R_Q$ ; this happens when  $C = Q$ , but also for all other choices of  $C$  which share the associated covariance matrix with  $Q$ . This implies that the Gaussian copula score is a proper, but not strictly so, scoring rule for copula distributions.

<sup>7</sup> $\mathbb{E} [X^T \Lambda X] = \text{tr} [\Lambda \Sigma] + \mu^T \Lambda \mu$ , for a symmetric matrix  $\Lambda$ , and where  $\mu$  and  $\Sigma$  are the mean and covariance matrix of  $X$  (which in general does not need to be normal, but only needs to have well defined second moments).

## C.4 Ratio estimation

We discuss here in more details the Ratio Estimation approach by Thomas et al. [2020], introduced in the main body in Sec. 3. In doing so, we also relax the assumption of having the same number of simulations in both datasets (which we used in the main body for ease of exposition).

Specifically, recall that logistic regression, given a function  $h$ , a predictor  $x$  and a response  $t \in \{0, 1\}$ , approximates the probability of the predictor being 1 as:

$$\Pr(T = 1|X = x; h) = \frac{1}{1 + \exp(-h(x))}. \quad (19)$$

Then, considering a training dataset of  $m_0$  elements  $\{x_j^{(0)}\}_{j=1}^{m_0}$  belonging to class 0 and  $m_1$  elements  $\{x_j^{(1)}\}_{j=1}^{m_1}$  belonging to class 1, the function  $h$  corresponding to the best classifier is determined by minimizing the cross entropy loss:

$$J_{\mathbf{m}}(h) = \frac{1}{m_0 + m_1} \left\{ \sum_{j=1}^{m_1} \log [1 + \exp(-h(x_j^{(1)}))] + \sum_{j=1}^{m_0} \log [1 + \exp(h(x_j^{(0)}))] \right\},$$

where  $\mathbf{m} = (m_0, m_1)$ .

In the setup of interest to the main body of this paper and for a fixed  $\theta$ , class 1 is associated to being sampled from the marginal  $p(\cdot|\theta)$  and class 0 to being sampled from  $p(\cdot)$ , which implies that  $X|T = 1 \sim p(\cdot|\theta)$  and  $X|T = 0 \sim p(\cdot)$ .

We will consider the setting in which  $m_1, m_0 \rightarrow \infty$  but such that the limit of their ratio is a constant  $\nu = \lim m_1/m_0$  which is equal to the ratio of prior probability  $\frac{P(T=1)}{P(T=0)}$ . In this limit case, we want to show that the minimizer of  $J_{\mathbf{m}}(h)$  over all scalar functions of  $\mathcal{X}$  is  $h^*(x) = \log r(x; \theta) + \log \nu$ , as long as the minimization of  $J$  is performed under the full set of functions  $h$ ; an alternative proof for this fact is given in Thomas et al. [2020].

We proceed in two steps: first, we show how  $\Pr(T = 1|X = x; h^*) = \Pr(T = 1|X = x)$ ; secondly, we use that fact to show that  $h^*(x) = \log r(x; \theta) + \log \nu$ .

Let us denote now  $g(h(X)) = \Pr(T = 1|X = x; h)$ . For the first part, we proceed by rewriting the objective in the infinite data limit as:

$$\begin{aligned} J(h) &= \mathbb{E}_{X,T}[-T \log g(h(X)) - (1 - T) \log(1 - g(h(X)))] \\ &= \mathbb{E}_X \mathbb{E}_{T|X}[-T \log g(h(X)) - (1 - T) \log(1 - g(h(X)))]. \end{aligned}$$

For fixed  $X$ ,  $g(h(X))$  is a probability value between  $(0, 1)$ .  $[-T \log g(h(X)) - (1 - T) \log(1 - g(h(X)))]$  is the logarithmic score for the binary variable  $T$ , which is a strictly proper scoring rule (see Example 3 in Gneiting and Raftery [2007]). Therefore,

$$\mathbb{E}_{T|X}[-T \log g(h(X)) - (1 - T) \log(1 - g(h(X)))]$$

is minimized for each fixed  $X$  whenever  $g(h(x)) = P(T = 1|X = x)$ , and the overall  $J(h)$  is minimized when the inner expectation is minimized for each value of  $X$ , so that  $h^*$  is such that

$$\Pr(T = 1|X = x; h^*) = \Pr(T = 1|X = x).$$

For the second part, let's now consider:

$$\begin{aligned} P(T = 1|X = x) &= \frac{\overbrace{p(X = x|T = 1)}^{p(x|\theta)} P(T = 1)}{p(X = x|T = 1)P(T = 1) + p(X = x|T = 0)P(T = 0)} \\ &= \frac{p(x|\theta)P(T = 1)}{p(X = x|T = 1)P(T = 1) + p(X = x|T = 0)P(T = 0)}, \end{aligned}$$

$$\begin{aligned}
P(T = 0|X = x) &= \frac{\overbrace{p(X = x|T = 0)}^{p(x)} P(T = 0)}{p(X = x|T = 1)P(T = 1) + p(X = x|T = 0)P(T = 0)} \\
&= \frac{p(x)P(T = 0)}{p(X = x|T = 1)P(T = 1) + p(X = x|T = 0)P(T = 0)}.
\end{aligned}$$

Moreover, the definition in Eq. (19) implies that:

$$h(x) = \log \frac{P(T = 1|X = x; h)}{P(T = 0|X = x; h)},$$

Therefore, by performing logistic regression in the infinite data limit, we get that:

$$h^*(x) = \log \frac{P(T = 1|X = x; h^*)}{P(T = 0|X = x; h^*)} = \log \frac{P(X = x|T = 1)}{P(X = x|T = 0)} + \log \frac{P(T = 1)}{P(T = 0)} = \log \frac{p(x|\theta)}{p(x)} + \log \nu,$$

which concludes our proof, with  $\nu = \frac{P(T=1)}{P(T=0)}$ .

## D Tuning the bandwidth of the Gaussian kernel

Consider the Gaussian kernel:

$$k(x, y) = \exp \left( -\frac{\|x - y\|_2^2}{2\gamma^2} \right);$$

inspired by Park et al. [2016], we fix the bandwidth  $\gamma$  with the following procedure:

1. Simulate a value  $\theta_j \sim \pi(\theta)$  and a set of samples  $x_{jk} \sim P_{\theta_j}$ , for  $k = 1, \dots, m_\gamma$ .
2. Estimate the median of  $\{\|x_{jk} - x_{jl}\|_2\}_{kl}^{m_\gamma}$  and call it  $\hat{\gamma}_j$ .
3. Repeat points 1) and 2) for  $j = 1, \dots, m_{\theta, \gamma}$ .
4. Set the estimate for  $\gamma$  as the median of  $\{\hat{\gamma}_j\}_{j=1}^{m_{\theta, \gamma}}$ .

Empirically, we use  $m_{\theta, \gamma} = 1000$  and we set  $m_\gamma$  to the corresponding value of  $m$  for the different models.

## E Further details on simulation studies reported in the main text

Across most experiments, we use correlated pseudo-marginal MCMC with independent normal proposals on each component of the parameter space; in those cases, we indicate by  $\sigma$  the standard deviation of the normal proposal distribution, which we report below. For the Recruitment, Boom and Bust model, we use instead a multivariate normal proposal in the MCMC, whose covariance matrix  $\Sigma$  is reported below (Appendix E.4).

In all cases, whenever the parameter space is bounded, we run MCMC on a transformed unbounded space obtained via a logistic transformation. Therefore, the proposal sizes refer to that unbounded space.

### E.1 The g-and-k model

#### E.1.1 Additional experimental details for well specified setup

We report here additional experimental details on the g-and-k model experiments (Sec. 4.1.1).

First, we discuss settings for the SR posteriors:

- For the Energy Score posterior, our heuristic procedure (Sec. 2.4) for setting  $w$  using BSL as a reference resulted in  $w \approx 0.35$  for the univariate model and  $w \approx 0.16$  for the multivariate one.

- For the Kernel Score posterior, we first fit the value of the Gaussian kernel bandwidth parameter as described in Appendix D, which resulted in  $\gamma \approx 5.50$  for the univariate case and  $\gamma \approx 52.37$  for the multivariate one. Then, the heuristic procedure for  $w$  using BSL as a reference resulted in  $w \approx 18.30$  for the univariate model and  $w \approx 52.29$  for the multivariate one.

Next, we discuss the proposal sizes for MCMC; recall that we use independent normal proposals on each component of  $\theta$ , with standard deviation  $\sigma$ . We report here the values for  $\sigma$  used in the experiments; we stress that, as the MCMC is run in the transformed unbounded parameter space (obtained applying a logit transformation), these proposal sizes refer to that space.

For the univariate g-and-k, the proposal sizes we use are the following:

- For BSL, we use  $\sigma = 1$  for all values of  $n$ .
- For Energy and Kernel Scores, we take  $\sigma = 1$  for  $n$  from 1 up to 25 (included),  $\sigma = 0.4$  for  $n$  from 30 to 50, and  $\sigma = 0.2$  for  $n$  from 55 to 100.

For the multivariate g-and-k:

- For BSL and semiBSL, we use  $\sigma = 1$  for all values of  $n$  for which the chain converges. We stress that we tried decreasing the proposal size, but that did not solve the non-convergence issue (discussed in the main text in Sec. 4.1.1).
- For Energy and Kernel Scores, we take  $\sigma = 1$  for  $n$  from 1 up to 15 (included),  $\sigma = 0.4$  for  $n$  from 20 to 35,  $\sigma = 0.2$  for  $n$  from 40 to 50 and  $\sigma = 0.1$  for  $n$  from 55 to 100.

In Table 2, we report the acceptance rates the different methods achieve for all values of  $n$ , with the proposal sizes mentioned above. We denote by “/” the experiments for which we did not manage to run MCMC satisfactorily. We remark how the Energy Score achieves a larger acceptance rates in all experiments compared to the Kernel Score.

### E.1.2 Poor MCMC performance for BSL and semiBSL

As discussed in the main text (Sec. 4.1.1), the correlated pseudo-marginal MCMC for BSL and semiBSL performed poorly for the multivariate g-and-k example, not being able to converge when using more than respectively 1 and 10 observations. In order to shed light on the reason for this behavior, we fix  $n = 20$  and run MCMC with 10 different initializations, for 10000 MCMC steps with no burn-in, for BSL and semiBSL, with  $m = 500$ . For all runs, we found that, after a short transient, the different chains get stuck in different parameter values and have very “sticky” behavior. The results can be seen in Fig. 9.

In order to understand the reason for this result, we investigate whether the poor performance is due to large variance in the estimate of the target; as increasing the number of simulations reduces such variance, we study the effect of this on the MCMC performance. Therefore, we report here the results of a study increasing the number of simulations for a fixed number of observations  $n = 20$  for the g-and-k model. Specifically, we tested  $m = 500, 1000, 1500, 2000, 2500, 3000, 30000$ ; as discussed in Appendix E.1.1, we used a proposal size  $\sigma = 0.4$ , with which the Energy and Kernel Score posteriors performed well. We report traceplots in Fig. 10 and corresponding acceptance rates in Table 3; from this experiment, we note that BSL achieves acceptance rate as large as few percentage points with larger  $m$  values, but there is no constant trend (for instance, acceptance rate with  $m = 3000$  is smaller than with  $m = 2000$ ), which means that the method is still prone to getting stuck. For semiBSL, the acceptance rate is abysmal even for very large  $m$ .

### E.1.3 Additional experimental details for misspecified setup

We report here additional experimental details on the misspecified g-and-k model experiments, where the observations were generated by a Cauchy distribution (Sec. 4.1.2).

In order to have coherent results with respect to the well specified case, we use here the values of  $w$  and  $\gamma$  determined in the well specified case (reported in Appendix E.1.1)

N. obs.	Univariate g-and-k			Multivariate g-and-k			
	BSL	Kernel Score	Energy Score	BSL	semiBSL	Kernel Score	Energy Score
1	0.362	0.507	0.420	0.216	0.190	0.468	0.445
5	0.221	0.329	0.375	0.069	/	0.136	0.224
10	0.133	0.252	0.272	0.036	/	0.127	0.216
15	0.109	0.253	0.217	/	/	0.077	0.154
20	0.100	0.154	0.207	/	/	0.151	0.278
25	0.092	0.149	0.208	/	/	0.126	0.233
30	0.085	0.218	0.343	/	/	0.124	0.222
35	0.080	0.172	0.315	/	/	0.076	0.166
40	0.076	0.152	0.293	/	/	0.119	0.246
45	0.070	0.130	0.256	/	/	0.103	0.223
50	0.062	0.121	0.220	/	/	0.103	0.219
55	0.060	0.189	0.317	/	/	0.139	0.297
60	0.059	0.185	0.324	/	/	0.129	0.286
65	0.057	0.173	0.314	/	/	0.133	0.273
70	0.052	0.172	0.289	/	/	0.119	0.256
75	0.048	0.161	0.273	/	/	0.123	0.247
80	0.048	0.159	0.267	/	/	0.117	0.233
85	0.045	0.150	0.252	/	/	0.098	0.213
90	0.044	0.143	0.247	/	/	0.087	0.198
95	0.044	0.136	0.244	/	/	0.089	0.198
100	0.042	0.129	0.236	/	/	0.076	0.190

Table 2: Acceptance rates for the univariate and multivariate g-and-k experiments with different values of  $n$ , with the MCMC proposal sizes reported in Appendix E.1.1. “/” denotes experiments for which MCMC did not run satisfactorily.

N. simulations $m$	500	1000	1500	2000	2500	3000	30000
Acc. rate BSL	$6.0 \cdot 10^{-3}$	$1.1 \cdot 10^{-2}$	$3.3 \cdot 10^{-2}$	$9.9 \cdot 10^{-3}$	$1.8 \cdot 10^{-2}$	$7.5 \cdot 10^{-3}$	$5.1 \cdot 10^{-2}$
Acc. rate semiBSL	$7.0 \cdot 10^{-3}$	$3.4 \cdot 10^{-3}$	$3.7 \cdot 10^{-3}$	$2.8 \cdot 10^{-3}$	$4.2 \cdot 10^{-3}$	$3.6 \cdot 10^{-3}$	$9.2 \cdot 10^{-3}$

Table 3: Acceptance rates for BSL and semiBSL and BSL for  $n = 20$  using different number of simulations  $m$ ; there is no improvement in the acceptance rate for increasing number of simulations. We recall that we were not able to run semiBSL for  $m = 30000$  due to its high computational cost.

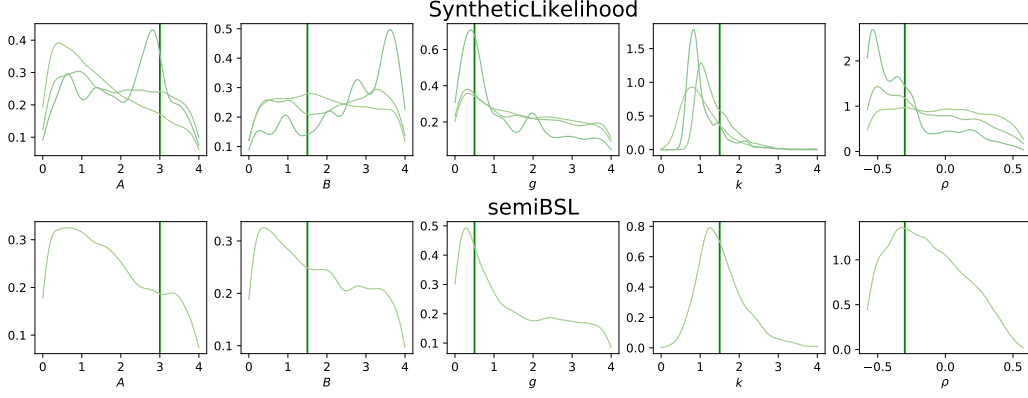


Figure 8: Marginal posterior distributions for the different parameters for the well specified multivariate g-and-k model. For BSL, we were able to run the inference for  $n = 1, 5, 10$ , while we were only able to do so for  $n = 1$  for semiBSL. Darker (respectively lighter) colors denote a larger (smaller) number of observations. The densities are obtained by KDE on the MCMC output thinned by a factor 10.

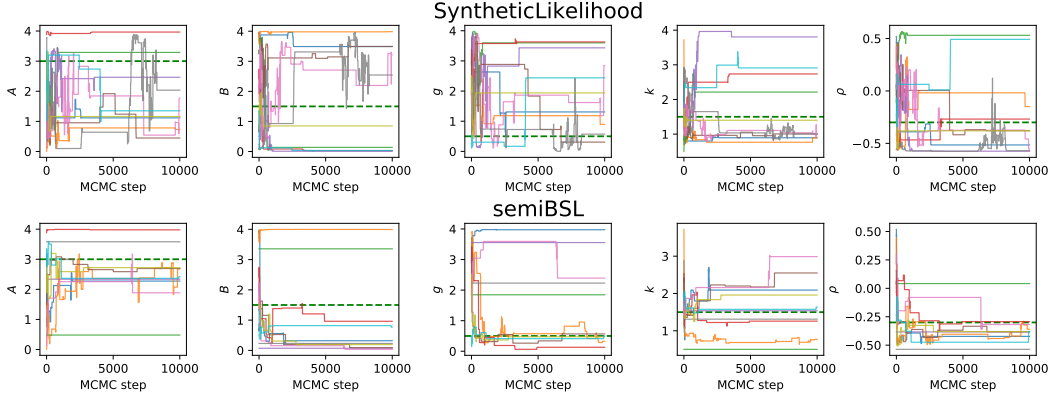


Figure 9: Traceplots for semiBSL and BSL for  $n = 20$  for 10 different initializations (different colors), with 10000 MCMC steps (no burn-in); the green dashed line denotes the true parameter value. It can be seen that the chains are very sticky, and that they explore different parts of the parameter space.

Next, we discuss the proposal sizes for MCMC (which is run with independent normal proposals on each component of  $\theta$  with standard deviation  $\sigma$ , in the same way as in the well specified case, after applying a logit transformation to the parameter space).

- For the univariate g-and-k, for all methods (BSL, Energy and Kernel Scores), we take  $\sigma = 1$  for  $n$  from 1 up to 25 (included),  $\sigma = 0.4$  for  $n$  from 30 to 50, and  $\sigma = 0.2$  for  $n$  from 55 to 100.
- For the multivariate g-and-k, recall that we did not report results for BSL and semiBSL here as we were not able to sample the posteriors with MCMC for large  $n$ , as already experienced in the well specified case. For the remaining techniques, we used the same values of  $\sigma$  as in the well specified experiments (Appendix E.1.3).

In Table 4, we report the acceptance rates the different methods achieve for all values of  $n$ , with the proposal sizes discussed above. We remark how the Energy Score achieves a larger acceptance rates in all experiments compared to the Kernel Score.

## E.2 Additional details on misspecified normal location model

As mentioned in the main text (Sec. 4.2.1), we set the weight  $w$  such that the variance achieved by our SR posteriors is approximately the same as the one achieved by the standard Bayes distribution for the well specified case ( $\epsilon = 0$ ). This resulted in  $w = 1$  for the Energy Score posterior and  $w = 2.8$

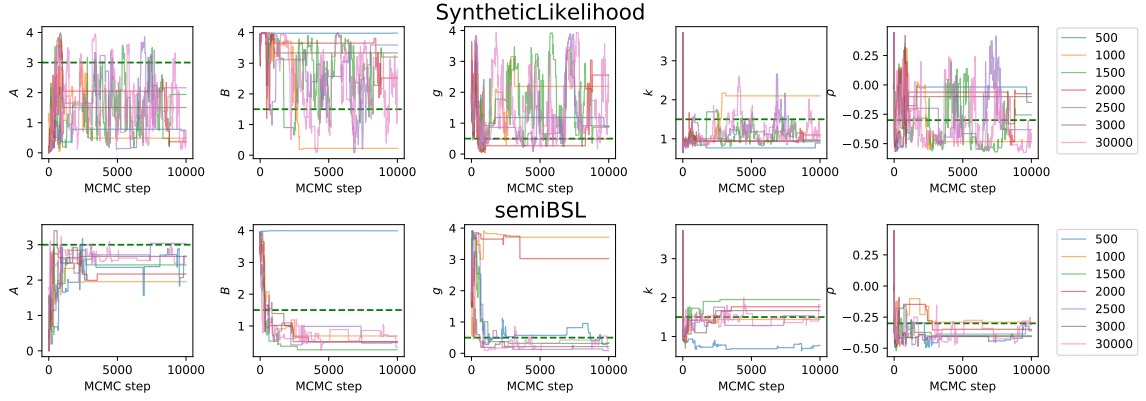


Figure 10: Traceplots for BSL and semiBSL and BSL for  $n = 20$  using different number of simulations  $m$ , reported in the legend for each row; green dashed line denotes the true parameter value. There is no improvement in the mixing of the chain for increasing the number of simulations.

N. obs.	Misspecified univariate g-and-k			Misspecified multivariate g-and-k	
	BSL	Kernel Score	Energy Score	Kernel Score	Energy Score
1	0.457	0.482	0.521	0.472	0.470
5	0.302	0.436	0.454	0.324	0.373
10	0.193	0.450	0.425	0.362	0.330
15	0.146	0.441	0.390	0.361	0.276
20	0.102	0.264	0.311	0.544	0.410
25	0.093	0.288	0.314	0.530	0.377
30	0.153	0.426	0.471	0.536	0.359
35	0.144	0.349	0.448	0.537	0.336
40	0.134	0.340	0.440	0.631	0.432
45	0.130	0.344	0.429	0.523	0.373
50	0.125	0.255	0.393	0.383	0.343
55	0.167	0.318	0.501	0.471	0.436
60	0.176	0.303	0.490	0.412	0.407
65	0.164	0.293	0.481	0.389	0.391
70	0.164	0.276	0.455	0.372	0.374
75	0.156	0.272	0.445	0.278	0.329
80	0.157	0.262	0.436	0.232	0.306
85	0.153	0.254	0.430	0.247	0.300
90	0.147	0.231	0.415	0.239	0.299
95	0.152	0.226	0.410	0.235	0.291
100	0.141	0.223	0.407	0.232	0.277

Table 4: Acceptance rates for the misspecified univariate and multivariate g-and-k experiments with different values of  $n$ , with the MCMC proposal sizes reported in Appendix E.1.3.

for the Kernel Score posterior. Additionally, the bandwidth for the Gaussian kernel was tuned to be  $\gamma \approx 0.9566$  (with the strategy discussed in Appendix D).

In Figure 11 we report the full set of posterior distributions for the different values of  $\epsilon$  and  $z$  obtained with the standard Bayes posterior and with our SR posteriors.

In the MCMC with the SR posteriors, a proposal size  $\sigma = 2$  is used for all values of  $\epsilon$  and  $z$ . For all experiments, Table 5 reports acceptance rates obtained with the SR posteriors, while Table 6 reports the obtained posterior standard deviation with SR posteriors and for the standard Bayes distribution (for which we do not give the proposal size and acceptance rate as it was sampled using more advanced

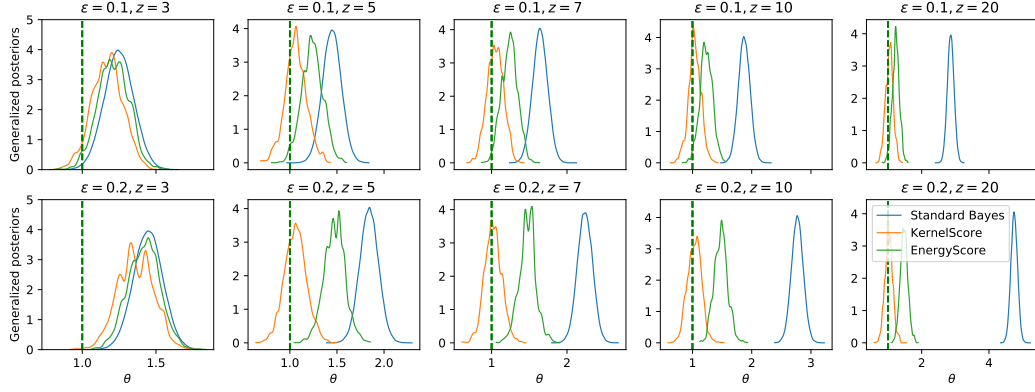


Figure 11: Posterior distribution obtained with the Scoring Rules and exact Bayes for the misspecified normal location model; each panel represents a different choice of  $\epsilon$  and  $z$ . It can be seen that both Kernel and Energy score are more robust with respect to Standard Bayes, with the Kernel Score one being extremely robust. The densities are obtained by KDE on the MCMC output thinned by a factor 10.

MCMC techniques than standard Metropolis-Hastings using the PyMC3 library [Salvatier et al., 2016]).

Setup	$\epsilon = 0$	$\epsilon = 0.1$					$\epsilon = 0.2$				
	-	$z = 3$	$z = 5$	$z = 7$	$z = 10$	$z = 20$	$z = 3$	$z = 5$	$z = 7$	$z = 10$	$z = 20$
<b>Kernel Score</b>	0.076	0.086	0.089	0.085	0.086	0.087	0.080	0.086	0.089	0.091	0.090
<b>Energy Score</b>	0.076	0.084	0.087	0.082	0.083	0.085	0.082	0.079	0.077	0.082	0.082

Table 5: Acceptance rates for MCMC targeting the Energy and Kernel Score posteriors for the different outlier setups, for the misspecified normal location model.

Setup	$\epsilon = 0$	$\epsilon = 0.1$					$\epsilon = 0.2$				
	-	$z = 3$	$z = 5$	$z = 7$	$z = 10$	$z = 20$	$z = 3$	$z = 5$	$z = 7$	$z = 10$	$z = 20$
<b>Standard Bayes</b>	0.100	0.100	0.099	0.099	0.099	0.100	0.099	0.099	0.100	0.099	0.099
<b>Kernel Score</b>	0.101	0.106	0.114	0.108	0.105	0.113	0.121	0.116	0.113	0.117	0.116
<b>Energy Score</b>	0.098	0.105	0.112	0.106	0.106	0.107	0.109	0.112	0.111	0.114	0.113

Table 6: Obtained posterior standard deviation for the standard Bayes and the Energy and Kernel Score posteriors, for the different outlier setups, for the misspecified normal location model.

Finally, as mentioned in the main text (Sec. 4.2.1), we attempted using BSL in this scenario. As the model is Gaussian, we expected the BSL posterior to be very close to the standard posterior. Indeed, this is what we observed in the well specified case and for small  $z$  (Figure 12). When however  $z$  is increased, the MCMC targeting the BSL posterior does not perform satisfactorily (see the trace plots in Figure 13). Neither reducing the proposal size nor running the chain for a longer number of steps seems to solve this issues, which reminds of the issue discussed in Sec. 4.1.

### E.3 Additional details on the Lorenz96 model experiments

As discussed in the main text, we consider observations from two parameter values here; Figure 14 shows the trajectory of some the simulations from  $\theta^*$  (blue) and from  $\theta^{\text{out}}$  (red).

For the Kernel Score posterior with the Gaussian Kernel, we first fit the value of the bandwidth of the Gaussian kernel as described in Appendix D, which resulted in  $\gamma \approx 0.8610$ .

Next, we used our heuristic procedure (Sec.2.4) to tune the value of the weight  $w$  for both the



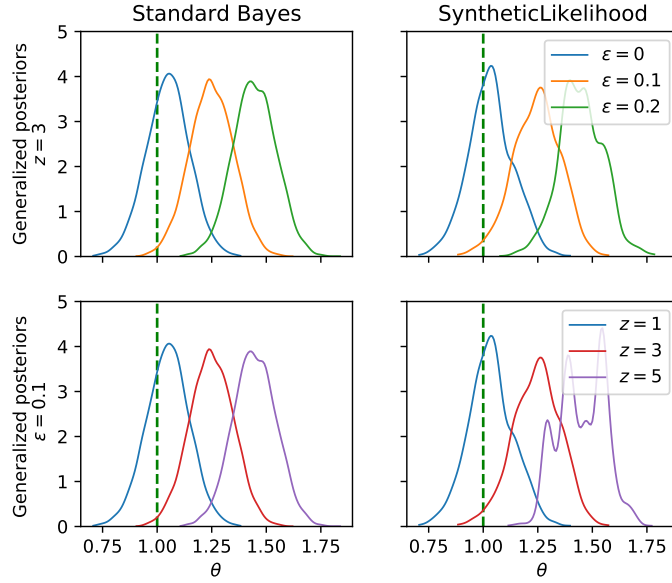


Figure 12: Standard Bayes and BSL posteriors for the normal location model, for different choices of  $\epsilon$  and  $z$ . First row: fixed outliers location  $z = 3$  and varying proportion  $\epsilon$ ; second row: fixed outlier proportion  $\epsilon$ , varying location  $z$ . As expected, the BSL posterior is very close to the standard Bayes posterior. The densities are obtained by KDE on the MCMC output thinned by a factor 10.

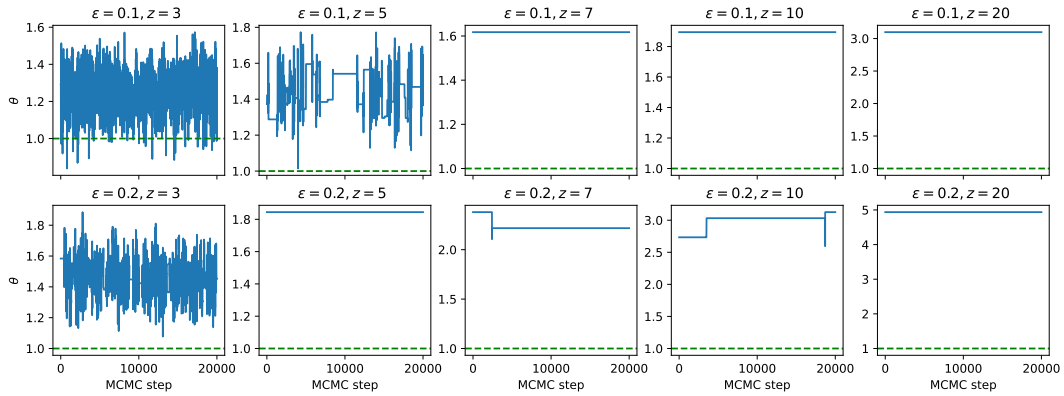


Figure 13: Trace plots for MCMC targeting the BSL posterior with different choices of  $z$  and  $\epsilon$ , for the misspecified normal location model. We used here proposal size  $\sigma = 2$  and 60000 MCMC steps, of which 40000 were burned in; reducing the proposal size or increasing the number of steps did not seem to solve this issue.

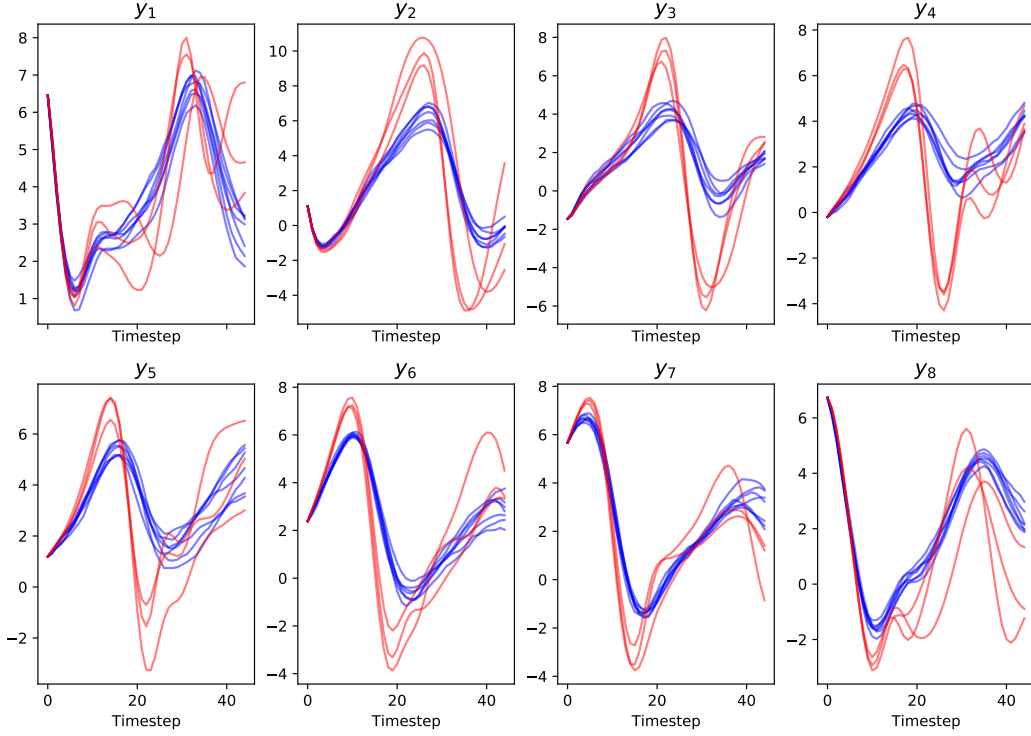


Figure 14: Simulations from  $\theta^*$  (blue) and from  $\theta^{\text{out}}$  (red; i.e., outliers). Here, we consider 7 simulations from  $\theta^*$  and 3 outliers. Each panel shows a different component of  $y$ .

Kernel and Energy Score Posteriors; this resulted in  $w \approx 0.8610$  for the Energy Score and  $w \approx 20.7138$  for the Kernel Score.

In Table 7 we report the proposal sizes  $\sigma$  and the resulting acceptance rates for the SR posteriors for the different values of  $\epsilon$  considered in the main text. We also report the trace of the posterior covariance matrix  $\Sigma_{\text{post}}$  for the SR posteriors and the one obtained with SMC ABC of Del Moral et al. [2012]. We stress again how the correlated pseudo-marginal MCMC for BSL and semiBSL were unable to run satisfactory.

$\epsilon$	Kernel Score			Energy Score			SMC ABC
	Prop. size $\sigma$	Acc. rate	Tr $[\Sigma_{\text{post}}]$	Prop. size $\sigma$	Acc. rate	Tr $[\Sigma_{\text{post}}]$	Tr $[\Sigma_{\text{post}}]$
0	0.1	0.21	0.1276	0.25	0.25	0.1805	0.1848
0.1	0.1	0.23	0.1596	0.25	0.27	0.2023	0.1919
0.2	0.1	0.27	0.2012	0.25	0.29	0.1884	0.1843

Table 7: Proposal size, acceptance rate and trace of the posterior covariance matrix for different outlier proportions  $\epsilon$  for the Lorenz96 model, for the Kernel and Energy Score posteriors.

We report posterior marginals for all values of  $\epsilon$  in Figure 15. There, all methods lead very broad posterior distributions, so that all of them seem fairly insensitive to outliers. Notice however how the ABC posterior is broader for the  $b_1$  parameter.

Finally, in Table 8 we report numerical values for the first predictive check discussed in Section 4.2.2 in the main text, from which Figure 6a in the main text is derived. Additionally, Figure 16 reports analogous results for the Energy Score posterior to Figure 7a in the main text for the Kernel Score posterior.

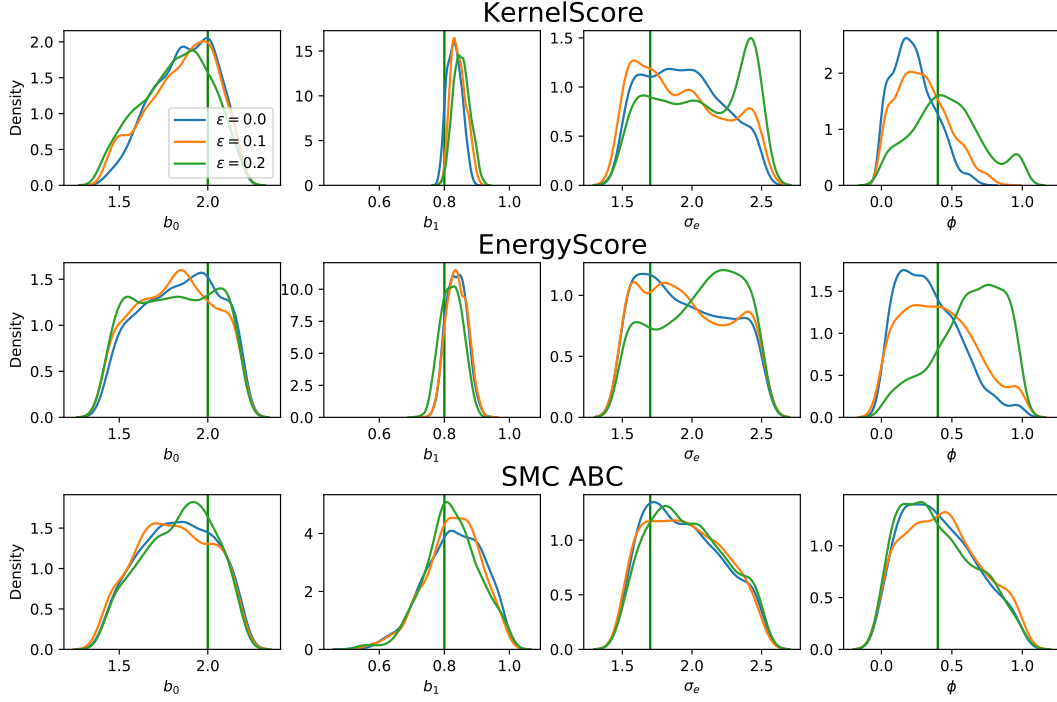


Figure 15: Marginal distribution for the posterior distributions obtained with the different methods and different outliers proportions  $\epsilon$ , for the Lorenz96 model. The posterior densities are obtained by KDE on the MCMC output thinned by a factor 10.

$\epsilon$	Kernel Score posterior		Energy Score posterior		SMC ABC posterior	
	Kernel Score	Energy Score	Kernel Score	Energy Score	Kernel Score	Energy Score
0	-797.391	538.401	-737.072	643.464	-556.662	985.031
0.1	-769.984	584.181	-695.978	716.861	-515.992	1054.11
0.2	-685.028	728.355	-541.48	989.387	-530.634	1020.09

Table 8: Posterior predictive check: SR values for Lorenz96 model computed after statistics computation. Each row refers to a different outliers proportion  $\epsilon$ . Each column reports the estimated Kernel and Energy Score for the different posteriors.

#### E.4 Additional details on the recruitment, boom and bust model experiments

For the Kernel Score posterior with the Gaussian Kernel, we first fit the value of the bandwidth of the Gaussian kernel as described in Appendix D, which resulted in  $\gamma \approx 23.3363$ .

Next, we used our heuristic procedure (Sec.2.4) to tune the value of the weight  $w$  for both the Kernel and Energy Score Posteriors; this resulted in  $w \approx 2.3298$  for the Energy Score and  $w \approx 5497.1406$  for the Kernel Score. Unfortunately, these values turn out to be too large and the posterior too concentrated for successfully running MCMC on it. Therefore, we hand-picked  $w = 1$  for the Energy Score and  $w = 20$  for the Kernel Score.

For this model, we use a multivariate normal proposal in the MCMC, with covariance matrix  $0.1 \cdot \Sigma$  for the Energy Score, and  $0.25 \cdot \Sigma$  for the KernelScore, where  $\Sigma$  is the covariance matrix given by the

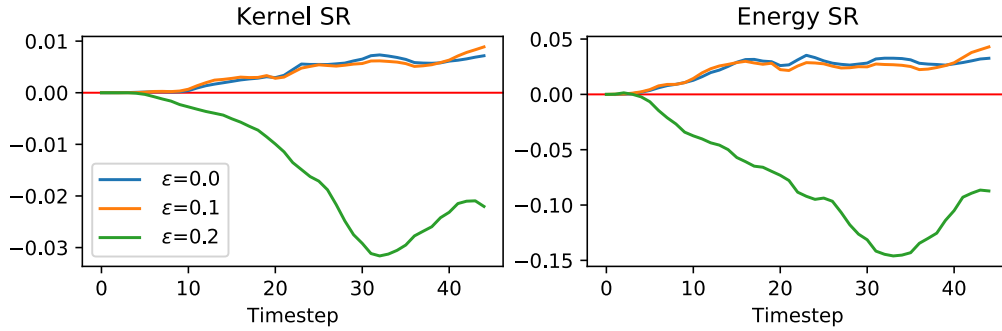


Figure 16: Posterior predictive check: difference of SR at each time-step (with respect to observations from  $\theta^*$ ) between posterior predictive obtained from the SMC ABC posterior and the Energy Score one, for the Lorenz96 model. Left (respectively right) panel report Kernel (resp. Energy) SR values. Positive values indicate the Energy Score posterior better represents the distribution at that time-step than the SMC ABC one, which happens for most time-steps for  $\epsilon = 0, 0.1$  but not for  $\epsilon = 0.2$ . Red horizontal line denotes 0.

average of the covariance matrix used for BSL and semiBSL in An et al. [2020], which results in:

$$\Sigma = \begin{pmatrix} 0.01472403 & -0.0008366 & -0.00101653 & -0.03552685 \\ -0.0008366 & 0.00992781 & 0.00074306 & 0.00612864 \\ -0.00101653 & 0.00074306 & 0.02028828 & -0.01096709 \\ -0.03552685 & 0.00612864 & -0.01096709 & 0.50033174 \end{pmatrix}$$

In Table 9 we report the acceptance rates for the SR posteriors for the different values of  $\epsilon$  considered in the main text. We also report the trace of the posterior covariance matrix  $\Sigma_{post}$  for the SR posteriors and the one obtained with SMCABC. For this model, the correlated pseudo-marginal MCMC for the Energy Score posterior had a very small acceptance rate for  $\epsilon > 0$ . In the following, we therefore exclude that from our analysis. Again, we also exclude BSL and semiBSL as the correlated pseudo-marginal MCMC results were unsatisfactory.

$\epsilon$	Kernel Score		Energy Score		SMC ABC
	Acc. rate	Trace of covariance	Acc. rate	Trace of covariance	Tr [ $\Sigma_{post}$ ]
0	0.47	0.8734	0.07	0.1463	94.9879
0.1	0.20	0.9753	0.01	0.1034	59.6868
0.2	0.13	2.5997	0.01	0.0339	92.1825

Table 9: Proposal size, acceptance rate and trace of the posterior covariance matrix for different outlier proportions  $\epsilon$  for the recruitment, boom and bust model, for the Kernel and Energy Score posteriors. Here, the acceptance rate for the Energy Score is extremely small.

We report posterior marginals for SMC ABC and the Kernel Score posterior for all values of  $\epsilon$  in Figure 17. There, you can notice how the Kernel Score posterior is much more concentrated close to the true parameter values with respect to the ABC one, which is broader. Notwithstanding its high concentration, the Kernel Score posterior is remarkably insensitive to outliers. The SMC ABC one looks also insensitive to outliers, but notice how it is very broad, covering large part of the parameter space.

Finally, in Table 10 we report numerical values for the first predictive check discussed in Section 4.2.2 in the main text, from which Figure 6b in the main text is derived.

## F Additional simulation studies: the MA(2) and M/G/1 models

We test now the performance of the different methods with one single observation on the MA(2) and the M/G/1 models [Marin et al., 2012, An et al., 2020]. We consider a well specified setting, and

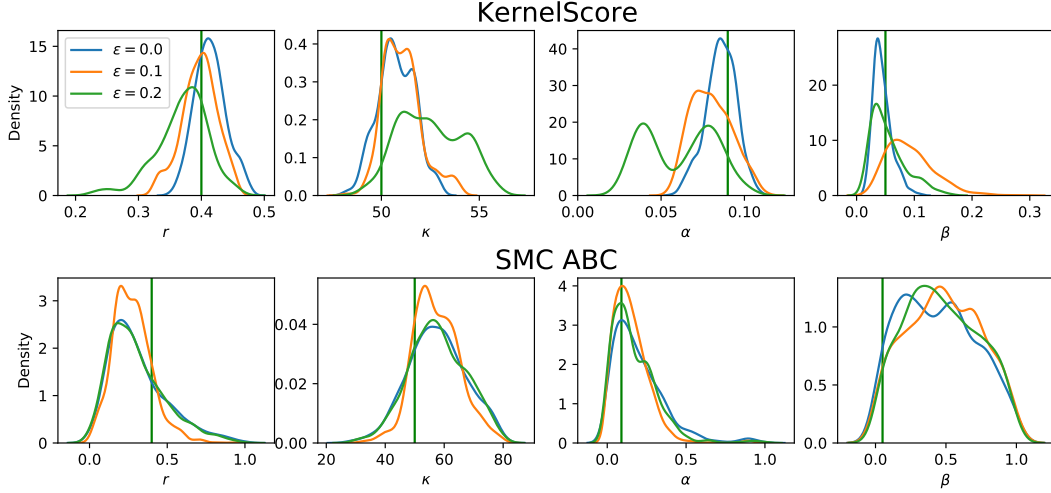


Figure 17: Marginal distribution for the posterior distributions obtained with the different methods and different outliers proportions  $\epsilon$ , for the recruitment, boom and bust model. Notice the different horizontal scale for panels corresponding to Kernel Score and SMC ABC posterior, which show larger concentration of the former. The posterior densities are obtained by KDE on the MCMC output thinned by a factor 100.

$\epsilon$	Kernel Score posterior		SMC ABC posterior	
	Kernel Score	Energy Score	Kernel Score	Energy Score
0	-178.629	115537	-19.1644	257156
0.1	-149.347	92216	-5.5363	174541
0.2	-50.8351	143102	89.9685	268772

Table 10: Posterior predictive check: SR values for the Recruitment, Boom and Bust model computed after statistics computation. Each row refers to a different outliers proportion  $\epsilon$ . Each column reports the estimated Kernel and Energy Score for the different posteriors.

also report the true posterior distribution, which is obtained via the `PyMC3` library [Salvatier et al., 2016] for the MA(2) model and with the custom strategy described in Shestopaloff and Neal, 2014 for the M/G/1 one. Let us stress here how the SR posterior does not approximate the standard Bayes posterior, but rather is defined as a generalized Bayesian update; for this reason, it is unfair to evaluate the SR posterior (with respect to, say, BSL) by assessing the mismatch from the standard Bayes one. Still, it is insightful to show the performance of our methods alongside the true posterior and its approximations BSL and semiBSL. With both models, we find that the SR posteriors are located on similar regions of the parameter space as the true posterior, but are centered on slightly different parameter values.

Additionally, we investigated the SR posteriors with different values of  $w$ : unsurprisingly, larger values of  $w$  lead to more concentrate posteriors.

## F.1 MA(2) model

The Moving Average model of order 2, or MA(2), is a time-series model for which simulation is easy and the likelihood is available in analytical form; it has 2 parameters  $\theta = (\theta^1, \theta^2)$ . Sampling from the model is achieved with the following recursive process:

$$x^1 = \xi^1, \quad x^2 = \xi^2 + \theta^1 \xi^1, \quad x^t = \xi^t + \theta^1 \xi^{t-1} + \theta^2 \xi^{t-2}, \quad t = 3, \dots, 50,$$

where  $\xi^t$ 's are i.i.d. samples from the standard normal distribution (recall here superscripts do not represent power but vector indices). The vector random variable  $X \in \mathbb{R}^{50}$  has a multivariate normal

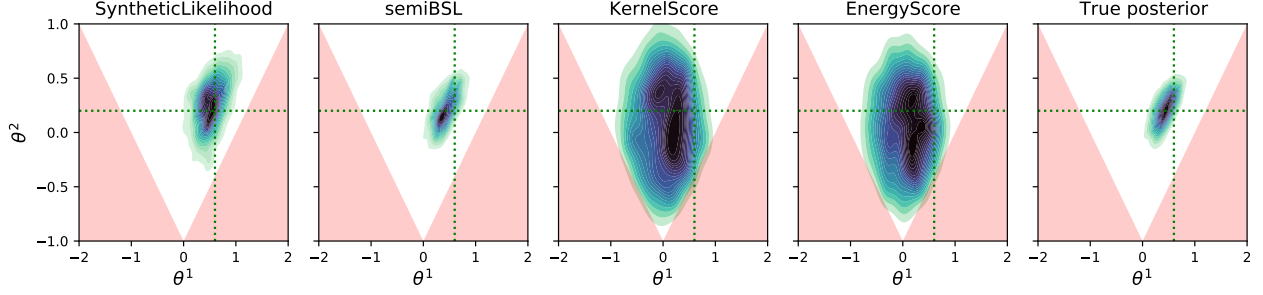


Figure 18: Contour plot for the posterior distributions for the MA(2) model, with darker colors denoting larger posterior density, and dotted line denoting true parameter value. The posterior densities are obtained by KDE on the MCMC output thinned by a factor 10. Here, the Energy and Kernel Score posteriors are similar and broader than the true posterior; notice that they do not approximate the true posterior but rather provide a general Bayesian update. BSL and semiBSL reproduce the true posterior well, as expected for this model. The prior distribution is uniform on the white triangular region.

distribution with sparse covariance matrix; therefore, this model satisfies the assumptions of both BSL and semiBSL. We set the prior distribution over the parameters to be uniform in the triangular region defined through the following inequalities:  $-1 < \theta^2 < 1$ ,  $\theta^1 + \theta^2 > -1$ ,  $\theta^1 - \theta^2 < 1$ . We consider an observation generated from  $\theta^* = (0.6, 0.2)$ ; further, we use  $m = 500$  simulations and 30000 MCMC steps, of which 10000 are burned-in, in order to sample from the different methods. Further, we take  $G = 50$  in the correlated pseudo-marginal MCMC.

Exact posterior samples are obtained with MCMC using the exact MA(2) likelihood with 6 parallel chains with 20000 steps, of which 10000 are burned in.

For the Kernel Score posterior with the Gaussian Kernel, we first fit the value of the bandwidth of the Gaussian kernel as described in Appendix D, which resulted in  $\gamma \approx 12.77$ .

Next, we used our heuristic procedure (Sec.2.4) to tune the value of the weight  $w$  for both the Kernel and Energy Score Posteriors; this resulted in  $w \approx 12.97$  for the Energy Score and  $w \approx 208$  for the Kernel Score.

In Table 11 we report the proposal sizes  $\sigma$  and the resulting acceptance rates and trace of the posterior covariance matrix  $\Sigma_{post}$  for BSL, semiBSL and the SR posteriors with the above values of  $w$ ; we also report the trace of  $\Sigma_{post}$  for the true posterior, for which we do not give the proposal size and acceptance rate as it was sampled using more advanced MCMC techniques than standard Metropolis-Hastings using the PyMC3 library [Salvatier et al., 2016].

Technique	BSL	semiBSL	True posterior	Kernel Score	Energy Score
Proposal size $\sigma$	1	0.2	/	1	1
Acceptance rate	0.16	0.16	/	0.51	0.46
$\text{Tr}[\Sigma_{post}]$	0.08595	0.05271	0.04483	0.3010	0.2600

Table 11: Proposal sizes and acceptance rates for the BSL, semiBSL, Kernel and Energy Score posteriors, and the true posterior for the MA2 model.

For all methods, we report the posteriors in Fig. 18. As expected, both BSL and semiBSL recover the true posterior well. The Energy Score and Kernel Score posterior perform similarly and are centered around the same parameter value as the true posterior, which is however narrower.

### F.1.1 Different values of $w$

In order to understand the behavior of the SR posterior for different choices of  $w$ , we run an MCMC chain with 30000 steps of which 10000 are burned in, by using  $m = 500$ , for a range of values of  $w$ .

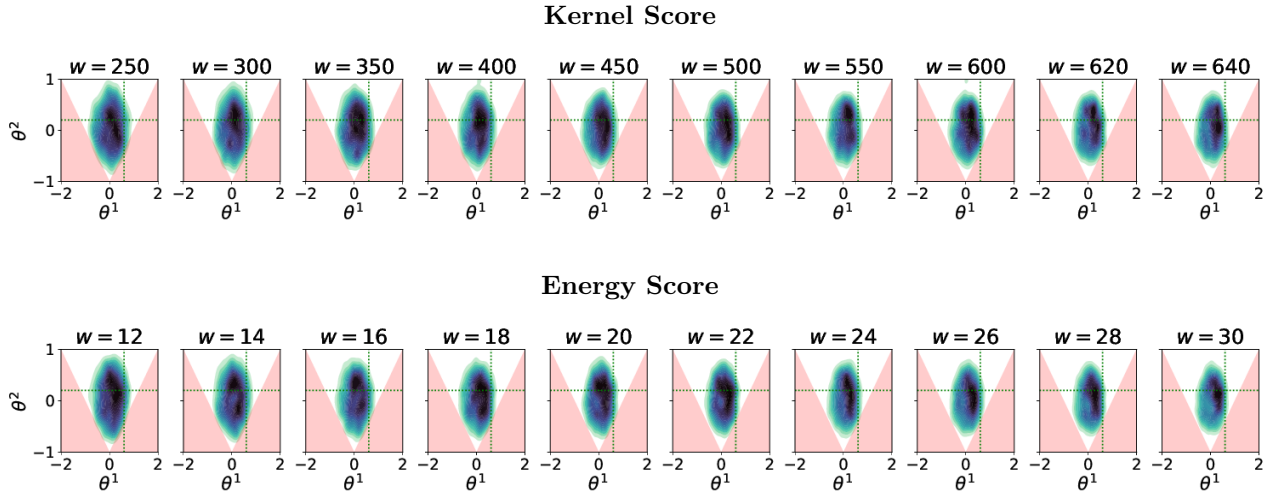


Figure 19: Contour plot for the posterior distributions for the MA(2) model with different values of  $w$ , with darker colors denoting larger posterior density and dotted line denoting true parameter value. The posterior densities are obtained by KDE on the MCMC output thinned by a factor 10. The prior distribution is uniform on the white triangular region. We remark how increasing  $w$  leads to narrower posteriors, as expected.

In Table 12, we report the proposal size, acceptance rate and the trace of the posterior covariance matrix for the different weights used, for both the Kernel and Energy Score posteriors. We highlight that increasing  $w$  leads to smaller posterior variance (as expected).

The posterior density plots for the different values of  $w$  are reported in Figure 19, where it can be seen that increasing  $w$  leads to narrower posteriors.

Kernel Score				Energy Score			
$w$	Prop. size $\sigma$	Acc. rate	Tr $[\Sigma_{\text{post}}]$	$w$	Prop. size $\sigma$	Acc. rate	Tr $[\Sigma_{\text{post}}]$
250	1	0.49	0.2828	12	0.3	0.67	0.2738
300	0.9	0.48	0.2653	14	0.3	0.65	0.2582
350	0.8	0.49	0.2537	16	0.3	0.63	0.2409
400	0.7	0.48	0.2437	18	0.3	0.62	0.2280
450	0.6	0.49	0.2273	20	0.15	0.69	0.2195
500	0.5	0.50	0.2192	22	0.15	0.67	0.2080
550	0.4	0.52	0.2164	24	0.15	0.64	0.2074
600	0.3	0.53	0.2160	26	0.15	0.63	0.2042
620	0.15	0.61	0.2068	28	0.1	0.65	0.1928
640	0.15	0.60	0.2037	30	0.1	0.63	0.1880

Table 12: Proposal size, acceptance rate and trace of the posterior covariance matrix for different weight values for MA2, for the Kernel and Energy Score posteriors.

## F.2 The M/G/1 model

The M/G/1 model is a single-server queuing system with Poisson arrivals and general service times. Specifically, the distribution of the service time is Uniform in  $(\theta^1, \theta^2)$  and the interarrival times have exponential distribution with parameter  $\theta^3$ ; the set of parameters is therefore  $\theta = (\theta^1, \theta^2, \theta^3)$ . The observed data is the logarithm of the first 50 interdeparture times; as shown in An et al. [2020], the distribution of simulated data does not resemble any common distributions; we give more details on the model and how to simulate from it in Appendix F.2.2. We set a Uniform prior on the region

$[0, 10] \times [0, 10] \times [0, 1/3]$  for  $(\theta^1, \theta^2 - \theta^1, \theta^3)$  and generate observations from  $\theta^* = (1, 5, 0.2)$ . We use  $m = 1000$  simulations and 30000 MCMC steps, of which 10000 are burned-in, in order to sample from the different methods. Further, we take  $G = 50$  in the correlated pseudo-marginal MCMC. To sample from the true posterior distribution, we employ the custom procedure described in Shestopaloff and Neal [2014].

For the Kernel Score posterior with the Gaussian Kernel, we first fit the value of the Gaussian kernel bandwidth parameter as described in Appendix D, which resulted in  $\gamma \approx 3.6439$ .

Next, we used our heuristic procedure (Sec.2.4) to tune the value of the weight  $w$  for both the Kernel and Energy Score Posteriors; this resulted in  $w \approx 10.98$  for the Energy Score and  $w \approx 797$  for the Kernel Score.

In Table 13 we report the proposal sizes  $\sigma$  and the resulting acceptance rates and trace of the posterior covariance matrix  $\Sigma_{post}$  for BSL, semiBSL and the SR posteriors with the above values of  $w$ ; we also report the trace of  $\Sigma_{post}$  for the true posterior, for which we do not give the proposal size and acceptance rate as it was sampled using more advanced MCMC techniques than standard Metropolis-Hastings [Shestopaloff and Neal, 2014].

Technique	BSL	semiBSL	True posterior	Kernel Score	Energy Score
Proposal size $\sigma$	1	0.2	/	0.01	1
Acceptance rate	0.12	0.11	/	0.2697	0.1477
$\text{Tr}[\Sigma_{post}]$	4.518	0.2726	0.2108	0.336	4.499

Table 13: Proposal sizes and acceptance rates for the BSL, semiBSL, Kernel and Energy Score posteriors, and the true posterior for the M/G/1 model.

For all methods, we report bivariate marginals of the posterior in Fig. 20. As already noticed in An et al. [2020], semiBSL is able to recover the true posterior quite well, while BSL performs worse. The Kernel and Energy Score posteriors are centered on slightly different parameter values from the true posterior, highlighting the fact that the SRs focus on different features in the data. However, we remark here that all posteriors are close in parameter space (notice that the axis in Fig. 20 do not span the full prior range). Notice that both the true posterior and the SR posteriors are guaranteed (by our Theorem 1) to concentrate on the exact parameter value as  $n \rightarrow \infty$ . For the used value of  $w$ , the SR posteriors are broader than the true posterior, and comparable to the BSL one, which is used as a reference for tuning  $w$ .

### F.2.1 Different values of $w$

In order to understand the behavior of the SR posterior for different choices of  $w$ , we run an MCMC chain with 30000 steps of which 10000 are burned in, by using  $m = 1000$ , for a range of values of  $w$ . In Table 14, we report the proposal size, acceptance rate and the trace of the posterior covariance matrix for the different weights used, for both the Kernel and Energy Score posteriors. We highlight here that the larger values of  $w$  lead to much smaller posterior variance than BSL, and almost as small as semiBSL and the true posterior.

The posterior density plots for the different value of  $w$  are reported in Figure 21, where it can be seen that increasing  $w$  leads to narrower posteriors.

### F.2.2 Simulating the M/G/1 model

We give here two different recursive formulations of the M/G/1 model which can be used to generate samples from it.

We follow the notation and the model description in Shestopaloff and Neal [2014]. Specifically, we consider customers arriving at a single server with independent interarrival times  $W_i$  distributed according to an exponential distribution with parameter  $\theta_3$ . The service time  $U_i$  is assumed to be  $U_i \sim \text{Uni}(\theta_1, \theta_2)$ ; the observed random variables are the interdeparture times  $Y_i$ .



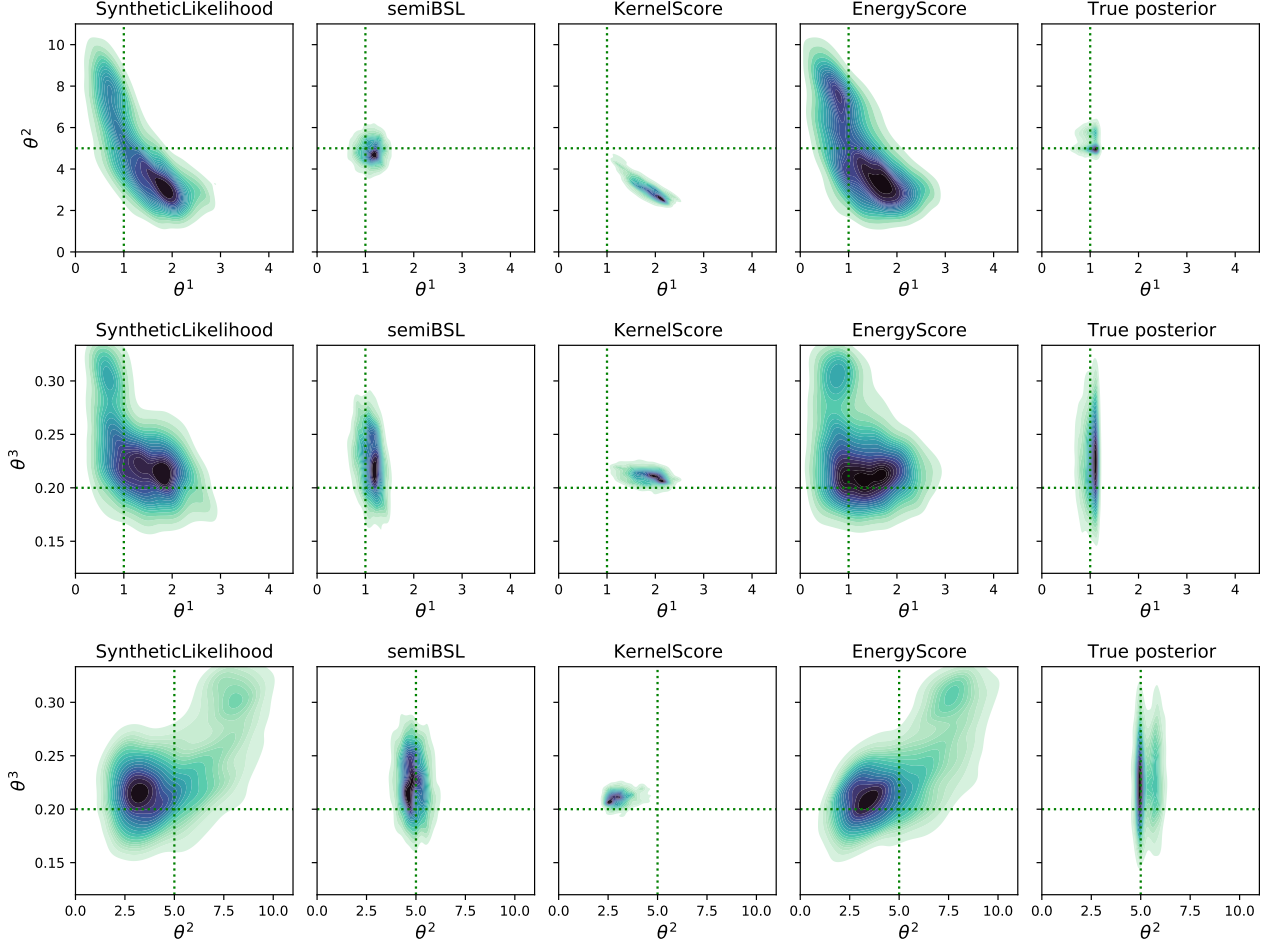


Figure 20: Posterior distributions for the M/G/1 model, with each row showing contour plots of the bivariate marginals for a different pair of parameters; darker colors denote larger posterior density, and dotted lines denote true parameter value. The posterior densities are obtained by KDE on the MCMC output thinned by a factor 10. All posteriors are close in parameter space (as the axis do not span the full prior range); however, the Energy and Kernel Score posteriors are different from each other as well as from the BSL and true posteriors. We remark that the SR posteriors do not approximate the true one but rather provide a general Bayesian update. As already noted in An et al. [2020], semiBSL recovers the true posterior well, while BSL performs worse.

In Shestopaloff and Neal [2014],  $Y_i$  is written using the following recursive formula:

$$Y_i = U_i + \max \left( 0, \sum_{j=1}^i W_j - \sum_{j=1}^{i-1} Y_j \right) = U_i + \max(0, V_i - X_{i-1}), \quad (20)$$

where  $V_i = \sum_{j=1}^i W_j$  and  $X_i = \sum_{j=1}^i Y_j$  is the departure time are respectively the arrival and departure time of the  $i$ -th customer.

A different formulation of the same process is given in Chapter 4.3 in Nelson [2013] by exploiting Lindley's equation, and is of independent interest. We give it here and we show how the two formulations correspond. Specifically, this formulation considers an additional variable  $Z_i$  which denotes the waiting time of customer  $i$ . For this, a recursion can be obtained to be:

$$Z_i = \max(0, Z_{i-1} + U_{i-1} - W_i),$$

where  $Z_0 = 0$  and  $U_0 = 0$ . Then, the interdeparture time is found to be:

$$Y_i = W_i + U_i - U_{i-1} + Z_i - Z_{i-1}; \quad (21)$$

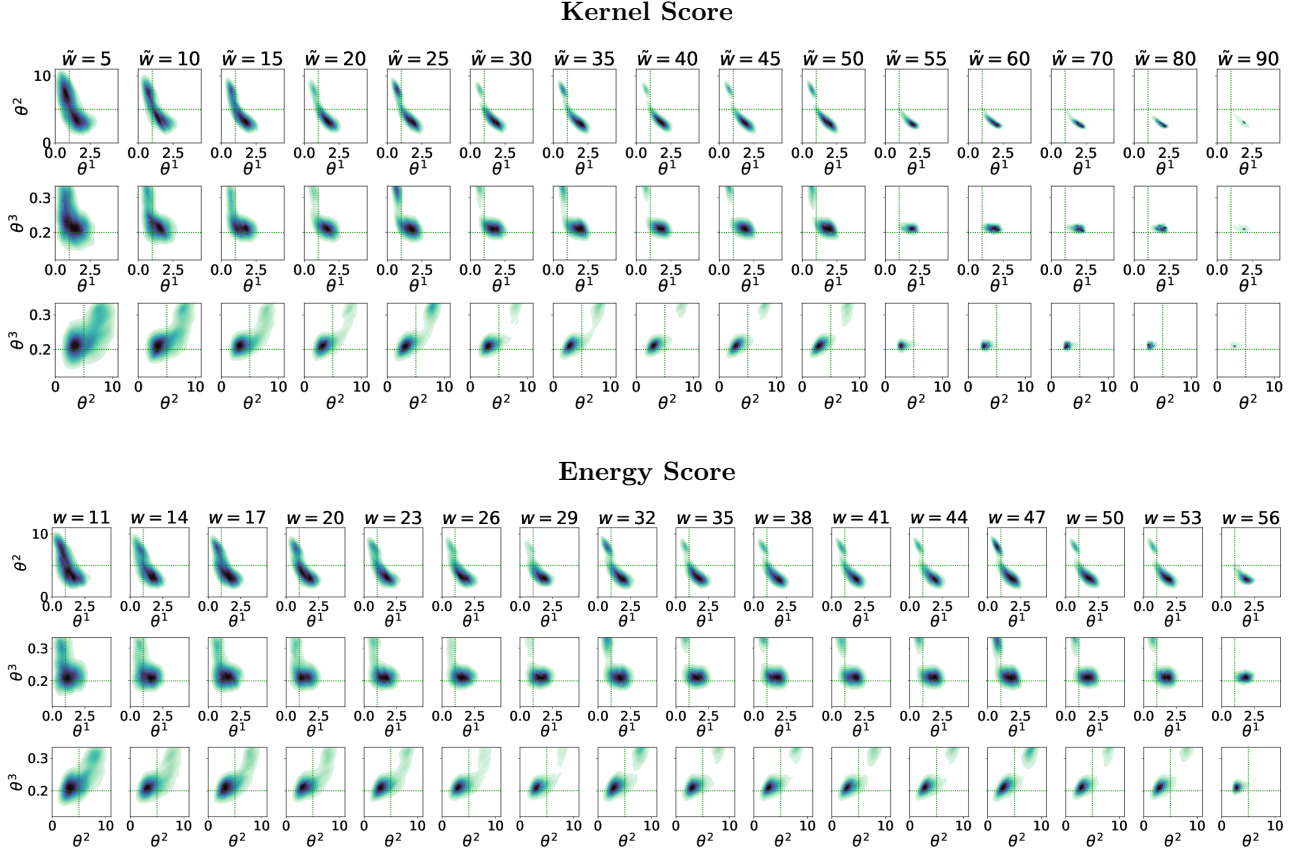


Figure 21: Posterior densities for the Kernel and Energy Score posteriors with different values of  $w$  for the M/G/1 model; for both methods, each row shows bivariate marginals for a different pair of parameters, with darker colors denoting larger posterior density and dotted line denoting true parameter value. In the figure for the Kernel Score posterior, we write  $\tilde{w} = w/10$  for brevity. The posterior densities are obtained by KDE on the MCMC output thinned by a factor 10. Notice that the axis do not span the full prior range of the parameters. We remark how increasing  $w$  leads to narrower posteriors, as expected.

Kernel Score				Energy Score			
$w$	Prop. size $\sigma$	Acc. rate	Tr $[\Sigma_{\text{post}}]$	$w$	Prop. size $\sigma$	Acc. rate	Tr $[\Sigma_{\text{post}}]$
50	1	0.20	5.2641	11	0.9	0.17	4.6423
100	1	0.11	4.5269	14	0.8	0.14	4.1235
150	0.4	0.16	4.0499	17	0.6	0.16	4.0349
200	0.3	0.13	3.2948	20	0.5	0.15	3.8567
250	0.2	0.17	4.6480	23	0.4	0.15	3.8503
300	0.1	0.21	2.7522	26	0.3	0.17	3.2135
350	0.07	0.25	3.9636	29	0.2	0.20	2.2610
400	0.05	0.26	2.5626	32	0.05	0.43	4.4932
450	0.05	0.23	3.3643	35	0.05	0.40	2.9258
500	0.05	0.22	3.7557	38	0.05	0.38	3.3495
550	0.02	0.31	0.6334	41	0.05	0.37	3.6486
600	0.02	0.29	0.4585	44	0.04	0.39	3.6295
700	0.01	0.31	0.3652	47	0.04	0.39	4.9781
800	0.01	0.27	0.2561	50	0.04	0.36	3.2886
900	0.01	0.12	0.1907	53	0.04	0.34	3.3311
-	-	-	-	56	0.01	0.56	0.5347

Table 14: Proposal size, acceptance rate and trace of the posterior covariance matrix for different weight values for M/G/1, for the Kernel and Energy Score posteriors.

this can be easily found as the absolute departure time for  $i$ -th client is  $\sum_{j=1}^i W_j + U_i + Z_i$ .

These two formulations are the same; indeed, the latter can be written as:

$$Y_i = U_i + \max(0, Z_{i-1} + U_{i-1} - W_i) - Z_{i-1} - U_{i-1} + W_i = U_i + \max(0, W_i - Z_{i-1} - U_{i-1}). \quad (22)$$

By comparing Eqs. (20) and (22), the two formulations are equal if the following equality is verified:

$$\max(0, W_i - Z_{i-1} - U_{i-1}) = \max\left(0, \sum_{j=1}^i W_j - \sum_{j=1}^{i-1} Y_j\right)$$

which is equivalent to:

$$W_i - Z_{i-1} - U_{i-1} = \sum_{j=1}^i W_j - \sum_{j=1}^{i-1} Y_j \iff Z_{i-1} + U_{i-1} = \sum_{j=1}^{i-1} (Y_j - W_j)$$

Now, from Eq. (21) we have:

$$\sum_{j=1}^{i-1} (Y_j - W_j) = \sum_{j=1}^{i-1} (U_j + Z_j - U_{j-1} - Z_{j-1}) = U_i + Z_i - U_0 - Z_0 = U_i + Z_i,$$

from which the chain of equalities are satisfied.

## G Study on the values of $m$

Here, we consider the univariate and multivariate g-and-k, both well specified and misspecified, the MA(2) and the M/G/1 models, and study the impact of varying  $m$  in the resulting MCMC target. As we span from very small to large values of  $m$ , we use here the vanilla pseudo-marginal MCMC of Andrieu et al. [2009] instead of the correlated pseudo-marginal MCMC which was used for all other simulations.

The choice of  $m$  has two different impacts on the MCMC:

1. first, it changes the pseudo-marginal MCMC target, as discussed in Section 2.3 in the main text; recall how, there, we proved that, for  $m \rightarrow \infty$ , the pseudo-marginal MCMC target converges to the original SR posterior defined in Eq. (2) in the main text. Therefore, we expect, for large enough  $m$ , the pseudo-marginal MCMC target to be roughly constant.
2. Additionally, smaller values of  $m$  imply that the target estimate has a larger variance. Therefore, we expect sampling to be harder for small  $m$ , in terms of acceptance rate of the MCMC, and easier for large  $m$  (albeit that is more computationally intensive).

In our simulation study below, we consider  $m$  values from 10 to 1000. Our results empirically verify our expectations above. In particular, we find that, for  $m$  larger than a threshold which is typically few hundreds, the pseudo-marginal MCMC target is roughly constant. Additionally, very small values of  $m$  (few tens) make sampling impractical.

Moreover, our empirical results suggest that larger values of  $m$  are required for the MCMC for semiBSL to be stable. For the other methods, the required  $m$  seem to be fairly similar, with slightly larger values for BSL for some models.

Typically, we found  $m$  values in the few hundreds to strike a good balance between larger computational cost and improved acceptance rate with larger  $m$ . Additionally, this consideration depends also on how quickly the simulation cost scales with  $m$ : even when not parallelizing model simulations across different processors, if the implementation is vectorized, the computational cost can scale sub-linearly in  $m$ , which means a better MCMC efficiency is reached for a larger  $m$ . A more extensive study considering for instance the effective sample size per CPU time could be carried out.

In all experiments, except where said otherwise, we use the value of  $w$  found via our heuristics strategy (Section 2.4 in the main text) and reported above.

## G.1 Univariate g-and-k

Here, we report results considering  $n = 10$  observations.

$m$	BSL		Kernel Score		Energy Score	
	Acc. rate	Tr $[\Sigma_{\text{post}}]$	Acc. rate	Tr $[\Sigma_{\text{post}}]$	Acc. rate	Tr $[\Sigma_{\text{post}}]$
10	0.104	4.5245	0.011	3.6030	0.063	3.9822
20	0.122	4.4439	0.035	3.6679	0.115	3.9642
50	0.129	4.3778	0.098	3.3803	0.179	3.6105
100	0.134	4.4095	0.157	3.2220	0.219	3.5335
200	0.136	4.1753	0.204	3.1628	0.243	3.4730
300	0.135	4.2261	0.220	3.1181	0.252	3.3537
400	0.135	4.1769	0.229	3.0716	0.257	3.3553
500	0.132	4.1702	0.234	3.1079	0.262	3.4362
600	0.130	4.2095	0.239	3.0295	0.259	3.2612
700	0.133	4.2417	0.243	3.0536	0.265	3.3629
800	0.132	4.2421	0.247	3.0216	0.265	3.3077
900	0.132	4.1084	0.248	3.0477	0.267	3.3815
1000	0.137	4.2930	0.253	3.1181	0.269	3.3570

Table 15: Acceptance rate and trace of the posterior covariance matrix for different values of  $m$  for the well specified univariate g-and-k, for the BSL, Kernel and Energy Score posteriors.

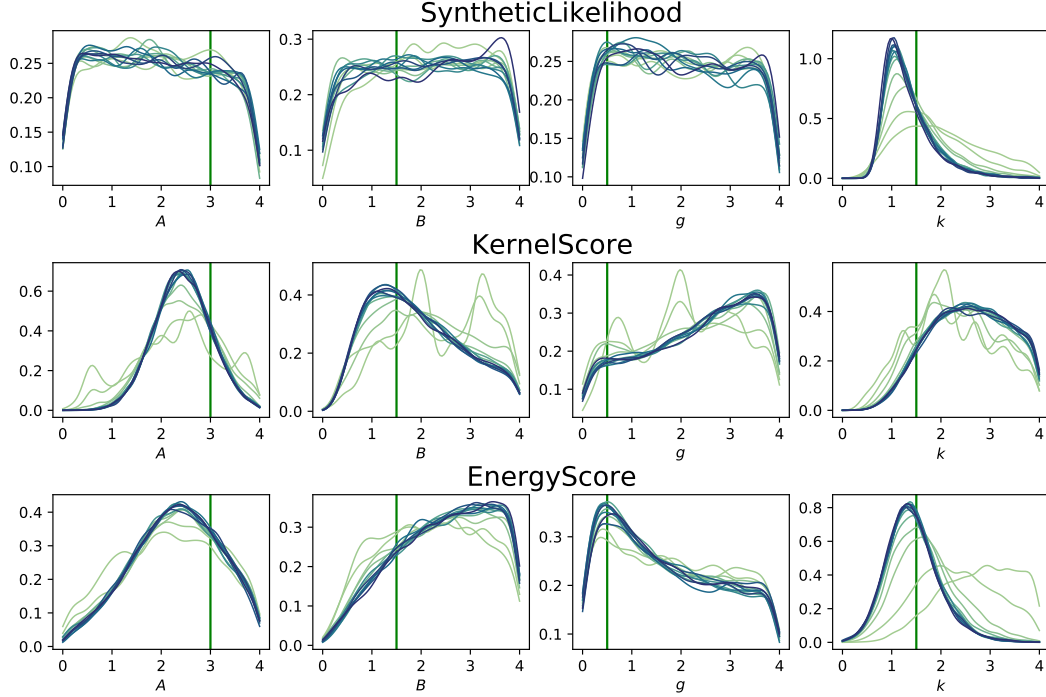


Figure 22: Univariate posterior marginals for different  $m$  values for the well specified univariate g-and-k distribution, for the BSL, Kernel and Energy Score posteriors. Lighter (respectively darker) colors denote smaller (resp. larger) values of  $m$ . For small values of  $m$ , the marginals are spiky, which is due to unstable MCMC. The densities are obtained by KDE on the MCMC output thinned by a factor 10.

## G.2 Misspecified univariate g-and-k

Here, we report results considering  $n = 10$  observations.

$m$	BSL		Kernel Score		Energy Score	
	Acc. rate	Tr $[\Sigma_{\text{post}}]$	Acc. rate	Tr $[\Sigma_{\text{post}}]$	Acc. rate	Tr $[\Sigma_{\text{post}}]$
10	0.038	3.3664	0.047	3.4141	0.164	3.8095
20	0.072	2.3207	0.069	3.2060	0.216	3.4900
50	0.130	1.9729	0.184	2.6690	0.306	2.9483
100	0.159	2.0145	0.298	2.4529	0.364	2.7232
200	0.179	1.8829	0.359	2.4037	0.391	2.7153
300	0.187	2.0198	0.389	2.3623	0.402	2.6055
400	0.188	1.9498	0.405	2.3403	0.410	2.6164
500	0.189	1.9092	0.412	2.3756	0.413	2.5579
600	0.191	1.8259	0.422	2.3461	0.414	2.5704
700	0.186	1.9207	0.430	2.3452	0.417	2.5484
800	0.184	1.9509	0.432	2.3810	0.419	2.6276
900	0.190	1.9475	0.434	2.4472	0.423	2.6468
1000	0.194	1.9763	0.436	2.3434	0.425	2.6386

Table 16: Acceptance rate and trace of the posterior covariance matrix for different values of  $m$  for the misspecified univariate g-and-k, for the BSL, Kernel and Energy Score posteriors.

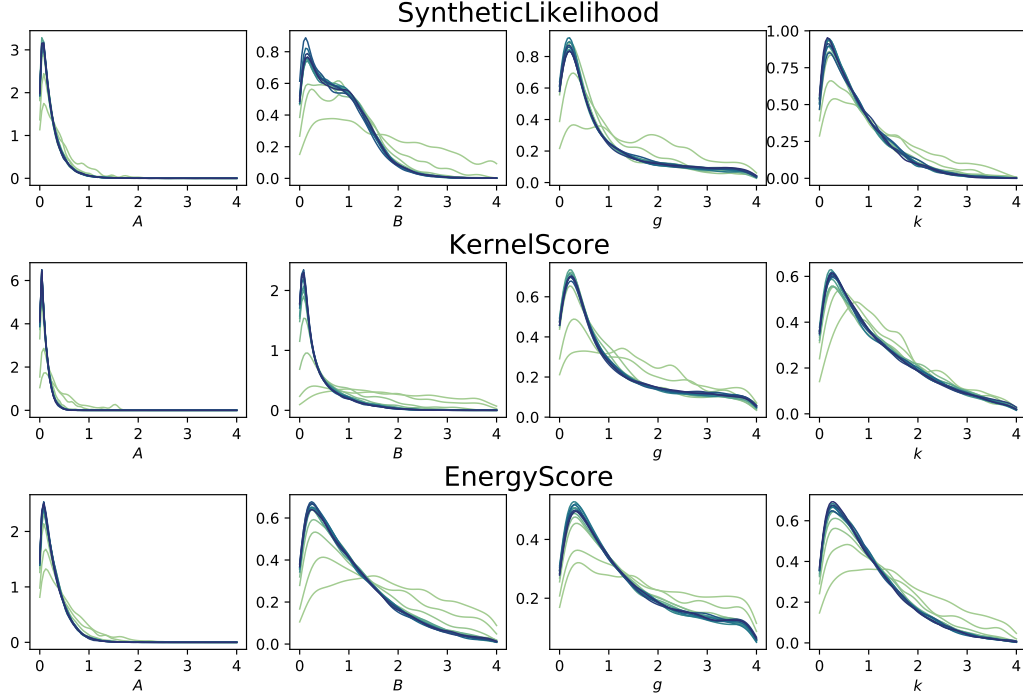


Figure 23: Univariate posterior marginals for different  $m$  values for the misspecified univariate g-and-k distribution, for the BSL, Kernel and Energy Score posteriors. Lighter (respectively darker) colors denote smaller (resp. larger) values of  $m$ . The densities are obtained by KDE on the MCMC output thinned by a factor 10.

### G.3 Multivariate g-and-k

Here, we report results considering  $n = 10$  observations.

For this model, small  $m$  lead to extremely small acceptance rates for BSL and semiBSL (Table 17); in those cases, the trace of the posterior covariance matrix is also very small due to the chain being almost still. Additionally, even large  $m$  values lead to small acceptance rate for semiBSL; that is consequence of the issues discussed in Section 4.1 in the main text and in Appendix E.1.2. We report nevertheless the results here.

$m$	BSL		semiBSL		Kernel Score		Energy Score	
	Acc. rate	Tr $[\Sigma_{\text{post}}]$	Acc. rate	Tr $[\Sigma_{\text{post}}]$	Acc. rate	Tr $[\Sigma_{\text{post}}]$	Acc. rate	Tr $[\Sigma_{\text{post}}]$
10	0.001	1.0566	0.001	0.4227	0.006	3.6061	0.070	4.5255
20	0.001	0.3674	0.001	0.6383	0.023	4.0455	0.123	3.9212
50	0.003	2.8320	0.001	0.6331	0.055	3.8924	0.170	3.8571
100	0.002	2.3666	0.001	0.6131	0.078	4.1250	0.194	3.8126
200	0.001	0.7140	0.001	0.8603	0.099	3.9624	0.206	3.7142
300	0.008	2.8229	0.002	2.2184	0.108	4.2766	0.208	3.9078
400	0.009	2.5694	0.001	0.6885	0.113	3.9710	0.212	3.8284
500	0.009	3.3583	0.002	1.2885	0.116	4.0250	0.217	3.8383
600	0.013	2.9646	0.005	1.3359	0.120	3.9632	0.216	3.7698
700	0.010	3.7043	0.005	0.6511	0.119	4.0173	0.214	3.7437
800	0.016	3.3017	0.006	0.6679	0.122	3.9607	0.214	3.7512
900	0.022	2.9915	0.005	0.6411	0.126	4.1293	0.216	3.9202
1000	0.017	3.1304	0.006	0.5892	0.122	3.9757	0.216	3.7959

Table 17: Acceptance rate and trace of the posterior covariance matrix for different values of  $m$  for the well specified multivariate g-and-k, for the BSL, semiBSL, Kernel and Energy Score posteriors.

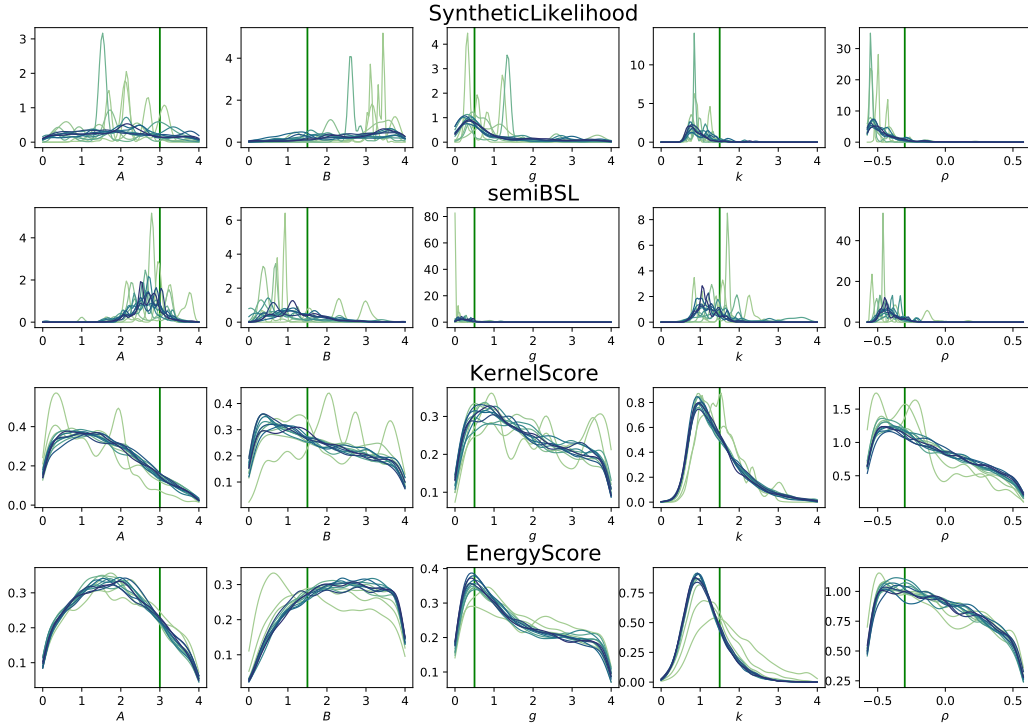


Figure 24: Univariate posterior marginals for different  $m$  values for the well specified multivariate g-and-k distribution, for the BSL, semiBSL, Kernel and Energy Score posteriors. Lighter (respectively darker) colors denote smaller (resp. larger) values of  $m$ . For small values of  $m$ , the marginals are spiky, which is due to unstable MCMC. The densities are obtained by KDE on the MCMC output thinned by a factor 10.

#### G.4 Misspecified multivariate g-and-k

Here, we report results considering  $n = 10$  observations. We do not report results for BSL and semiBSL as those were unable to run satisfactorily for that number of observations, for all considered values of  $m$ .

$m$	Kernel Score		Energy Score	
	Acc. rate	Tr $[\Sigma_{\text{post}}]$	Acc. rate	Tr $[\Sigma_{\text{post}}]$
10	0.017	4.5045	0.174	3.4306
20	0.108	3.6950	0.252	3.2373
50	0.243	3.4612	0.300	3.0291
100	0.308	3.4759	0.316	3.0081
200	0.344	3.4666	0.323	2.9303
300	0.348	3.4583	0.321	2.9160
400	0.355	3.4158	0.331	3.0031
500	0.359	3.4047	0.332	2.9743
600	0.363	3.3847	0.330	2.9321
700	0.360	3.3485	0.329	2.9249
800	0.361	3.3505	0.332	2.9854
900	0.363	3.3627	0.331	3.0155
1000	0.363	3.3307	0.330	2.9277

Table 18: Acceptance rate and trace of the posterior covariance matrix for different values of  $m$  for the misspecified multivariate g-and-k, for the Kernel and Energy Score posteriors.



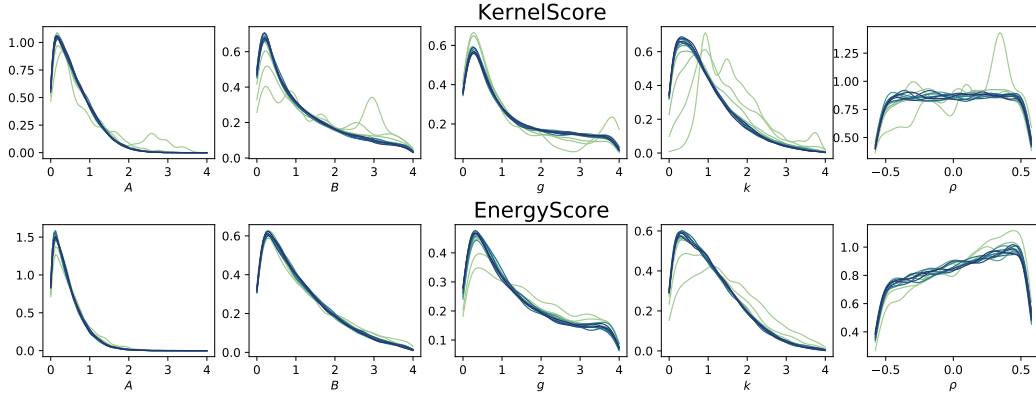


Figure 25: Univariate posterior marginals for different  $m$  values for the misspecified multivariate g-and-k distribution, for the Kernel and Energy Score posteriors. Lighter (respectively darker) colors denote smaller (resp. larger) values of  $m$ . For small values of  $m$ , the marginals are spiky, which is due to unstable MCMC. The densities are obtained by KDE on the MCMC output thinned by a factor 10.

## G.5 MA2 model

Here, we consider a single observation ( $n = 1$ ). Notice additionally how small  $m$  values lead to very small acceptance rates for all methods except BSL; in those cases, the trace of the posterior covariance matrix is also very small due to the chain being almost still. Moreover, running semiBSL failed altogether for  $m = 10$  and  $m = 50$  due to numerical errors in the estimate of some quantities. That problem does not happen for larger  $m$  values.

$m$	BSL		semiBSL		Kernel Score		Energy Score	
	Acc. rate	Tr $[\Sigma_{\text{post}}]$	Acc. rate	Tr $[\Sigma_{\text{post}}]$	Acc. rate	Tr $[\Sigma_{\text{post}}]$	Acc. rate	Tr $[\Sigma_{\text{post}}]$
10	0.031	0.1667	nan	nan	0.001	0.0001	0.001	0.0001
20	0.123	0.2149	0.001	0.0151	0.008	0.3371	0.001	0.2041
50	0.178	0.1901	nan	nan	0.106	0.3288	0.041	0.2709
100	0.178	0.1392	0.003	0.0214	0.215	0.3189	0.111	0.2748
200	0.168	0.1128	0.041	0.0565	0.303	0.3042	0.203	0.2772
300	0.170	0.0958	0.081	0.0496	0.360	0.3062	0.251	0.2554
400	0.165	0.0890	0.123	0.0505	0.392	0.2974	0.303	0.2516
500	0.157	0.0860	0.155	0.0527	0.414	0.2940	0.330	0.2546
600	0.154	0.0817	0.165	0.0441	0.434	0.2956	0.347	0.2574
700	0.143	0.0749	0.191	0.0458	0.442	0.2975	0.372	0.2617
800	0.137	0.0722	0.209	0.0494	0.446	0.2900	0.375	0.2511
900	0.132	0.0678	0.222	0.0505	0.454	0.2886	0.384	0.2576
1000	0.144	0.0684	0.230	0.0481	0.463	0.2956	0.395	0.2611

Table 19: Acceptance rate and trace of the posterior covariance matrix for different values of  $m$  for MA2, for the BSL, semiBSL, Kernel and Energy Score posteriors. **nan** values corresponds to settings in which semiBSL failed.

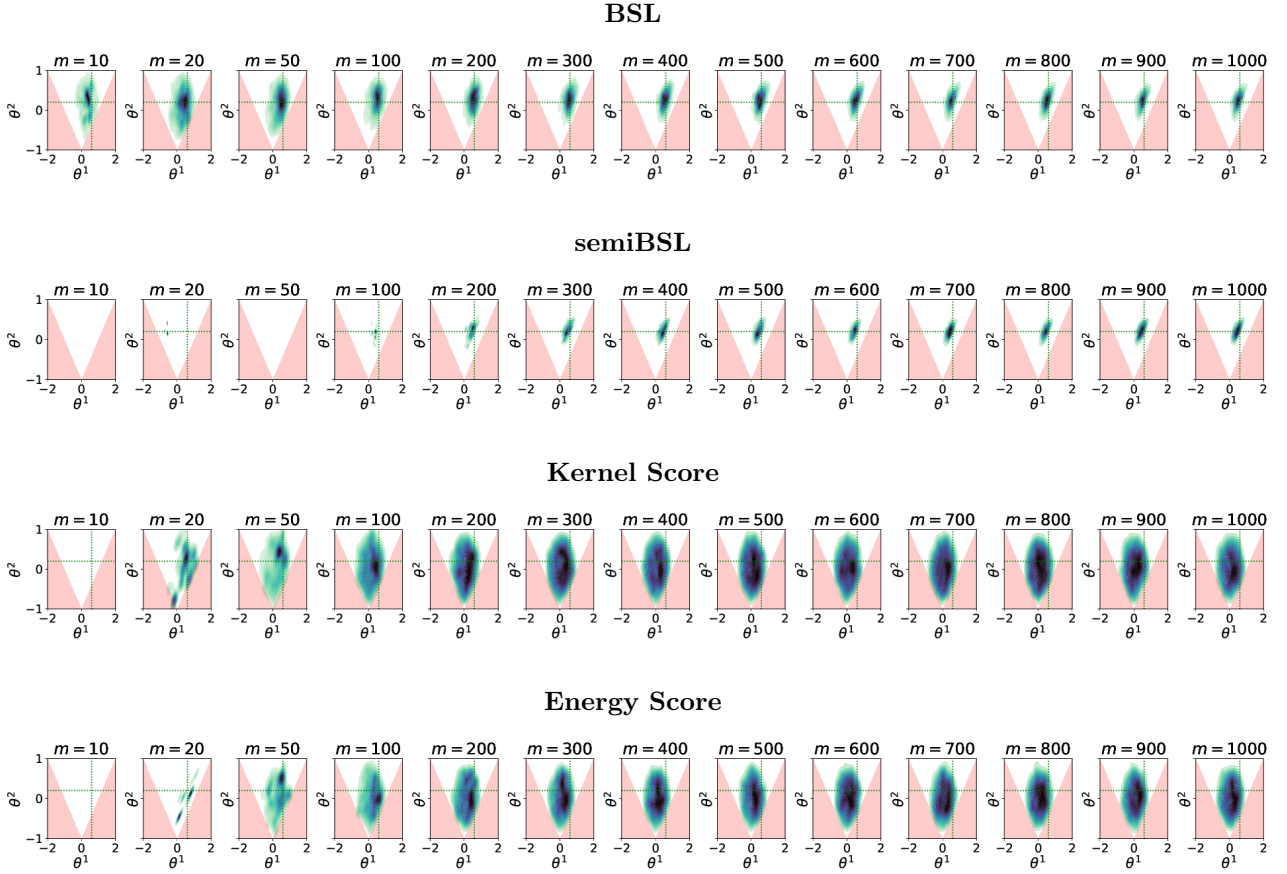


Figure 26: Bivariate posterior marginals for different  $m$  values for the MA(2) model, for the BSL, semiBSL, Kernel and Energy Score posteriors. Lighter (respectively darker) colors denote smaller (resp. larger) values of  $m$ . For small values of  $m$ , the marginals are spiky, which is due to unstable MCMC. Additionally, panels for  $m = 10$  and  $m = 50$  for semiBSL are empty as MCMC failed for those setups. The densities are obtained by KDE on the MCMC output thinned by a factor 10.

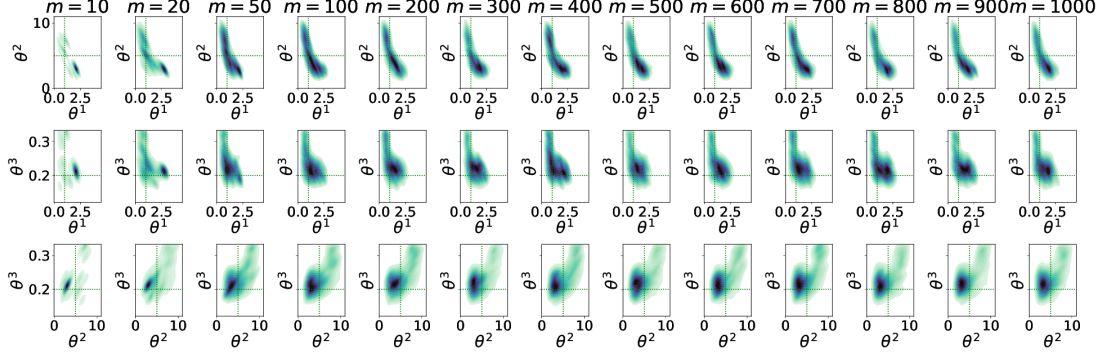
## G.6 M/G/1 model

Here, we consider a single observation ( $n = 1$ ). Additionally, we set  $w = 200$  for the Kernel Score experiment, which leads to nicer visualizations. Notice additionally how small  $m$  values lead to very small acceptance rates for all methods except Energy Score; in some of those cases, the trace of the posterior covariance matrix is also very small due to the chain being almost still. Moreover, running semiBSL failed altogether for  $m = 50$  due to numerical errors in the estimate of some quantities. That problem does not happen for larger  $m$  values.

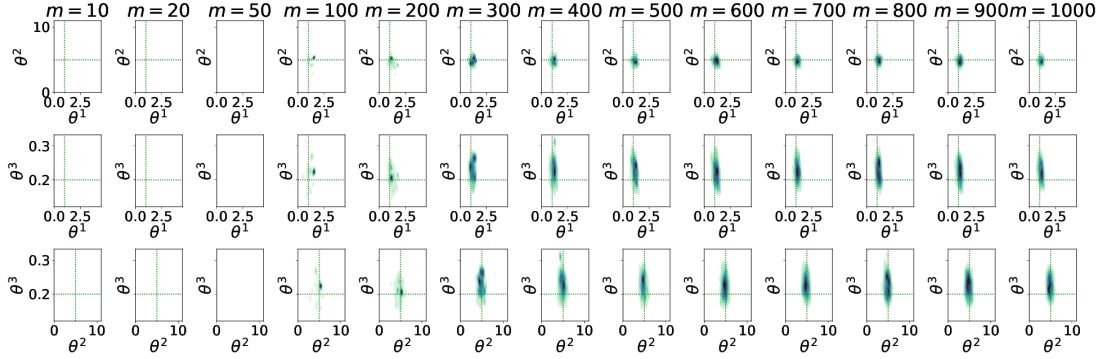
$m$	BSL		semiBSL		Kernel Score		Energy Score	
	Acc. rate	Tr $[\Sigma_{\text{post}}]$	Acc. rate	Tr $[\Sigma_{\text{post}}]$	Acc. rate	Tr $[\Sigma_{\text{post}}]$	Acc. rate	Tr $[\Sigma_{\text{post}}]$
10	0.004	3.4400	0.001	1.1318	0.001	0.0072	0.015	7.1089
20	0.039	4.7629	0.001	0.001	0.001	0.4960	0.032	6.9773
50	0.084	4.6943	nan	nan	0.007	0.7041	0.082	4.9889
100	0.100	5.0199	0.002	0.3024	0.048	4.1120	0.104	4.4941
200	0.113	4.9298	0.018	0.3448	0.059	2.4117	0.127	5.0424
300	0.109	4.2174	0.036	0.3350	0.067	1.2283	0.133	4.3495
400	0.115	4.9477	0.066	0.3468	0.099	3.2122	0.142	5.2047
500	0.119	4.5245	0.072	0.3241	0.100	2.9637	0.144	4.7920
600	0.113	4.7229	0.086	0.3383	0.109	3.7342	0.148	5.1760
700	0.112	4.9816	0.091	0.3082	0.120	4.5793	0.146	4.5703
800	0.114	4.7486	0.089	0.2843	0.114	3.1445	0.151	5.1457
900	0.113	4.6482	0.114	0.3123	0.110	2.5299	0.154	4.9276
1000	0.120	4.5183	0.106	0.2726	0.120	3.0236	0.147	4.7525

Table 20: Acceptance rate and trace of the posterior covariance matrix for different values of  $m$  for M/G/1, for the BSL, semiBSL, Kernel and Energy Score posteriors. **nan** values corresponds to settings in which semiBSL failed.

### BSL



### semiBSL



### Kernel Score

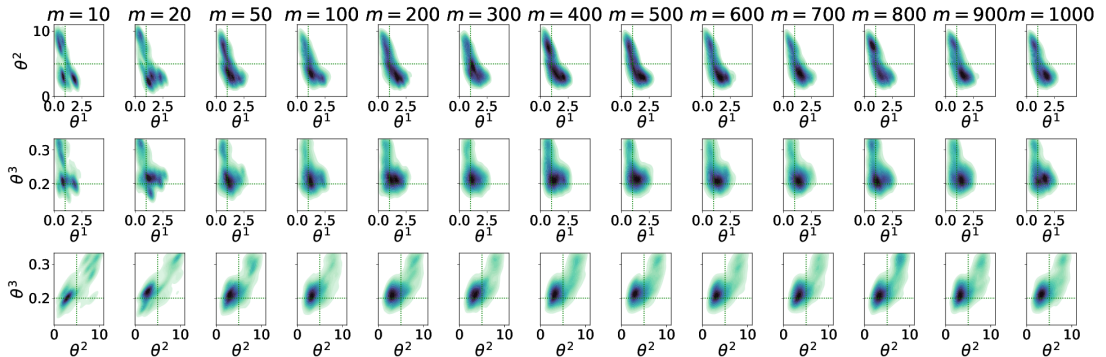
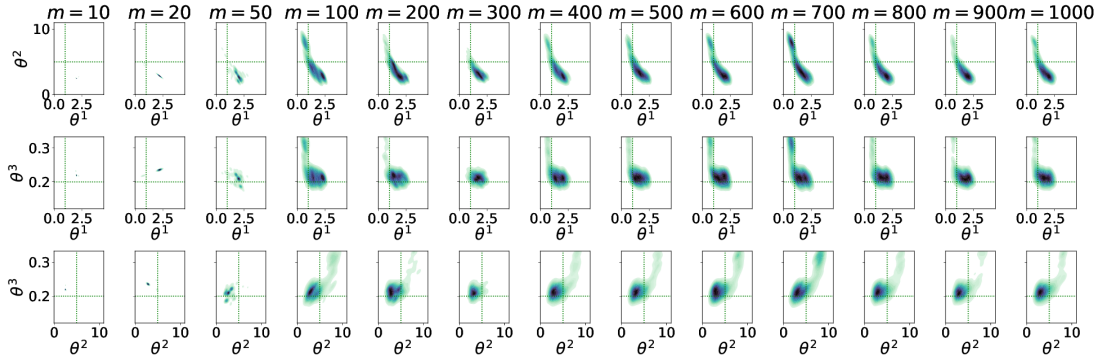


Figure 27: Bivariate posterior marginals for different  $m$  values for the M/G/1 model, for the BSL, semiBSL, Kernel and Energy Score posteriors. Lighter (respectively darker) colors denote smaller (resp. larger) values of  $m$ . For small values of  $m$ , the marginals are spiky, which is due to unstable MCMC. Additionally, panels for  $m = 50$  for semiBSL are empty as MCMC failed for those setups. The densities are obtained by KDE on the MCMC output thinned by a factor 10.